The coverage-dependent adsorption of carbon monoxide on copper catalysts studied by a combination of adsorption microcalorimetry, temperature-programmed desorption and Fourier transform infrared spectroscopy

DISSERTATION

zur Erlangung des Grades

eines Doktors der Naturwissenschaften

vorgelegt von

Raoul Naumann d'Alnoncourt

aus Göttingen

Ruhr-Universität Bochum

Lehrstuhl für Technische Chemie

2005

Die vorliegende Arbeit wurde in der Zeit vom Dezember 2001 bis Dezember 2004 am Lehrstuhl für Technische Chemie der Ruhr-Universität Bochum angefertigt.

Vorsitzender der Prüfungskommission: Prof. Dr. Ch. Wöll

Referent: Prof. Dr. M. Muhler

Korreferent: Prof. Dr. W. Grünert

Dritter Prüfer: Prof. Dr. R. Fischer

Tag der mündlichen Prüfung: 31. Januar 2005

Danksagung

Mein besonderer Dank gilt Prof. Dr. Martin Muhler für die wissenschaftliche Leitung dieser Arbeit, für sein stetes Interesse und seine Geduld.

Prof. Dr. Wolfgang Grünert danke ich für die Übernahme des Korreferats.

Den Mitgliedern der Methanol-Gruppe möchte ich für die gute Zusammenarbeit danken:
Elke, Hagen, Jenny, Lamy, Maurits, Melanie und Olaf.

Vielen Dank dem technischen und administrativen Personal des Lehrstuhls, ohne deren Hilfe die Doktorarbeit nicht möglich gewesen wäre:
Astrid, Heinz, Manuela, Sandy, Sigrid und Sigrid, Susanne und die Herren Otto.

Ich möchte an dieser Stelle auch den Werkstätten der Fakultät Chemie der RUB danken.

Ich bedanke mich bei meinen Eltern, die mich während meines gesamten Studiums immer voll und ganz unterstützt haben.

Vielen Dank an Silke für Hilfe und Unterstützung, im Alltag wie in besonderen Zeiten.

Vielen Dank auch an Euch:

Wilma, Markus, Obi Wan Volker, die Ethanolgruppe ...

Contents

1 Introduction **1**

2 The combined application of microcalorimetry, TPD and FTIR spectroscopy **9**

2.1 Introduction 9

2.2 Experimental 11

2.2.1 Adsorption microcalorimetry 11

2.2.2 CO TPD experiments 15

2.2.3 Transmission FTIR spectroscopy 16

2.2.4 Investigated samples 17

2.3 Results and discussion 18

2.3.1 Calorimetry 18

2.3.2 CO TPD results 20

2.3.3 Results by FTIR spectroscopy 22

2.4 Conclusions 24

3 Part I: The reduced catalyst **27**

3.1 Introduction 27

3.2 Experimental 28

3.3 Results 30

3.4 Discussion 35

3.5 Conclusions 43

4 Part II: The state of the catalyst after pretreatment in CO **47**

4.1 Introduction 47

4.2 Experimental 49

4.3 Results 51

4.4 Discussion 56

4.5 Conclusions 64

5 Part III: The state of the catalyst after methanol synthesis 69

5.1 Introduction . . . 69

5.2 Experimental . . . 70

5.3 Results . . . 72

5.4 Discussion . . . 77

5.5 Conclusions . . . 81

6 Conclusions 85

6.1 Introduction . . . 89

6.2 Experimental . . . 90

6.2.1 Connectors and flanges . . . 90

6.2.1.1 Swagelok connectors and tube fittings . . . 90

6.2.1.2 The Cajon VCR connection . . . 91

6.2.1.3 The CF Flange . . . 93

6.2.1.4 The KF Flange . . . 94

6.2.2 The adsorption microcalorimetry set-up . . . 94

6.2.2.1 The microcalorimeter . . . 95

6.2.2.2 The volumetric dosing section . . . 96

6.2.2.3 Controlling the temperature of the set-up . . . 98

6.2.2.4 The measuring cells . . . 99

6.2.2.5 The gas supply system . . . 100

6.2.2.6 The vacuum system . . . 102

6.2.2.7 The Baratron pressure gauges . . . 103

6.2.3 Operation of the adsorption microcalorimetry set-up . . . 104

6.2.3.1 Controlling the calorimeter via the Setsoft 2000 software . . . 104

6.2.3.2 Controlling the volumetric dosing section via LabView programs . . . 107

6.2.3.3 Volume calibration . . . 111

6.2.3.4 Sample pretreatment . . . 113

6.2.3.5 Measurement of heats of adsorption . . . 115

6.3 Data processing . . . 116

6.3.1 Calculation of the adsorption isotherm 117
6.3.2 Calculation of the differential heat of adsorption 120

1 Introduction

Methanol is together with ammonia and sulphuric acid one of the three most important products synthesized industrially. Copper catalysts are widely used for the synthesis of methanol. The industrially applied catalyst is a ternary system containing copper (Cu), zinc oxide (ZnO), and alumina (Al_2O_3) [1, 2]. Although this catalyst system has been used for about 40 years and in spite of the importance of the methanol synthesis process, the nature of the active site, the role of the different catalyst components and the mechanism of the methanol synthesis are still subject of investigations.

Klier [3] proposed copper species incorporated in interstitial and substitutional sites in ZnO to be the active site in methanol synthesis. Okamoto et al. [4] correlated the activity of Cu/ZnO catalysts to Cu^0-Cu^+ species in a two-dimensional epitaxial layer on ZnO. Other authors [5, 6] identified copper in its metallic state as the active site and ZnO as inert supporting material that stabilizes a high copper surface [5]. Frost [7] assumed that the active sites are located at the Cu/ZnO interface. Nakamura and co-workers [8, 9, 10] reported that ZnO_x species migrated under reducing conditions onto the Cu surfaces forming Cu-Zn alloys and stabilizing Cu(I) species. Clausen et al. [11, 12] found no experimental evidence for Cu(I) species when investigating $Cu/ZnO/Al_2O_3$ samples in an in situ X-ray diffraction (XRD) and an in situ X-ray absorption fine structure (XAFS) study under the conditions of methanol synthesis while measuring the catalytic activity using on-line gas chromatography. X-ray photoelectron spectroscopy (XPS) data presented by Fleisch and Mieville [13] included also no evidence for Cu(I) species under methanol synthesis conditions.

Chinchen et al. [14] investigated the synthesis of methanol from ^{14}C-labelled reactants over $Cu/ZnO/Al_2O_3$. The authors concluded that methanol is predominantly produced from carbon dioxide (CO_2) and not from carbon monoxide (CO) for a wide range of CO_2/CO ratios in the feed gas. Askgaard et al. [15] presented a detailed kinetic model of the methanol synthesis over copper catalysts based on surface science studies. In their model methanol is synthesized from carbon dioxide only. Adsorbed carbon dioxide is hydrogenated to methanol and water via formate as stable intermediate product. The model includes the water-gas shift reaction of carbon monoxide and water and a route from formate to formaldehyde as by-product.

Carbon monoxide is an often used probe molecule. In literature, many studies are found investigating copper, binary (e. g. Cu/ZnO, Cu/Al_2O_3) or ternary copper catalysts (e. g. $Cu/ZnO/Al_2O_3$) by microcalorimetry, temperature-programmed desorption (TPD) or Fourier transform infrared (FTIR) spectroscopy.

In 1934, Beebe and Wildner [16] measured calorimetrically the heat of adsorption of CO on reduced copper granules. They observed a decrease with increasing coverage from an initial value of about 85 kJ/mol to a value of about 57 kJ/mol at a pressure of about 50 Pa of CO.

Tracy [17] measured the isosteric heat of adsorption of CO on the Cu(100) single crystal plane and reported values of about 70 kJ/mol at low coverage and 56 kJ/mol at high coverage. Hollins and Pritchard [18] reported isosteric heats of adsorption of CO on Cu(111) of 50 and 38 kJ/mol at low and high coverage, respectively. More recently, Vollmer et al. [20] derived site-specific adsorption energies of CO on single crystal faces and polycrystalline copper by thermal desorption spectroscopy (TDS). For the close packed surfaces Cu(111) and Cu(110), integral heats of adsorption of 47 and 51 kJ/mol, respectively, were determined. Higher values of 58 kJ/mol were found for kinks, steps, and defect structures.

In an FTIR study Dulaurent et al. [19] found a band at 2092 cm^{-1} after the adsorption of CO on a completely reduced 4.7 % Cu/Al_2O_3 at 300 K for pressures of 1 and 10 kPa. They reported isosteric heats of adsorption of 82 kJ/mol at low coverages and 57 kJ/mol at high coverages. Boccuzzi et al. [21] investigated the adsorption of CO on Cu/ZnO catalysts by FTIR spectroscopy. They observed a strong and narrow band at 2098 cm^{-1} and a broad and weak band at 2070 cm^{-1} after the adsorption of CO on the reduced catalyst. Giamello et al. [22] presented a microcalorimetric study of the adsorption of CO on Cu/ZnO. They assigned heats of adsorption of about 300–110 kJ/mol to the adsorption of CO on Cu(II) species, heats of adsorption in the range from 110–70 kJ/mol to the adsorption on Cu(I) species, and heats of adsorption of 70–40 kJ/mol to the adsorption on Cu(0).

1975 Pritchard et al. [23] presented an infrared spectroscopy study of carbon monoxide chemisorbed on copper. The authors compared own data and literature data concerning copper single crystals and copper catalyst samples with various supports. The frequency of the stretching vibration of adsorbed CO is significantly different for different copper single crystal planes. The frequency is lower for low-indexed single crystal planes than for high-indexed planes, i. e. 2085, 2076 and 2093 cm^{-1} for Cu(100), Cu(111) and Cu(110) and 2100, 2102 and 2098 cm^{-1}

for Cu(211), Cu(311) and Cu(755). It is interesting to note that only the high-frequency bands were observed in the case of supported copper (evaporated films and dispersed metal), even though other characterization methods indicated the presence of low-indexed surface planes. The authors stated that this effect was not due to incomplete reduction of the copper or temperature differences in the experimental conditions (77 K in the case of copper single crystal studies, about 300 K in the case of supported copper). In 1992 Hollins [24] gave an explanation of this apparent contradiction. Dipole-dipole coupling of chemisorbed species leads to an intensity shift from low-frequency to high-frequency bands. In the case of CO chemisorbed on copper, this intensity shift leads to an increase of the bands assigned to CO adsorbed on defect sites (high-indexed planes, high-frequency bands) and a decrease of the bands assigned to CO on terrace sites (low-indexed planes, low-frequency bands). Hollins showed that the resulting spectrum can be completely dominated by the bands assigned to defect sites, even when the defect sites are a minority species of less than 10 %.

In 1978 Tauster et al. [25] reported that the state of noble metal catalysts using TiO_2 as support depended on the reduction conditions. The investigated samples showed different behavior in the adsorption of hydrogen and carbon monoxide after low-temperature reduction and high-temperature reduction. After low-temperature reduction all samples adsorbed hydrogen and CO in reasonable agreement to literature data. The adsorption capacity of the samples decreased to nearly zero after high-temperature reduction. The effect was reversible as the adsorption capacity was fully restored by an oxidizing treatment and subsequent low-temperature reduction. Using electron microscopy and X-ray diffraction the authors showed that the loss of adsorption capacity was not due to metal agglomeration or encapsulation. They concluded that the loss of adsorption capacity should be related to the formation of bonds between the noble metal atoms and titanium atoms or cations of the support, thus changing the electronic properties of the metal clusters. They referred to these processes as strong metal-support interactions (SMSI). Several recent studies [26, 27, 28, 29, 30] using different investigation methods indicate that there are strong metal-support interactions (SMSI) between copper and zinc oxide in these catalysts.

Based on in situ EXAFS and XRD experiments Grunwaldt et al. [26] presented a model for the SMSI between copper and ZnO as a function of the surrounding atmosphere: Under the reducing conditions of methanol synthesis, metallic copper particles spread on the support and

their surfaces are covered by zinc and oxygen species. Under more severe conditions, i. e. in an atmosphere of a higher reduction potential, surface and bulk alloying leads to the formation of brass.

Hansen et al. [27] gave experimental evidence of dynamic shape changes of copper nanocrystals supported on ZnO. The changes were directly observed by in situ transmission electron microscopy under high pressures. The effects were caused by changes of the reduction potential of the surrounding gas phase and were fully reversible. The authors concluded that the processes were due to adsorbate-induced changes of the Cu/ZnO interfacial energies. They assumed that oxygen vacancies in the ZnO play a role in the observed processes. Only negligible shape changes were found for copper nanocrystals supported on SiO_2.

Wagner et al. [29] investigated the SMSI between copper and ZnO by applying in situ electron energy loss spectroscopy. They reported that the support induced a tensile strain in the Cu nanoclusters. The degree of this strain was dependent on the reduction potential of the surrounding gas phase. They found no indication for strained Cu nanoclusters in Cu/SiO_2 samples.

Hinrichsen and co-workers [28, 30] investigated the interaction of hydrogen and nitrous oxide with Cu/Al_2O_3, Cu/ZnO and $Cu/ZnO/Al_2O_3$ samples after different pretreatments. The applied pretreatment conditions included reduction in hydrogen, methanol synthesis and a strongly reducing pretreatment in CO. The authors found that Cu/Al_2O_3 is hardly influenced by the pretreatment, while dynamical changes of the copper content were found in the case of ZnO-containing samples. The strongly reducing conditions of the pretreatment in CO led to a loss in free copper surface area. The free copper surface area was derived from hydrogen TPD experiments. The authors concluded that zinc and oxygen species migrated onto the copper surface thus decreasing the free surface area. The presence of the zinc species was confirmed by nitrous oxide reactive frontal chromatography.

It is difficult to draw conclusions from a comparison of all these studies, as the samples are never prepared and pretreated following identical procedures. For example, Giamello et al. [22] found in their microcalorimetric study the presence of Cu(I) species in a Cu/ZnO sample after hydrogen reduction and postulated that these species were dissolved in the ZnO matrix. Following the authors, their results supported the role of Cu(I) species as active site in the synthesis of methanol. However, the authors also pointed out that Boccuzzi et al. [21] using FTIR spectroscopy did not find any evidence for Cu(I) species investigating the same catalyst sample

after a similar pretreatment.

The goal of this study is to reach a better understanding of the SMSI between copper and zinc oxide. For several reasons the adsorption of carbon monoxide was chosen as investigation tool. The adsorption of carbon monoxide on copper catalysts is non-dissociative and not activated, and the stretching vibration of CO is active in FTIR spectroscopy. One single investigation method cannot give all desired information. For example FTIR spectroscopy can be used to identify chemically different adsorption sites, but the strength of the bond between adsorbate and adsorption site cannot be directly measured. On the other hand, microcalorimetry can be used to measure the heat of adsorption of a specific adsorbate on a substrate, but cannot distinguish between chemically different sites with the same heat of adsorption. Therefore, a combination of microcalorimetry, temperature-programmed desorption experiments and FTIR spectroscopy was applied to study the adsorption of CO. In order to obtain a high degree of comparability with the work of Hinrichsen and co-workers [28, 30, 31], the same samples were included in the present study. In addition, the samples were pretreated using the same set-up and following the same procedures applied in ref. [28, 30]. The building of a microcalorimetry set-up including a special pretreatment reactor that can be attached to the flow set-up used for the TPD experiments was one of the main tasks in this study. In addition, an already existing FTIR cell was modified to allow pretreatments in flowing gas and the dosing of CO at pressures below 100 Pa. The FTIR cell was also connected to the flow set-up used for the TPD experiments. All these efforts were made to avoid the problems that arise when data produced with different or differently pretreated samples are compared.

A complete description of the set-up and all experimental conditions is given in the second chapter. Analogous to the work in ref. [28, 30], the catalyst samples were studied after three different pretreatments: after a complete reduction of the copper content of the sample in hydrogen, after a 12 h period of methanol synthesis and after a 50 h pretreatment in strongly reducing CO gas. The results obtained with all samples after a specific pretreatment are presented in one chapter, respectively. The final chapter summarizes the conclusions of each chapter.

Bibliography

[1] J.B. Hansen,in: ”Handbook of Heterogenous Catalysis”, VCH Verlagsgesellschaft, Weinheim, 4 (1997) 1856.

[2] K. Kochloefl,in: ”Handbook of Heterogenous Catalysis”, VCH Verlagsgesellschaft, Weinheim, 4 (1997) 1831.

[3] K. Klier, Adv. Catal., 31 (1982) 243.

[4] Y. Okamoto, K, Fukino, T. Imanaka, and S. Teranishi, J. Phys. Chem., 87 (1983) 3747.

[5] G.C. Chinchen, K.C. Waugh and D.A. Whan, Appl. Catal., 25 (1986) 101.

[6] J.L. Robbins, E. Iglesia, C.P. Kelkar, and B. DeRites, Catal. Lett., 10 (1991) 1.

[7] J.C. Frost, Nature, 334 (1988) 577.

[8] I. Nakamura, T. Fujitani, T. Uchijima, and J. Nakamura, J. Vac. Sci. Technol. A, 14 (1996) 1464.

[9] I. Nakamura, T. Fujitani and T. Uchijima, und J. Nakamura, Surf. Sci., 400 (1998) 387.

[10] Y. Kanai, T. Watanabe, T. Fujitani, M. Saito, J. Nakamura, and T. Uchijima, Energy Convers. Mgmt, 36 (1995) 649.

[11] B.S. Clausen and H. Topsøe, Catal. Today, 9 (1991) 189.

[12] B.S. Clausen, G. Steffensen, B. Fabius, J. Villadsen, R. Feidenhans’l, and H. Topsøe, J. Catal., 132 (1991) 524.

[13] T.H. Fleisch and R.L. Mieville, J. Catal., 90 (1984) 165.

[14] G.C. Chinchen, P.J. Denny, D.G. Parker, M.S. Spencer and D.A. Whan, Appl. Catal., 30 (1987) 333.

[15] T.S. Askgaard, J.K. Nørskov, C.V. Ovesen, and P. Stoltze, J. Catal., 156 (1995) 229.

[16] R.A. Beebe and E.L. Wildner, J. Am. Chem. Soc., 56 (1934) 642.

[17] J.C. Tracy, J. Chem. Phys., 56 (1972) 2748.

[18] P. Hollins and J. Pritchard, Surf. Sci., 89 (1979) 486.

[19] O. Dulaurent, X. Courtois, V. Perrichon, and D. Bianchi, J. Phys. Chem. B, 104 (2000) 6001.

[20] S. Vollmer, G. Witte and C. Wöll, Catal. Lett., 77 (2001) 97.

[21] F. Boccuzzi, G. Ghiotti and A. Chiorino, Surf. Sci., 156 (1985) 933.

[22] E. Giamello, B. Fubini and V. Bolis, Appl. Catal., 36 (1988) 287.

[23] J. Pritchard, T. Catterick and R.K. Gupta, Surf. Sci., 53 (1975) 1.

[24] P. Hollins, Surf. Sci. Rep., 16 (1992) 53.

[25] S.J. Tauster, S.C. Fung and R.L. Garten, J. Am. Chem. Soc., 100 (1978) 170.

[26] J.-D. Grunwaldt, A.M. Molenbroek, N.-Y. Topsøe, H. Topsøe, and B.S. Clausen, J. Catal., 194 (2000) 452.

[27] P.L. Hansen, J.B. Wagner, S. Helveg, J.R. Rostrup-Nielsen, B.S. Clausen, and H. Topsøe, Science, 295 (2002) 2053.

[28] H. Wilmer and O. Hinrichsen, Catal. Lett., 82 (2002) 117.

[29] J.B. Wagner, P.L. Hansen, A.M. Molenbroek, H. Topsøe, B.S. Clausen, and S. Helveg, J. Phys. Chem. B, 107 (2003) 7753.

[30] H. Wilmer, T. Genger and H. Hinrichsen, J. Catal., 215 (2003) 188.

[31] M. Kurtz, H. Wilmer, T. Genger, O. Hinrichsen, and M. Muhler, Catal. Lett., 86 (2003) 77.

2 The combined application of microcalorimetry, TPD and FTIR spectroscopy

Abstract

The strong metal-support interactions between Cu and ZnO are strongly influenced by the pretreatment of the Cu/ZnO catalysts. The objective of this contribution is to demonstrate that by pretreating binary Cu/ZnO and ternary Cu/ZnO/Al_2O_3 samples under the same conditions, the Cu metal surface in identical states is accessible to adsorption microcalorimetry, TPD experiments and transmission FTIR spectroscopy. Carbon monoxide is used as probe molecule to investigate the state of the Cu surface after H_2 reduction. All results show that a fully reduced and adsorbate-free Cu surface is obtained after a reduction pretreatment in flowing hydrogen. The adsorption of CO on these surfaces is fully reversible at room temperature, with heats of adsorption ranging between 70 kJ/mol at low coverages and 45 kJ/mol at high coverages.

2.1 Introduction

Copper catalysts are widely used for the industrial methanol synthesis. These catalysts are ternary systems containing copper, zinc oxide and alumina [1]. Several recent studies indicate there are strong metal-support interactions (SMSI) between copper and zinc oxide in these catalysts. Under the reducing conditions of the methanol synthesis, the metallic copper surfaces are covered by zinc and oxygen species [2]. Under more severe conditions, surface and bulk alloying leads to the formation of brass [3]. The adsorption of CO can be applied as a tool to investigate the nature of the SMSI effect.

In this contribution, three different techniques are used to study the adsorption of CO on copper catalysts, which are linked by the same gas supply and gas analysis units for sample pretreatment. The goal of this contribution is to demonstrate that by pretreating samples under the same

conditions, the metallic copper surface is accessible to the different investigation methods in identical states.

The heat of adsorption can be derived from temperature programmed desorption (TPD) experiments using the Redhead equation, or from adsorption isotherms using the Clausius-Clapeyron equation. A more direct approach is to measure the differential heat of adsorption as a function of coverage by adsorption microcalorimetry. The value of this tool for the characterization of catalyst surfaces is demonstrated in numerous examples in literature, focusing e. g. on acid sites in zeolites or on metal oxide surfaces [4, 5]. Spiewak and Dumesic [6] presented a technique, which allows to study reactive catalyst surfaces unimpaired by poisoning. For example, they applied this technique to determine the heat of adsorption of nitrogen on reduced and extremely air-sensitive iron catalysts. Samples were pretreated ex situ in ultra-pure flowing gases, and then sealed in pyrex capsules in inert gas. These capsules were transferred into the calorimeter, and were broken after degassing the microcalorimetric cells. Small doses of the adsorptive gas were subsequently admitted to the adsorbent, and while the heat of adsorption was measured calorimetrically, the amount of adsorbed species was measured volumetrically. A crucial point is the required very low leakage rate of the complete set-up. This procedure prevents the contamination of the sample with oxygen or moisture and yields data of the clean catalyst surface. A further developed version of the adsorption microcalorimetry set-up described in [6] was used in this contribution to study the adsorption of CO on copper catalysts as a function of coverage and pretreatment.

The adsorption of CO can be indirectly investigated by TPD experiments. For non-activated adsorption, the activation energy of the desorption equals the heat of adsorption as is the case for CO adsorption on metallic Cu surfaces [7]. Consequently, the TPD peaks are shifted to higher temperatures due to readsorption within the fixed bed. The coverage dependence of the heat of adsorption can be investigated by varying the initial coverage. The experiments were carried out in a stainless steel U-tube reactor connected to a flow set-up, and the desorption of CO into a stream of helium was monitored by on-line mass spectrometry.

CO is a often used probe molecule in Fourier transform infrared (FTIR) spectroscopy studies. CO adsorbs onto copper surfaces at low coverages non-dissociatively and linearly in on-top position. The ν(C–O) stretching vibration of adsorbed CO is sensitive to the strength of the bond to the adsorbent, and thus sensitive to the state of reduction of copper. In transmission IR

studies, relative coverages can be determined according to the Lambert-Beer law thus allowing to determine adsorption isotherms. In this contribution, the adsorption of CO was investigated using a modified transmission IR cell designed by Karge et al. [8]. The pressure of CO was varied stepwise between 0–100 Pa, in order to investigate the adsorption of CO as a function of coverage.

The interaction of Cu catalysts with hydrogen has been studied extensively by the Bochum group [12, 13, 2]. The catalysts had been investigated in different states: directly after hydrogen reduction, after a period of 12 h of methanol synthesis, and after a pretreatment of 64 h in CO/He. In order to compare the results of the studies investigating the interaction of the copper catalysts with hydrogen and with carbon monoxide, the same reduction procedure was applied in this present manuscript. All results refer to the state of the catalyst samples after hydrogen reduction. The investigated samples are a Cu/ZnO catalyst with a molar Cu:Zn ratio of 50:50, an industrial catalyst with a copper content of 50 %, and a ternary catalyst with a molar Cu:Zn:Al ratio of 10:60:30.

2.2 Experimental

2.2.1 Adsorption microcalorimetry

The adsorption microcalorimetry set-up consists mainly of three sections: the calorimeter, the microcalorimetric cells and the thermostated volumetric dosing section. A schematic diagram of the set-up is shown in Fig. 2.1. The calorimeter is a commercial Tian-Calvet heat-flux microcalorimeter (C80 II, Setaram). It can be operated from room temperature up to 573 K. The calorimetric resolution is 0.1 μW and the detection limit is 2–5 μW. The calorimeter is equipped with a homemade heating element fitted into the upper part of the calorimeter. The calorimeter is connected to the volumetric dosing section by specially designed microcalorimetric cells. The heating element keeps all parts of the cells that are not in the calorimetric block or the volumetric dosing section thermostated.

The microcalorimetric cells are shown in Fig. 2.2. They fit exactly into the calorimeter and the heating element. The cells are designed as symmetrically and simply as possible. They are made of five parts: the central part is a tee piece with two double-sided DN40 CF vacuum flanges and one standard DN40 CF vacuum flange. Two identical receptacles for the sample and

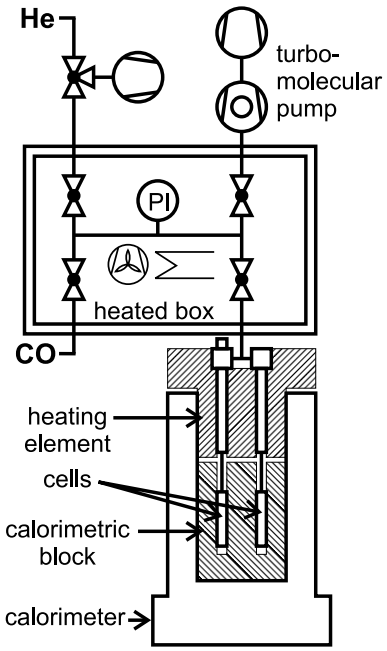

Figure 2.1: Flow scheme of the adsorption microcalorimetry set-up.

the reference sample are connected to the two double-sided flanges. A bellows-sealed linear motion feedthrough (E-LMD-133-2, Caburn MDC) and a dummy resembling the form of the half-expanded feedthrough are connected to the other side of the flanges. The linear motion feedthrough can be used to crush the pyrex capsules in the sample receptacle via a steel rod. The standard flange is used to connect the cells to the volumetric dosing section. All parts of the cells are made of stainless steel and are UHV (ultrahigh vacuum) tight.

The volumetric dosing section is made of four completely metal-tightened bellows valves and a Baratron capacity manometer (range: 0–100 Pa). The complete dosing section is placed in a heated box. The four valves are connected to the microcalorimetric cells, a CO gas line, a helium gas line and a turbomolecular drag pump (TMU 071 P, Pfeiffer). The turbomolecular pump is equipped with a membrane pump as backing pump and a compact full range gauge (PKR 251, Pfeiffer) to monitor the pressure. The helium gas line can be switched to a membrane pump, which is used as a rough pump for the turbomolecular pump.

The set-up completely consists of UHV tight components. Adsorption processes can be investigated at constant temperatures between room temperature and 423 K. The leakage rate of the set-up including the microcalorimetric cells is less than 10^{-10} Pa m^3/min after degassing for more than 72 h at 423 K. The leakage rate is derived from the measured increasing rate

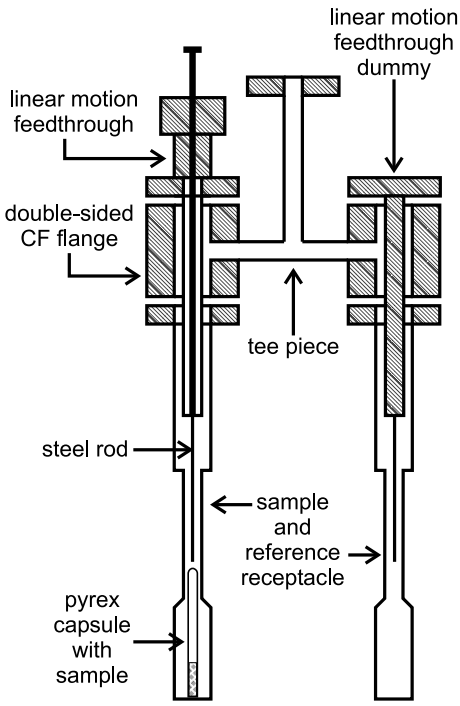

Figure 2.2: Schematic drawing of the microcalorimetric cells.

of the pressure under static vacuum conditions and the volume of the dosing section and the microcalorimetric cells (app. 100 cm^3).

Typically, 100 mg of the sieve fraction of 250–355 μm is used for the investigations. Samples are pretreated ex situ in a specially designed pretreatment reactor, and then sealed in a pyrex capsule of 5 mm diameter and 80–90 mm length under a reduced pressure of helium (200–500 hPa). The pyrex capsule is then placed into the sample receptacle of the microcalorimetric cells. The cells are placed into the calorimeter and are connected to the volumetric dosing section. The complete set-up is evacuated at a temperature of 418 K for at least 72 h. This leads to a dynamic vacuum of less than 10^{-5} Pa. After cooling the calorimeter to 303 K and the volumetric dosing section to 313 K overnight, the capsule is broken via a linear motion feedthrough. The pressure of the released helium is reduced to about 80 Pa. After reaching thermal equilibrium and a steady baseline of the heat flow signal, the adsorption measurement is started. The period of time between the breaking of the capsule and the start of the measurement typically amounts to less than 60 min.

Fig. 2.3 shows a schematic diagram of the specially designed pretreatment reactor used for the sample pretreatment. It consists of a glass-lined stainless steel U-tube, a pyrex-metal

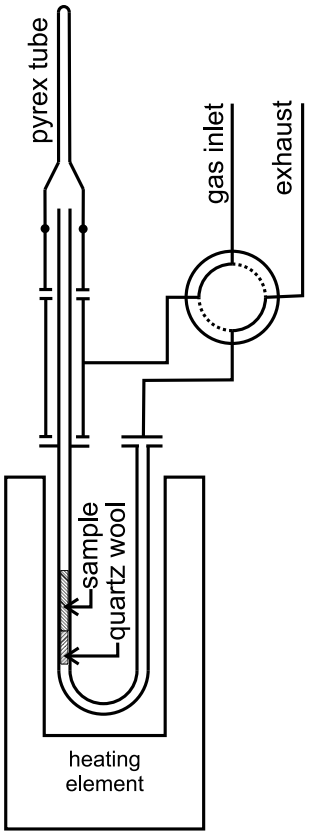

Figure 2.3: U-tube reactor used for the pretreatment of microcalorimetric samples.

joint (GA-050P-S, Caburn MDC) with a pyrex NMR tube welded to it, a manometer (-1000 to +2000 hPa, Millipore), and a four-way valve (4UWE, Valco, VICI). The complete reactor is metal-tightened. Samples are placed into the U-tube and kept in place by a quartz wool plug. The reactor can be heated by a vertically movable heating element. The thermocouple which controls the heating element is fixed onto the outside of the reactor at the position of the sample. The reactor can be connected by Cajon VCR connectors with the flow set-up used for CO TPD experiments (see section 2.2.2). The pressure in the reactor may not exceed atmospheric pressure, and the temperature can be raised up to 873 K. After pretreating the sample and purging in helium, the four-way valve of the reactor is closed and the reactor is disconnected from the flow set-up. The heating element is lowered and the reactor is cooled down. In the following step, the pressure of helium in the reactor is decreased to 200–500 hPa using a rotary vane pump (DUO 2.5, Pfeiffer). The reactor itself is then turned vertically by 180°. Thus, the sample falls out of the U-tube into the pyrex tube, while the quartz wool plug stays in the U-tube. Using a small torch fuelled by liquid gas, the pyrex tube is welded to yield a sealed

capsule of 80–90 mm length containing the pretreated sample in helium. The sealed capsule is finally placed into the calorimeter. All pretreatment procedures that can be applied to samples in the standard U-tube reactor can be carried out in the pretreatment reactor (except for high pressure treatments) and are monitored by mass spectrometry.

2.2.2 CO TPD experiments

A schematic diagram of the set-up is given in Fig. 2.4. It includes a gas supply unit with seven gas lines, a heated reactor, and a quadrupole mass spectrometer for on-line gas analysis. The

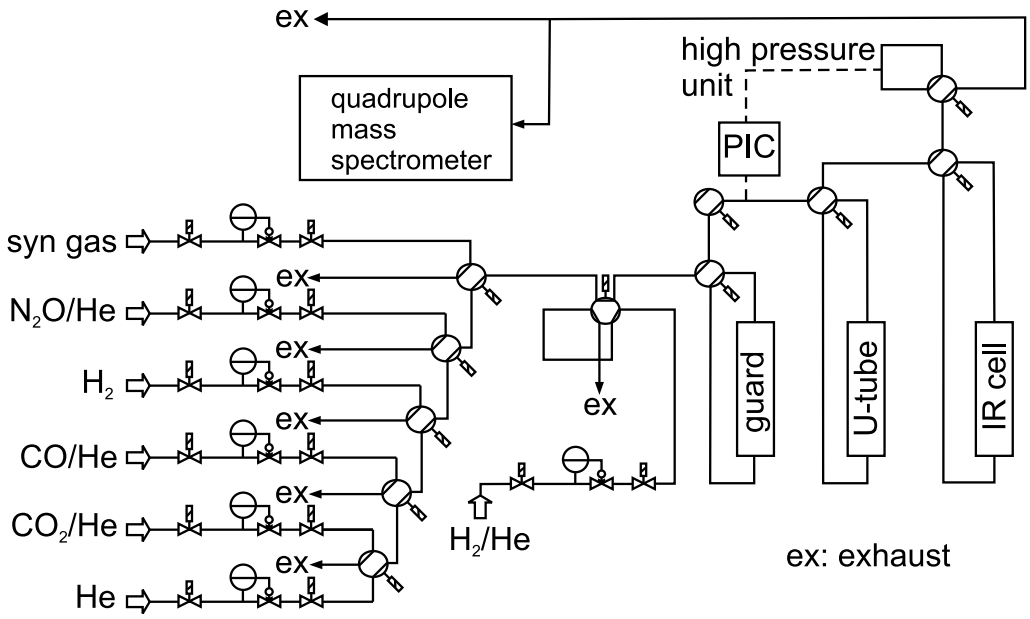

Figure 2.4: Flow scheme of the set-up used for CO TPD experiments and sample pretreatment.

reactor is a glass-lined stainless steel U-tube reactor of 3.8 mm inner diameter with two Cajon VCR connectors. The set-up can be operated at pressures of up to 6 MPa and reactor temperatures of up to 873 K. A personal computer equipped with the software package LabView is used to control the set-up. All tubings are made of glass-lined stainless steel to avoid adsorption or reaction of any gas components on the inner tube walls. Tubings between the reactor and the mass spectrometer are heated to a temperature of 366 K to prevent the condensation of products such as water or methanol. The gas lines of the gas supply unit are all of similar design. They consist of a gas cylinder, a pressure reducing valve, and a mass flow controller (0–100 Ncm^3/min). A pneumatically actuated shut-off valve is installed before and after each

mass flow controller. The gas lines are connected with four-way valves (4UWE, Valco, VICI). Only the gas of one line can flow through the reactor at the same time. The employed gases are helium, a 4 % CO_2/He mixture, a 10 % CO/He mixture, hydrogen, a 1 % N_2O/He mixture, a methanol synthesis gas mixture, and a 2 % H_2/He mixture. The methanol synthesis gas consists of 72 % H_2, 10 % CO, 4 % CO_2 and 14 % He. The gases are all of ultra-high purity ($>$ 99.9995 %). Three four-way valves (4UWE, Valco, VICI) are used to connect a guard reactor filled with ZnO, the standard U-tube reactor, and the transmission IR cell described below to the flow set-up. All reactors can be switched on-line or by-pass to the flowing gas. The U-tube reactor fits into an aluminium block with heating elements and a gas line for cooling air, which can be controlled by the LabView software. The gas analysis is performed by an on-line quadrupole mass spectrometer (GAM 400, Balzers) connected via a heated capillary and a tee piece to the exhaust side of the reactor. Data evaluation is performed with the software package Quadstar.

2.2.3 Transmission FTIR spectroscopy

The FTIR experiments are performed using a Nicolet Nexus FTIR spectrometer equipped with a MCT-A detector. Experiments can be performed in transmission using a further developed IR cell originally designed by Karge et al. [8]. Its design is shown in Fig. 2.5. The original IR cell designed by Karge et al. [8] is connected with a sample pretreatment section and a CO dosing system. The cell itself consists of a bronze body soldered to a stainless steel tube of 25 mm diameter. The bronze body is heatable to 403 K and has 9×18 mm sized openings for the IR beam. The openings are closed by CaF_2 windows of 43 mm diameter sealed with viton O-rings. The sample is positioned into the IR beam in a sample holder made of tantalum which fits exactly into the bronze body. The sample holder can be moved to the pretreatment section by a magnetic manipulator. The pretreatment section is a stainless steel tube of 120 mm length and an inner diameter of 25 mm. Three Swagelok tube stubs with 1/8” fittings are welded to the tube. It is connected to the cell and the dosing section by DN40 CF vacuum flanges. One Swagelok fitting is used to introduce a thermocouple into the pretreatment section. The other two fittings are connected to the flow set-up described above via a four-way valve (4UWE, Valco, VICI). The sample holder is placed directly between the gas inlet and the outlet during pretreatment. The pretreatment section can be heated by a heating tape to 673 K. All

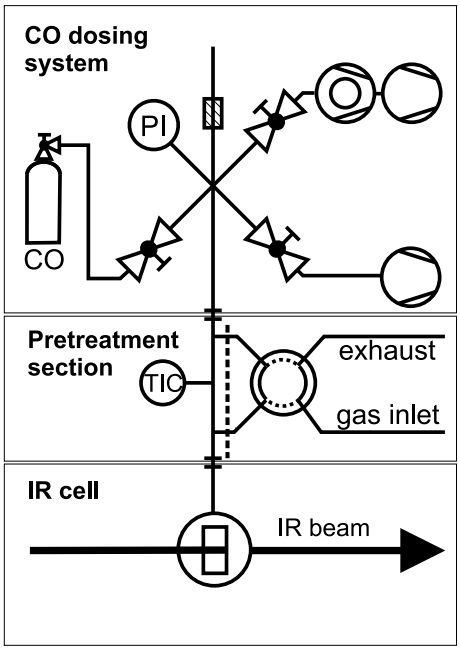

Figure 2.5: Flow scheme of the transmission IR cell.

pretreatment procedures can be monitored by on-line mass spectrometry, but due to the large dead zones of the IR cell only qualitative results can be obtained. CO is admitted to the sample via a mini leak valve (E-MLV-22, Caburn MDC).

All investigations in transmission are carried out using wafers of an area of about 2 cm^2 and a mass of less than 50 mg. The wafers are prepared by grinding powdered samples in an agate mortar, sieving the powder through a piece of cotton fabric directly into the pressing tool, and then pressing the powder for 60 s at a pressure of less than 1 MPa. The resulting wafer is cut to fit into the sample holder, and is transferred into the IR cell. For the pretreatment, the wafer is lifted into the pretreatment section by the magnetic manipulator. It is then pretreated under conditions resembling those of the microcalorimetric and CO TPD experiments. After the pretreatment, the wafer is lowered into the IR beam, and the IR cell is evacuated.

2.2.4 Investigated samples

The investigated samples are binary and ternary catalysts containing copper, zinc oxide and alumina with the following molar compositions: Cu/ZnO (50:50), Cu/ZnO/Al_2O_3 (50:35:15) and Cu/ZnO/Al_2O_3 (10:60:30).

The samples were prepared by coprecipitation using solutions of nitrates and sodium carbon-

ate, and calcined afterwards. In order to obtain reproducible results, the preparation follows a standardized procedure under controlled conditions (e. g. pH, temperature, reaction and ageing time). The samples were characterized by physisorption measurements (BET surface area), temperature programmed reduction (copper content), N_2O reactive frontal chromatography (reduced copper surface area), tests of activity for the methanol synthesis reaction, and X-ray diffraction measurements (before and after calcination). The preparation and the characterization of the samples are described in detail elsewhere [9, 10, 11].

The hydrogen reduction is carried out in two steps. The samples are first treated for 12 h in a mixture of H_2/He at 448 K and then for 30 min in pure hydrogen at 513 K. The synthesis pretreatment starts with the hydrogen reduction. The catalyst is then treated additionally for 12 h in a methanol synthesis gas mixture (see section 2.2.2). The CO pretreatment also starts with the hydrogen reduction, and the catalyst is treated additionally for 60 h in a mixture of CO/He at 498 K. All samples are flushed for at least 30 min at elevated temperatures in a flow of pure helium after the pretreatment. The flow rates are always fixed to 10 Ncm^3/min, all heating rates are set to 1 K/min.

2.3 Results and discussion

2.3.1 Calorimetry

In order to measure the differential heat of adsorption of carbon monoxide on the sample, small doses of CO (ca. 1 μmol) are sequentially admitted to the sample until the saturation of the sample surface at an equilibrium pressure of ca. 80 hPa is reached. The admission of each dose of CO follows the same cycle consisting of four steps. The first step is the evacuation of the volumetric dosing section to a pressure of less than 10^{-5} Pa, while the valve to the microcalorimetric cells is closed. In the second step, the dosing section is filled with ca. 80 Pa of CO. The admission of CO into the microcalorimetric cells is step three. The fourth step is to measure the heatflow and the pressure drop for 1 h. A complete experiment can consist of up to 50 cycles. The differential heat of adsorption and the adsorption isotherm can be derived from the experimental data. For each cycle, the evolved heat is determined by integrating the measured heat flow, and the amount of the adsorbed CO is determined from the measured pressure drop using the universal gas equation. The volume of the dosing section is constant

and was determined by the expansion of He into a calibration chamber. The volume of the microcalorimetric cells changes with the position of the linear motion feedthrough and the sample volume. This volume was measured after each experiment by the expansion of He into the evacuated microcalorimetric cells. To distinguish between reversible and irreversible adsorption, the complete set-up is evacuated overnight without raising the temperature. After filling the microcalorimetric cells with ca. 80 Pa of helium and reaching a steady baseline of the heatflow signal, the adsorption experiment is repeated. Any differences between the first and the second adsorption experiment are related to irreversible adsorption. In total, one experiment can last longer than one week. This explains why the leakage rate of the set-up has to be less than 10^{-10} Pa m^3/min.

Fig. 2.6 shows the results of the CO adsorption experiments on the binary Cu/ZnO catalyst (50:50). The sample was reduced by hydrogen as described above. Integration of the mass

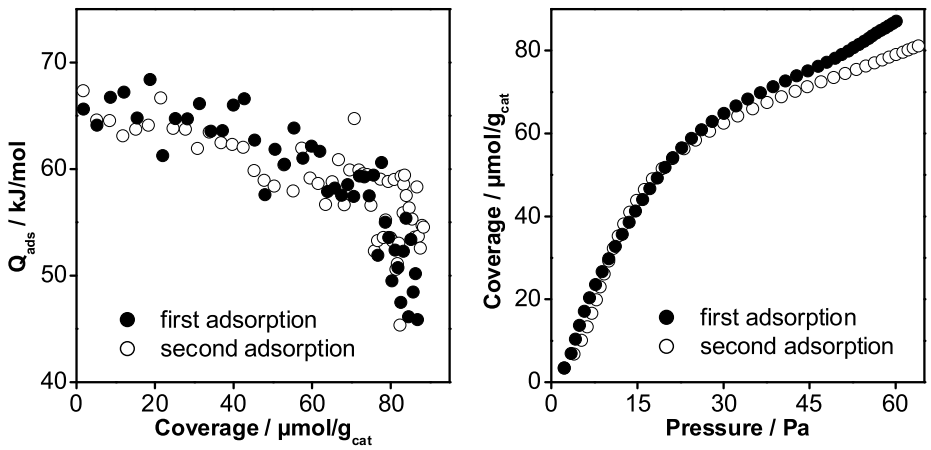

Figure 2.6: Differential heat of adsorption and adsorption isotherms of CO on Cu/ZnO (50:50) determined at 300 K.

spectrometry traces confirmed the complete reduction of the copper content. The differential heat of adsorption is found to decrease almost linearly from 68 kJ/mol at very low coverage to 57 kJ/mol at a coverage of about 80 μmol$_{CO}$/g$_{cat}$, followed by a steep decrease to nearly 45 kJ/mol. The saturation coverage of the sample with CO was about 90 μmol$_{CO}$/g$_{cat}$ at a pressure of 60 Pa.

The low initial value of the heat of adsorption confirms the absence of Cu(I) species and the

complete reduction of copper [14]. There are only negligible differences between the first adsorption and the second adsorption after evacuating at room temperature, indicating that the adsorption process is fully reversible even at room temperature. This can be seen in the plot of the differential heat as well as in the plot of the adsorption isotherms (Fig. 2.6). The repeated adsorption experiment shows also that the contamination of the sample with air by leakage is without measurable effect. The reversibility of the adsorption on the ternary catalysts can be safely assumed, considering the results presented above and in [15]. Microcalorimetric results of Cu/Al_2O_3 (85:15), Cu/ZnO (70:30) and $Cu/ZnO/Al_2O_3$ (50:35:15) samples pretreated by hydrogen reduction have been presented in [15]. The differential heat of adsorption of CO on $Cu/ZnO/Al_2O_3$ (50:35:15) ranges from 68–50 kJ/mol with a saturation coverage of ca. 85 $\mu mol_{CO}/g_{cat}$. Following the argumentation of Cardona-Martinez and Dumesic in [16] leads to the same conclusion. The adsorption isotherms can be described by simple models such as the Temkin or Freundlich isotherm. This will be shown elsewhere [17].

2.3.2 CO TPD results

For CO TPD experiments with the ternary catalyst (50:35:15), 100 mg of the sieve fraction of 250–355 μm are used. After the catalyst pretreatment, CO is adsorbed at 300 K in a flowing mixture of CO in He (10 % CO, 10 Ncm^3/min). The sample is then cooled to 78 K rapidly in flowing CO/He by pouring liquid nitrogen into the heating block. It is purged with pure He (10 Ncm^3/min) for 10 min and then heated to 450 K with a heating rate of 6 K/min in flowing helium. The effluent mole fraction of CO is monitored by the mass spectrometer. This procedure yields the CO TPD data from the fully covered catalyst surface. To vary the initial coverage of the CO TPD experiments, the catalyst samples are heated to 450 K in two steps, e. g. the sample is first heated to 275 K, again cooled to 78 K, and finally heated to 450 K. In the first step, all loosely bound CO species are desorbed. The final temperature of the first step defines the initial surface coverage of the second step. In order to investigate the influence of the coverage on the desorption, the complete experiment is repeated at different final temperatures of the first step ($T_{1st\ step}$). Typical temperatures are 275, 300, 325, and 350 K. This technique leads to surface coverages of CO which are comparable to the coverages obtained in the microcalorimetric experiments (2.1).

Fig. 2.7 shows the results of the experiments with varying initial surface coverage. The char-

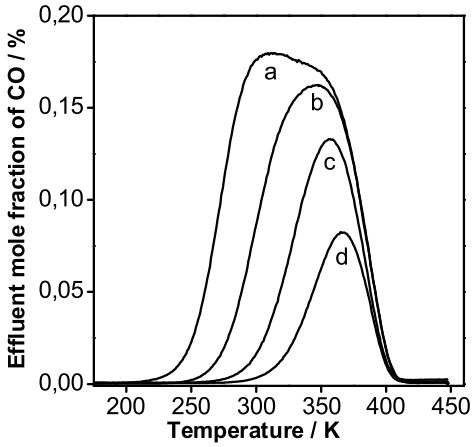

Figure 2.7: CO TPD spectra obtained with Cu/ZnO/Al_2O_3 (50:35:15) with varying initial coverage of CO, $T_{1st\ step}$: 275 K (a), 300 K (b), 325 K (c), and 350 K (d).

acteristics of the four peaks (a–d) are summarized in table 2.1. The final temperature of the

Table 2.1: CO TPD data obtained with Cu/ZnO/Al_2O_3 (50:35:15)

Peak	$T_{1st\ step}$ / K	T_{max} / K	FWHM / K	coverage / $\mu mol_{CO}/g_{cat}$	ΔH_{ads}^{TPD} / kJ/mol	ΔH_{ads}^{exp} / kJ/mol
a	275	315	112	145	50.8	-[a]
b	300	346	87	102	55.6	56.4[b]
c	325	357	61	62	57.3	58.4[c]
d	350	367	49	33	58.9	61.7[d]

[a]: not available; [b]: 0–84 $\mu mol_{CO}/g_{cat}$; [c]: 0–62 $\mu mol_{CO}/g_{cat}$; [d]: 0–33 $\mu mol_{CO}/g_{cat}$; ΔH_{ads}^{exp} is the integral molar heat of the adsorption of CO on Cu/ZnO/Al_2O_3 (50:35:15) derived from the microcalorimetric data in [15].

first heating step is $T_{1st\ step}$. The temperature of the absolute peak maximum is T_{max}. The peak maxima are shifted by more than 100 K to higher temperatures, compared with a thermal desorption spectroscopy (TDS) study by Vollmer et al. [7]. These experiments included low- and high-indexed copper single crystal surfaces and polycrystalline copper. The temperature shift between experiments using single crystals and fixed catalyst beds is due to re-adsorption occurring in the catalyst bed. The full width at half maximum is given in the column FWHM. The TPD peaks are asymmetric to lower temperatures, indicating a first order desorption process, and are broadened by re-adsorption. An additional broadening of the largest peak (a) is

due to contributions from a second desorption site occupied at lower temperatures. The initial coverages are calculated by integrating the mass spectrometry traces over the complete range of the desorption peak. ΔH_{ads}^{TPD} designates a rough estimate of the heat of adsorption based on the results of the TPD experiments. The estimation follows the method of Konvalinka and Scholten [18], as applied by Sandoval and Bell [19] in a study of the adsorption of CO on Cu/SiO_2. ΔH_{ads}^{TPD} is derived using standard values for the Arrhenius parameters of adsorption and desorption (10^1 Pa $^{-1}$ s^{-1} and 10^{13} s^{-1}, respectively) given by Dumesic et al. [20]. The values of ΔH_{ads}^{TPD} are slightly lower than ΔH_{ads}^{exp}, the integral molar heat calculated from the microcalorimetric data in [15], for corresponding coverages. The CO TPD data confirm the decrease of the heat of adsorption with increasing coverage measured by microcalorimetry in good quantitative agreement.

It can be assumed that the TPD experiments are carried out under thermodynamically controlled near-equilibrium conditions. This assumption is based on the following arguments: the desorption is very fast (see section 2.3.3), there is non-activated re-adsorption over the length of the catalyst bed, and the heating rate of the experiments is sufficiently moderate. A modelling of the peaks b–d using the integral molar heat of adsorption measured by microcalorimetry and considering re-adsorption is in progress [17]. The modelling intends to validate the data obtained by the different investigation methods.

2.3.3 Results by FTIR spectroscopy

The industrial ternary catalyst (50:35:15) has a very low transparency in the mid-IR region when completely reduced due to its high copper content. Therefore, a ternary catalyst system (10:60:30) with a lower copper content was investigated in the transmission FTIR experiments. A wafer of ca. 45 mg was prepared as described above. The sample was pretreated by the hydrogen reduction pretreatment. The reduction of the copper to its zero valent state could only be qualitatively confirmed by mass spectrometry. After the IR cell had been cooled down to room temperature, a single beam spectrum was recorded under dynamic vacuum conditions. This spectrum served as background spectrum for the adsorption experiment. The background spectrum was recorded with 2000 scans at a resolution of 2 cm^{-1}. The surface coverage of the sample with CO was then increased in steps by increasing the partial pressure of CO stepwise. At each pressure step, a spectrum with 500 scans at a resolution of 2 cm^{-1} was recorded. Typ-

ically, the pressure steps were 0, 0.5, 1, 2.5, 5, 10, 20, 40, 80, and 100 Pa. A period of 10 min between each CO dosing and the recording of the spectrum ensured near-equilibrium adsorption/desorption conditions. After recording the spectrum at 100 Pa pressure of CO, the cell was evacuated and two spectra were recorded after 1 min (250 scans) and 10 min (2000 scans).

Fig. 2.8 shows the CO stretching vibration in the region 1900–2300 cm^{-1} during the adsorption of CO in the pressure range 0–100 Pa. Only one broad and asymmetric band with a peak maxi-

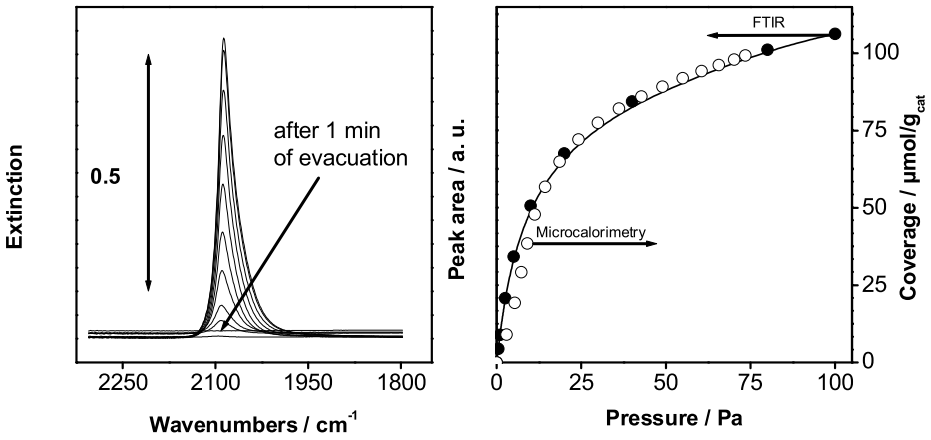

Figure 2.8: FTIR spectra obtained with $Cu/ZnO/Al_2O_3$ (10:60:30) (left) and adsorption isotherms of CO obtained with $Cu/ZnO/Al_2O_3$ (10:60:30) and $Cu/ZnO/Al_2O_3$ (50:35:15) (right) determined in the pressure range of 0–100 Pa and at room temperature.

mum shifting from 2090 to 2086 cm^{-1} with increasing coverage can be seen. This band can be ascribed to the vibration of CO adsorbed on metallic copper [21]. The band gets broader and more asymmetric with increasing coverage. It decreases instantly when the cell is evacuated. There is no band in the spectrum recorded 1 min after evacuation.

A qualitative adsorption isotherm can be derived from the IR data by integrating the peak areas (Fig. 2.8, right). The adsorption isotherm of the industrial ternary catalyst measured by microcalorimetry is included for comparison. The shape of the qualitative adsorption isotherm of the ternary catalyst (10:60:30) fits well to the adsorption isotherm of the industrial catalyst measured by microcalorimetry. While the absolute coverages ($\mu mol_{CO}/g_{cat}$) will surely be different for the two catalysts, the relative coverages ($\mu mol_{CO}/\mu mol_{Cu,surface}$) appear to follow the same adsorption isotherm. This confirms that the copper surfaces of the two ternary catalysts are in

the same state after the hydrogen reduction pretreatment.

2.4 Conclusions

The microcalorimetric results prove the efficiency of the applied technique for the sample transfer into the calorimeter without contamination by air. The results also show that the leakage rate of the microcalorimetry set-up is sufficiently low to investigate the air-sensitive copper surfaces of the reduced samples.

The CO TPD data confirms the microcalorimetry results. Similar surface coverages were obtained by both investigation methods. The decrease of the heat of adsorption with increasing coverage measured by microcalorimetry is also observed in the TPD experiments.

The results obtained by FTIR spectroscopy support the conclusions of the microcalorimetric experiments: copper is completely reduced to its zero valent state after hydrogen pretreatment (even under the non-ideal flow conditions of the IR cell), and the adsorption of CO is fully reversible at room temperature. The adsorption isotherms measured by the two different investigation methods fit to each other. The results prove that the FTIR set-up is suitable to investigate air-sensitive copper samples without contamination by air before or during the CO adsorption.

All results are in good agreement. The three different investigation methods were successfully combined by applying identical pretreatment conditions, which is further demonstrated by the modelling of the isotherm and the CO TPD data in [17]. Publications covering other model catalysts and the additional pretreatments described above are in preparation.

Acknowledgments

Financial support by the Deutsche Forschungsgemeinschaft within the Collaborative Research Center (SFB 558) ‘Metal-Substrate Interactions in Heterogenous Catalysis’ are gratefully acknowledged.

Bibliography

[1] J.B. Hansen, in: ”Handbook of Heterogenous Catalysis”, VCH Verlagsgesellschaft, Weinheim, 4 (1997) 1856.

[2] H. Wilmer, T. Genger, and H. Hinrichsen, J. Catal., 215 (2003) 188.

[3] J.-D. Grunwaldt, A.M. Molenbroek, N.-Y. Topsøe, H. Topsøe, and B.S. Clausen, J. Catal., 194 (2000) 452.

[4] A. Auroux, Topics in Catalysis, 19 (2002) 205.

[5] M.G. Cutrufello, I. Ferino, R. Monaci, E. Rombi, and V. Solinas, Topics in Catalysis, 19 (2002) 225.

[6] B.E. Spiewak and J.A. Dumesic, Thermochim. Acta, 290 (1996) 43.

[7] S. Vollmer, G. Witte, and C. Wöll, Catal. Lett., 77 (2001) 97.

[8] H.G. Karge and W. Nießen, Catal. Today, 8 (1991) 451

[9] B. Bems, M. Schur, A. Dassenoy, H. Junkes, D. Herein, and R. Schlögl, Chem. Eur. J., 9 (2003) 2039.

[10] O. Hinrichsen, T. Genger, and M. Muhler, Chem. Eng. Technol., 11 (2000) 956.

[11] H. Bielawa, M. Kurtz, T. Genger, and O. Hinrichsen, Ind. Eng. Chem. Res., 40 (2001) 2793.

[12] T. Genger, O. Hinrichsen, and M. Muhler, Catal. Lett., 59 (1999) 137.

[13] H. Wilmer and O. Hinrichsen, Catal. Lett., 82 (2002) 117.

[14] E. Giamello, B. Fubini, and V. Bolis, Appl. Catal. 36 (1988) 287.

[15] R. Naumann d’ Alnoncourt, M. Kurtz, H. Wilmer, E. Löffler, V. Hagen, J. Shen, and M. Muhler, J. Catal., 220 (2003) 249.

[16] N. Cardona-Martinez and J.A. Dumesic, Adv. Catal., 38 (1992) 149.

[17] J. Strunk, R. Naumann d’Alnoncourt, M. Bergmann, O. Hinrichsen, and M. Muhler, in preparation.

[18] J.A. Konvalinka, J.J.F. Scholten, and J.C. Rasser, J. Catal., 48 (1977) 365.

[19] M.J. Sandoval and A.T. Bell, J. Catal., 144 (1993) 227.

[20] J.A. Dumesic, D.F. Rudd, L.M. Aparicio, J.E. Rekoske, and A.A. Treviño, ACS Professional Reference Book, Washington, DC, (1993).

[21] K.I. Hadjiivanov and G.N. Vayssilov, Adv. Catal., 47 (2002) 307.

3 Part I: The reduced catalyst

Abstract

Our goal is a detailed understanding of the strong metal-support interactions between copper and zinc oxide in copper catalysts. These interactions are significantly influenced by the pretreatment. The adsorption of carbon monoxide is used as investigation tool in microcalorimetric, temperature-programmed desorption and infrared spectroscopy experiments. Many efforts were taken to assure that the pretreatment conditions are identical for all investigation methods. The results in the present contribution refer to the state of the catalysts after reduction by hydrogen at 513 K. All investigation methods confirm that the presence of zinc oxide lowers the initial heat of adsorption, while catalysts containing alumina have higher fractional coverages. The adsorbed carbon monoxide species are at low coverages less mobile on samples free of zinc oxide.

3.1 Introduction

Copper catalysts are industrially used for the synthesis of methanol. These catalysts are ternary systems containing copper (Cu), zinc oxide (ZnO) and alumina (Al_2O_3) [1]. Several recent studies [2, 3] indicate there are strong metal-support interactions (SMSI) between copper and zinc oxide in these catalysts. Grunwaldt et al. [4] presented a model for these effects: Under the reducing conditions of the methanol synthesis, the metallic copper surfaces are covered by zinc and oxygen species. Under more severe conditions, surface and bulk alloying leads to the formation of brass.

In literature, many studies are found investigating copper, binary (e. g. Cu/ZnO, Cu/Al_2O_3) or ternary copper catalysts (e. g. Cu/ZnO/Al_2O_3) by microcalorimetry, temperature-programmed desorption (TPD) or Fourier transform infrared (FTIR) spectroscopy [5, 6, 7, 8, 9, 10]. Carbon monoxide (CO), carbon dioxide (CO_2) and hydrogen (H_2) are often used probe molecules. In most cases a comparison of these studies is difficult, as the samples are prepared and pretreated following different procedures. For example, Giamello et al. [8] detected in a microcalorimetric study the presence of Cu(I) species in a Cu/ZnO sample after hydrogen reduction and postulated

these species to be dissolved in the ZnO matrix. They assumed that these species might play a role in the synthesis of methanol. The authors also pointed out that Boccuzzi et al. [9] using FTIR spectroscopy did not find any evidence for Cu(I) species investigating the same catalyst sample after a similar pretreatment.

In our studies, we compare different catalyst samples after identical pretreatment using a combination of calorimetry, TPD experiments and FTIR spectroscopy. By doing so, we hope to get a deeper understanding of the nature of the SMSI between copper and ZnO and its importance for the synthesis of methanol.

The interaction of Cu catalysts with hydrogen has been studied extensively by Hinrichsen and co-workers [11, 12, 2]. The catalysts have been investigated in different states: directly after hydrogen reduction, after a period of 12 h of methanol synthesis, and after a pretreatment of 64 h in CO/He.

The present study is the first of three parts investigating the same catalyst systems after analogous pretreatments and using the adsorption of CO as investigation tool. All results in this contribution refer to the state of the catalyst after hydrogen reduction.

3.2 Experimental

The investigated samples are binary and ternary catalysts containing copper, zinc oxide and alumina. Industrial and model catalysts are included in this study. The samples were prepared by coprecipitation using solutions of nitrates and sodium carbonate, followed by ageing, washing, drying, and calcining. The catalysts were characterized by physisorption measurements (BET surface area), temperature programmed reduction (copper content), N_2O reactive frontal chromatography (reduced copper surface area), tests of activity for the methanol synthesis reaction, and X-ray diffraction measurements (before and after calcination). The preparation and the characterization of the samples are described in detail elsewhere [13, 14, 15]. Table 3.1 summarizes the main characteristics of the used samples. The adsorption of carbon monoxide on these samples was studied by adsorption microcalorimetry, TPD experiments and FTIR spectroscopy in transmission mode. In the case of all three applied investigation methods, the set-up used for the TPD experiments was also used for the sample pretreatment. The fact that the pretreatment was always carried out using the same gas supply and on-line gas analysis

Table 3.1: Characterization and catalytic data

Catalyst	CZA1	CZA2	CZ1	CA1	CA2
BET surface area (m^2/g_{cat})	73	-	64	51	124
Cu content (wt% CuO)	47	7	68	76	20
Specific amount of Cu surface atoms[a] (μmol/g_{cat})	513	134	513	176	139
Specific Cu surface area[b] (m^2/g_{cat})	21	6	21	7	6
Specific methanol production rate[c] (μmol/s g_{cat})	0.112	0.065	0.077	0.015	0.012
Turnover frequency (10^{-5} s^{-1})	21.8	48.5	15.0	8.3	9.0

[a]: Derived by N_2O RFC. [b]: Assuming that 1 m^2 of Cu surface area equals 24.41 μmol Cu atoms. [c]: Obtained at ambient pressure using 100 mg catalyst in synthesis gas (72 % H_2, 10 % CO, 4 % CO_2 and 14 % He) and a volumetric flow rate of 50 cm^3 min^{-1} (STP).

gives access to the copper surface of the samples in identical states with all three investigation methods.

All results in this contribution refer to the state of the catalyst samples after hydrogen reduction. The reduction was carried out in two steps. The samples were first treated for 12 h in a mixture of H_2/He at 448 K and then for 30 min in pure hydrogen at 513 K. All samples were flushed for at least 30 min at elevated temperatures in a flow of pure helium after the pretreatment. The flow rates were always fixed to 10 Ncm^3/min, all heating rates were set to 1 K/min. The complete reduction of the copper content to its zero-valent state was confirmed for each experiment by on-line mass spectrometry.

For the microcalorimetric experiments, 100 mg of the sieve fraction of 250–355 μm were pretreated in a specially designed pretreatment reactor, and then sealed in a pyrex capsule. Next, the pyrex capsule was placed into the sample receptacle of the microcalorimeter (C80 II, Setaram). The calorimetric set-up was degassed and the capsule was broken. After reaching thermal equilibrium (at 303 K) the adsorption measurement was started. Small doses of the adsorptive gas were subsequently admitted to the adsorbent, and while the heat of adsorption was measured calorimetrically, the amount of adsorbed species was measured volumetrically. The employed measurement technique was adopted from the pioneering work by Spiewak and Dumesic [16]. The technique allows to investigate air-sensitive samples unimpaired by poisoning. A detailed description of the experimental procedure and the set-up is given elsewhere [17].

The TPD experiments were carried out in a stainless steel U-tube reactor connected to a flow

set-up. Typically, 100 mg of the sieve fraction of 250–355 μm were investigated *in situ*, directly after the pretreatment. The samples were cooled from room temperature to 78 K in a flow of a 10 % CO/He mixture and afterwards heated to 450 K in a flow of ultra-pure He. The desorption of CO into the stream of helium was monitored by on-line mass spectrometry. The coverage dependence of the CO desorption was investigated by varying the initial coverage. This was achieved by heating the samples to 450 K in two steps, i. e. after dosing CO the sample was first heated to $T_{1st\ step}$ (275, 300, 325, 350, and 375 K) again cooled to 78 K, and finally heated to 450 K. The experimental conditions and the set-up are fully described elsewhere [17].

The infrared spectroscopy experiments were performed using a modified transmission IR cell designed by Karge et al. [18] in a Nicolet Nexus FTIR spectrometer. The cell was connected to a sample pretreatment section and a CO dosing system. The investigations were carried out using wafers of an area of about 2 cm^2 and a mass of less than 50 mg. After the pretreatment the wafer was brought into the IR beam and spectra (250 scans, resolution: 2 cm^{-1} in the region 800 – 6000 cm^{-1} were recorded. The pressure of CO was varied stepwise between 0–100 Pa (0, 0.5, 1, 2.5, 5, 10, 20, 40, 80, 100 Pa and evacuation), in order to investigate the adsorption of CO as a function of coverage. Details about the experimental conditions and the set-up are given elsewhere [17].

3.3 Results

The heat of adsorption was measured calorimetrically using only the samples with a high copper content. Fig. 3.1 shows the results (left: differential heat of adsorption; right: adsorption isotherm) obtained with the samples CZA1, CZ1 and CA1. The adsorption of CO is strongly influenced by the presence of ZnO. The initial heat of adsorption of CO on zinc-containing catalysts (CZA1, CZ1) is about 10 kJ/mol lower than on the ZnO-free sample BA1. The heat of adsorption monotonously decreases in all cases with increasing coverage. In the observed pressure range, the final heat of adsorption is significantly lower in the case of the ZnO-free sample. The absolute coverage of the samples for a given equilibrium pressure, e.g. 60 Pa, is higher for ZnO-containing catalysts. CZA1, the sample most active for the production of methanol(see table 3.1) shows the highest coverage (fig. 3.1, right). A summary of the calorimetric data is given in table 3.2. Differences between the data published here and in ref. [19]

are due to a reprocessing of the raw data. The results in ref. [19] are calculated using the mass of the reduced sample as weighed directly after the experiment. The characterization data in table 3.1 is correlated to the mass of the calcined sample prior to reduction. The calorimetric data was reprocessed using the sample mass prior to reduction in order to obtain a better correlation with the characterization data.

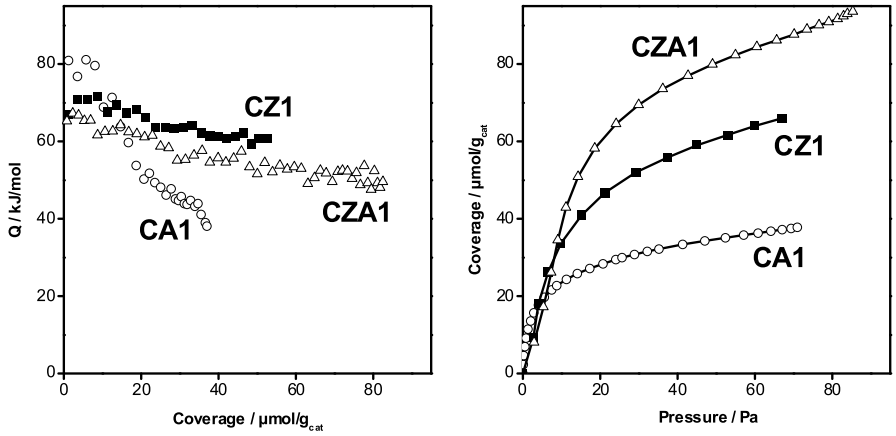

Figure 3.1: Differential heat of adsorption and adsorption isotherms of CO on CZA1, CZ1 and CA1 determined at 303 K.

Table 3.2: Calorimetric results

Catalyst	CZA1	CZ1	CA1
Initial heat of adsorption (kJ/mol)	68	71	81
Final heat of adsorption (kJ/mol)	50	60	38
Equilibrium coverage[a] (μmol$_{CO}$/g$_{cat}$	84	64	36
Fractional coverage[a,b]	0.16	0.12	0.20

[a]: at a CO partial pressure of 60 Pa; [b]: calculated by dividing the amount of adsorbed CO by the number of copper surface atoms.

The reversibility of the adsorption of CO under the conditions of the adsorption microcalorimetry was experimentally confirmed [17]. Following the argumentation of Cardona-Martinez and Dumesic [20] a near-equilibrium state between the adsorbed CO and the gas phase can be safely assumed. Therefore, it is possible to calculate the entropy of adsorption, ΔS_{ads} from the heat

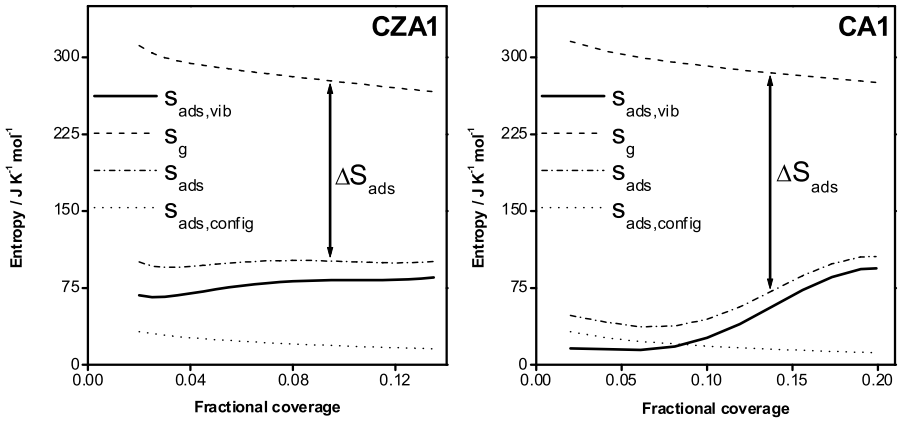

Figure 3.2: The entropy of adsorption of CO on CZA1 and CA1 at 303 K and its contributions.

of adsorption ΔH_{ads} using eq. (3.1).

$$\Delta S_{ads} = \frac{\Delta H_{ads}}{T} \tag{3.1}$$

The entropy of the adsorbed CO, s_{ads}, can be calculated with the eq. (3.2), (3.3) and (3.4). s_g is the entropy of the gas phase, the superscript ^{0} refers to the standard state.

$$\Delta S_{ads} = s_{ads} - s_g \tag{3.2}$$

$$s_g = s_g^0 - R \ln \frac{p}{p^0} \tag{3.3}$$

$$\Delta S_{ads}^0 = \frac{\Delta H_{ads}}{T} - R \ln \frac{p}{p^0} \tag{3.4}$$

s_{ads} can be interpreted as a sum of $s_{ads,config}$ and $s_{ads,vib}$ (eq. (3.5)). $s_{ads,config}$ is the configurational contribution of the entropy and is only a function of the fractional coverage θ (eq. (3.6)). $s_{ads,vib}$ is the vibrational contribution and can be correlated with the mobility of the adsorbed species.

$$s_{ads} = s_{ads,config} + s_{ads,vib} \tag{3.5}$$

$$s_{ads,config} = R \ln \frac{1-\theta}{\theta} \tag{3.6}$$

Fig. 3.2 shows s_g, s_{ads}, $s_{ads,config}$, and $s_{ads,vib}$ as a function of the fractional coverage for the samples CZA1 and CA1. s_g can be correlated to the coverage by the adsorption isotherm.

Only small changes of $s_{ads,vib}$ can be observed in the case of CZA1. $s_{ads,vib}$ increases from about 65 J/K mol to 85 J/K mol with increasing coverage. The CO species on CA1 are less mobile at low coverage ($s_{ads,vib}$ = 15 J/K mol)and similar mobile at higher coverages ($s_{ads,vib}$ = 95 J/K mol), compared to the CO species on CZA1.

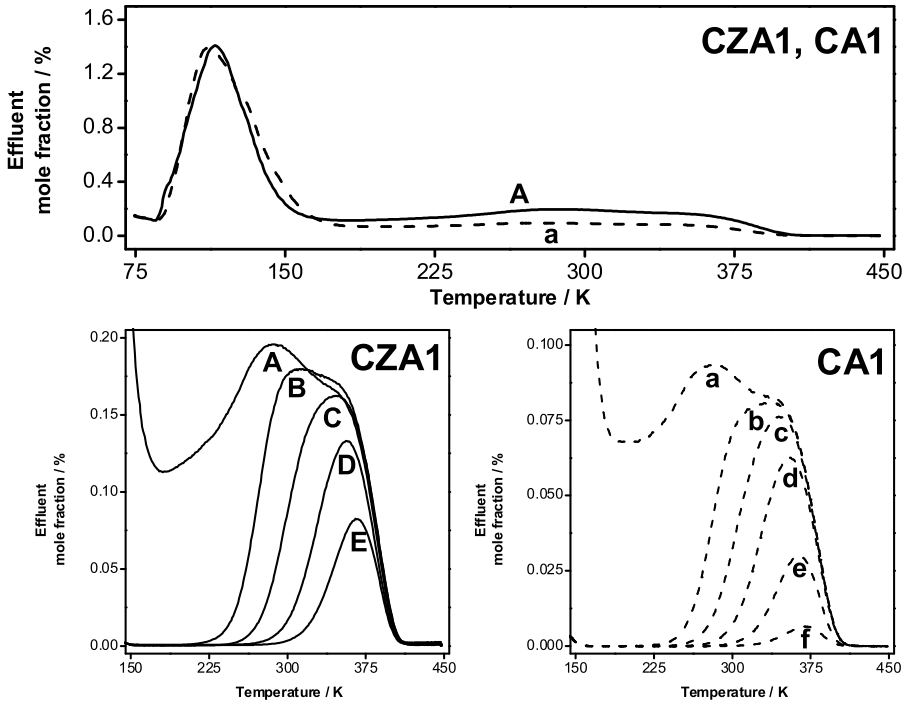

Figure 3.3: CO TPD spectra obtained with CZA1 and CA1 fully covered (A, a) and partially covered (B–E, b–f) with CO, $T_{1st\ step}$: 275 K (B, b), 300 K (C, c), 325 K (D, d), 350 K (E, e) and 375 K (f).

The CO TPD experiments include the two samples CZA1 and CA1. Fig. 3.3 shows the results of the TPD experiments. The desorption from the fully covered copper surface (experiments A and a) results in an intense peak at 115 K and a broad signal in the temperature range 200–400 K with a maximum at about 285 K and a shoulder at about 345 K, in the case of CZA1 and CA1. The desorption from the partially covered surface (experiments B–E and b–f) results in a broad peak that is asymmetric to lower temperatures. The peak maximum is shifted to higher temperatures with decreasing initial coverage. Tab. 3.3 summarizes the results of the TPD experiments. The final temperature of the first heating step is $T_{1st\ step}$. The temperature

of the absolute peak maximum is T_{max}. The full width at half maximum is given in the column FWHM. The initial coverages are calculated by integrating the mass spectrometry traces over the complete range of the desorption peak. The fractional coverage is calculated by dividing the total amount of desorbed CO by the number of copper surface atoms.

Table 3.3: CO TPD data obtained with CZA1 and CA1

Sample	Peak	$T_{1st\ step}$ / K	T_{max} / K	FWHM / K	coverage / $\mu mol_{CO}/g_{cat}$	fractional coverage[a]
CZA1	B	275	315	112	145	0.28
	C	300	346	87	102	0.20
	D	325	357	61	62	0.12
	E	350	367	49	33	0.06
CA1	b	275	336	98	58	0.32
	c	300	345	76	42	0.23
	d	325	355	59	27	0.15
	e	350	364	46	11	0.06
	f	375	369	40	2	0.01

[a]: calculated by dividing the total amount of desorbed CO by the number of copper surface atoms.

The FTIR results of the experiments using the reduced samples CZA2 (42 mg/2 cm^2) and CA2 (31 mg/2 cm^2) are shown in fig. 3.4 and 3.5. In the case of CZA2, mainly one broad and to lower wavenumbers asymmetric band with a peak maximum shifting from 2090 to 2086 cm^{-1} with increasing coverage is observed. The band becomes broader and more asymmetric with increasing coverage. Additionally, weak bands can be observed below 2000 cm^{-1} at 1689, 1246, 1228, and 1166 cm^{-1}. No bands appear above 2100 cm^{-1}. It is found that the main band at 2086 cm^{-1} decreases instantly when the cell is evacuated, while the weak bands change only little in intensity. The adsorption of CO induces a strong baseline shift to lower extinction in the range above 3000 cm^{-1}. Only minimal shifts are observed at lower wavenumbers. The spectra of CA2 show only one broad and asymmetric band with a peak maximum at 2090 cm^{-1}. The band becomes also broader and more asymmetric with increasing coverage. No further bands and no baseline shift is found. The band decreases instantly when the cell is evacuated.

Fig. 3.6 shows single beam spectra of CZA1, CZA2 and CA2. For CZA1 only a spectrum of the calcined sample can be achieved. The transparency of the sample is reduced to zero upon reduction. For CZA2 and CA2, samples with a low copper content, spectra of the calcined

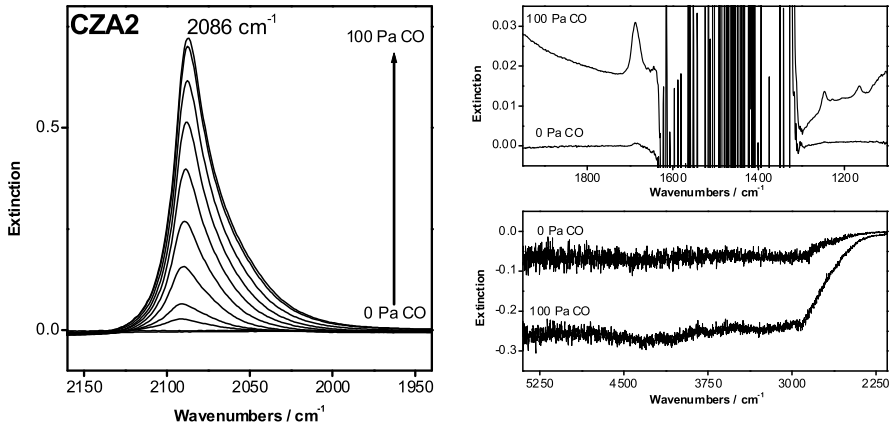

Figure 3.4: FTIR spectra obtained with CZA2 after reduction in the pressure range of 0–100 Pa of CO and at room temperature. The left side shows the range of the CO stretching vibration. The spectra are not corrected for a baseline or the gas phase CO vibrational contribution. The right side shows the range below (upper right) and above (lower right) the CO stretching vibration for a pressure of 0 and 100 Pa of CO. The upper right spectrum at 100 Pa CO is shifted by an extinction of 0.025 to allow a better comparison.

and the reduced state are presented. The transparency of the samples decreases strongly after reduction. This effect is stronger for CA2, which has a copper content three times higher than CZA2. The single beam spectra showing gas phase contributions of carbon dioxide and water were recorded while the spectrometer was purged by a commercial air dryer, the spectra without gas phase contributions were recorded while purging with a nitrogen gas cylinder.

Prior to the reduction of the samples, CO was adsorbed on the calcined samples. Fig. 3.7 shows the range of the CO stretching vibration for CZA1, CZA2 and CA2 at a pressure of 100 Pa of CO. The resulting broad and symmetric band has a peak maximum at 2112 cm^{-1} in the case of CZA1, and at about 2100 cm^{-1} for CZA2 and CA2.

3.4 Discussion

The differential heat of adsorption of CO on CA1 is in good agreement with data in literature. In 1972, Tracy [21] measured the isosteric heat of adsorption of CO on a Cu(100) single crystal plane in the temperature range from 77 to 300 K as a function of the coverage. An isosteric heat of adsorption of about 70 kJ/mol was reported for very low coverages, decreasing to about

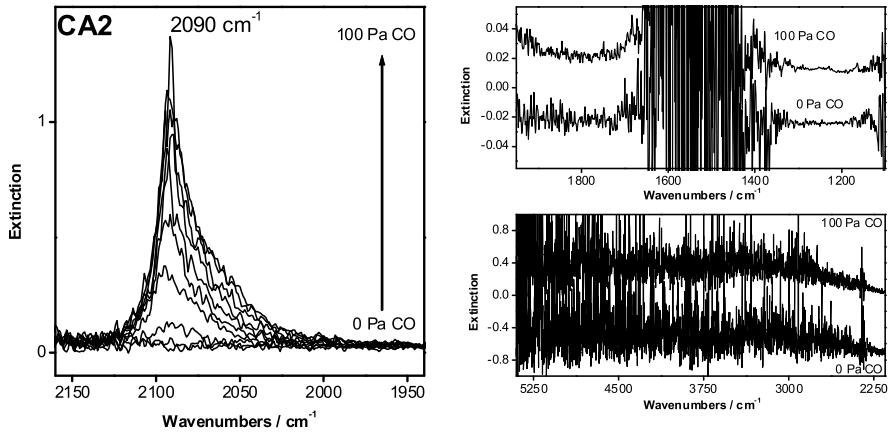

Figure 3.5: FTIR spectra obtained with CA2 after reduction in the pressure range of 0–100 Pa of CO and at room temperature.The left side shows the range of the CO stretching vibration. The spectra are not corrected for a baseline or the gas phase CO vibrational contribution. The right side shows the range below (upper right) and above (lower right) the CO stretching vibration for a pressure of 0 and 100 Pa of CO. The upper right and the lower right spectrum at 0 Pa CO are shifted by an extinction of -0.04 and -0.75, respectively, to allow a better comparison.

55 kJ/mol at a fractional coverage of 0.1. The isosteric heat was found to be constant in the coverage range 0.1–0.5. The initial value and the coverage dependence are in good agreement with the results obtained with CZA1. More recently Vollmer et al. [6] derived site-specific adsorption energies of CO on single crystal faces and poly-crystalline copper by thermal desorption spectroscopy (TDS). For the close packed surfaces Cu(111) and Cu(110), binding energies of 47 and 51 kJ/mol, respectively, were determined. Higher values of 58 kJ/mol were found for kinks, steps, and defect structures. Keeping in mind, that TDS gives only integral heats of adsorption, the two single crystal studies confirm the experimental data obtained with CA1. Borgard et al. [22] presented calorimetric data concerning the adsorption of CO on a supported catalyst in its reduced state. They reported values of 64-46 kJ/mol for the adsorption of CO on Cu/SiO_2. These values were measured for the adsorption of CO on CA1 in the coverage range of 14–35 μmol/g_{cat}. A more detailed comparison of these measurements is not possible due to the lack of any characterization data in Ref. [22]. However, the total amount of adsorbed CO on the Cu/SiO_2 catalyst is less than 14 μmol/g_{cat} suggesting a very small specific Cu surface area. Therefore, the initial heat of adsorption could not be measured reliably with the first dose

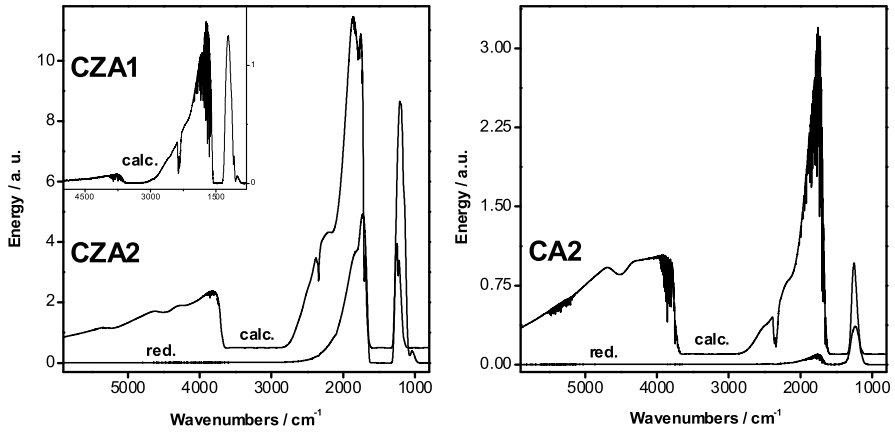

Figure 3.6: Single beam spectra obtained at room temperature with CZA1, CZA2 and CA2 in the calcined state (cal) and after reduction (red). The spectra of the calcined samples CZA2 and CA2 are shifted to higher energy to allow a better comparison. The single beam spectra served as background for the spectra in fig. 3.4, 3.5 and 3.7, respectively.

of CO. A study which can more directly be compared with our data was presented by Dulaurent et al. [7]. They derived isosteric heats of adsorption of CO on a reduced 4.7 % Cu/Al_2O_3 sample from FTIR spectroscopy experiments in the temperature range from 298 to 740 K. The reported isosteric heats of 82 kJ/mol (initial value) and 57 kJ/mol (equilibrium coverage at a pressure of 1 kPa of CO) are in excellent agreement with our differential heats of adsorption of CO on CA1. In summary, the obtained differential heat of adsorption of CO on CA1 is in good agreement with literature results obtained with various methods on Cu single crystals and supported Cu catalysts including SiO_2 and Al_2O_3 as non-interacting supports.

Giamello et al. [8] measured the differential heat of adsorption of CO on Cu/ZnO samples. The samples were prepared by coprecipitation from a solution of nitrates. They measured values of 70–40 kJ/mol for the adsorption of CO on zero-valent copper in a sample with a copper content of 30 wt-%. These values are in perfect agreement with the results obtained using CZ1. The fact that the authors measured slightly lower values at high coverages can be rationalized by the higher equilibrium pressure (5.33 kPa) and the resulting higher fractional coverage (0.23), which were not investigated in our study. The adsorption of CO on CZA1 yields results which are very similar to the results obtained with CZ1. The heat of adsorption is slightly lower over

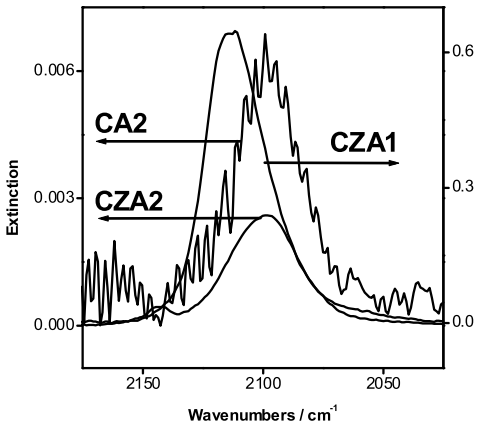

Figure 3.7: FTIR spectra obtained with CZA1, CZA2 and CA2 in the calcined state at a pressure of 100 Pa of CO and at room temperature. Only the spectrum of CZA2 is corrected for a baseline and the gas phase CO spectral contribution.

the complete coverage range and the fractional coverage at 60 Pa of CO is significantly higher in the case of CZA1.

In summary, the microcalorimetric experiments indicate that ZnO-containing catalysts show lowered initial values of the heat of adsorption, compared to unsupported copper (literature data) or Cu/Al_2O_3 catalysts (literature data and this study). Al_2O_3-containing samples show higher fractional coverages for a given equilibrium pressure of CO as shown in fig. 3.8. The lowered heat of adsorption in combination with the higher fractional coverage for a given equilibrium pressure result in a higher mobility of the adsorbed CO species as indicated by the entropy values for $s_{ads,vib}$ shown in fig. 3.2. Many authors found a linear correlation between the methanol synthesis activity and the free copper surface area of a catalyst. Hinrichsen and co-workers [23] confirmed this correlation, but postulated three classes of catalysts: Cu/Al_2O_3 (lowest activity/area), Cu/ZnO (slightly higher activity/area) and $Cu/ZnO/Al_2O_3$ (highest activity/area). The here presented results give a possible interpretation for the different activities of the different catalyst classes.

The TPD experiments cannot be directly compared to the TDS study of Vollmer et al. [6]. Readsorption phenomena cannot occur under the UHV conditions of a TDS experiments, but have a strong influence on the results of a TPD experiment. The peak maxima in a TPD experi-

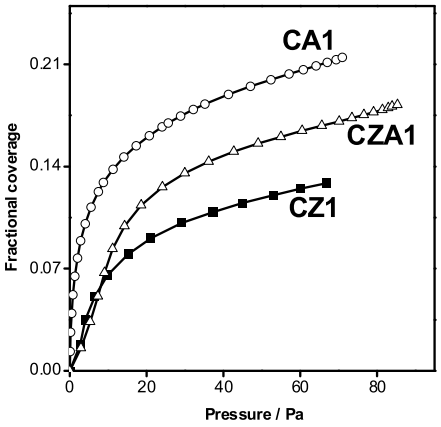

Figure 3.8: Comparison of adsorption isotherms derived from microcalorimetric results using the samples CZA1, CZ1 and CA1. The fractional coverage is calculated by dividing the amount of adsorbed CO by the specific amount of copper surface atoms, respectively.

ment are broadened and shifted to higher temperatures by readsorption processes, compared to the TDS experiment. A comparison with TPD studies in literature is also difficult as the TPD experiment is influenced by many parameters like the flow rate of the inert gas, the length of the catalyst bed or the heating rate.

The coverage dependence of the heat of adsorption of CO measured by microcalorimetry can also be found in the CO TPD experiments. The peak maximum shifts with decreasing initial coverage to higher temperatures, indicating an increase of the heat of adsorption with decreasing coverage. The higher fractional coverage for a given equilibrium pressure of CA1 in comparison to CZA1 can also be found in the TPD results. The fractional coverage measured for the experiments b–d is significantly higher than for the corresponding experiments B–D.

The integral heat of adsorption can be roughly estimated from the peak maximum following the method of Konvalinka and Scholten [24]. Values for the Arrhenius parameters of adsorption (A_{ads}) and desorption (A_{des}) are needed to apply this method. Tab. 3.4 shows the values obtained by this method and the integral heats of adsorption for the corresponding coverages calculated from the microcalorimetric data. A detailed description of the calculations is given elsewhere [25]. In the case of CZA1, standard values were used for A_{ads} ($10^3\,s^{-1}$) and A_{des} ($10^{15}\,s^{-1}$), as given by Dumesic et al. [26]. The estimation fits well with the experimental val-

ues. To estimate the integral heat of adsorption on CA1, A_{des} was kept at $10^{15}\,s^{-1}$, but A_{ads} was lowered to $10^{1}\,s^{-1}$, in order to take into account the lowered mobility of the adsorbed CO species found by microcalorimetry. The estimated heat is too high for trace c and too low for trace e and f, only for trace d the values are in good agreement. This may be rationalized by the microcalorimetric results. The mobility of the adsorbed CO strongly depends on the coverage in the case of CA1, but changes only little for CZA1.

Microkinetic modelling was used to confirm the agreement between the TPD experiments and the microcalorimetric results quantitatively. The TPD peaks were simulated using the integral heats of adsorption as measured by microcalorimetry. Fig. 3.9 shows the results of the calculations for the peaks C–E and c–f. Values for A_{ads} and A_{des} were optimized in order to give the best fit between simulated and experimental TPD peaks. The used values are included in table 3.4. The peak maxima are given correctly by the simulations, but the peaks are to narrow. This is due to the fact that the heat of adsorption was kept constant for the simulation of each peak. The peaks simulated E, e and f fit best as the integral heat of adsorption differs only slightly from the differential heat of adsorption in the regarded coverage range. A detailed description of the simulation is given elsewhere [25]. The simulation confirms also qualitatively the entropies of adsorption measured by microcalorimetry. There are only small changes of A_{ads} in the simulation of the experiments C–E using CZA1, in the case of CA1 A_{ads} ranges from $2\,s^{-1}$ at low coverage (experiments e and f) to $111\,s^{-1}$ at high coverage (experiment c).

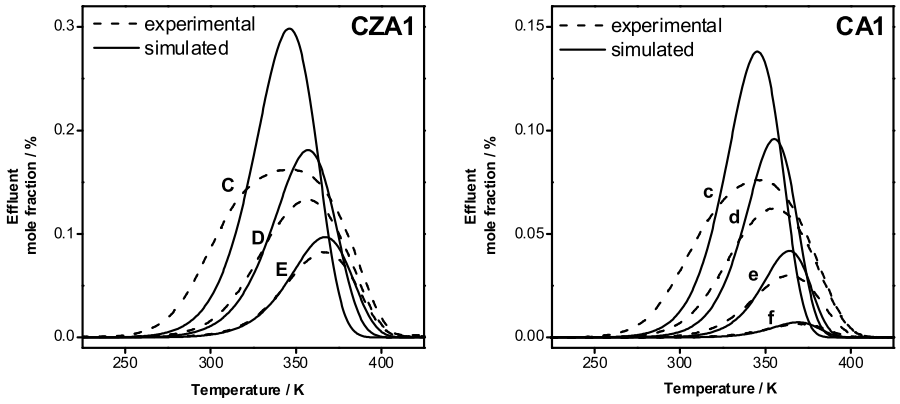

Figure 3.9: Simulation of the TPD peaks obtained with CZA1 and CA1.

Table 3.4: Simulated data

Sample	Peak	ΔH_{ads}^{TPD} / kJ/mol	ΔH_{ads}^{exp} / kJ/mol	A_{ads} s^{-1}	A_{des} s^{-1}
CZA1	C	55.6	56.4[a]	755	10^{15}
	D	57.3	58.4[b]	681	10^{15}
	E	58.9	61.7[c]	377	10^{15}
CA1	c	71.7	65.1[d]	111	10^{15}
	d	73.6	73.1[e]	12	10^{15}
	e	75.3	79.6[f]	2	10^{15}
	f	75.9	80.9[g]	2	10^{15}

ΔH_{ads}^{TPD} is estimated from the peak maximum following the method of Konvalinka and Scholten; ΔH_{ads}^{exp} is the integral molar heat of the adsorption of CO derived from the microcalorimetric data ; [a]: 0–84 $\mu mol_{CO}/g_{cat}$; [b]: 0–62 $\mu mol_{CO}/g_{cat}$; [c]: 0–33 $\mu mol_{CO}/g_{cat}$; [d]: 0–42 $\mu mol_{CO}/g_{cat}$; [e]: 0–27 $\mu mol_{CO}/g_{cat}$; [f]: 0–11 $\mu mol_{CO}/g_{cat}$; [g]: 0–4 $\mu mol_{CO}/g_{cat}$.

In summary, the CO TPD experiments confirm the results by microcalorimetry. The experimental heats of adsorption could be used to simulate the CO TPD experiments in good agreement. The simulation also reflects the differences in the entropies of adsorption in the case of CZA1 and CA1. The higher fractional coverage of CA1 at a given equilibrium pressure of CO can also be found in the TPD data.

Pritchard et al. [5] presented a detailed IR study of the adsorption of CO on copper single crystal surfaces and on supported copper samples. They assigned bands at 2093, 2085 and 2076 cm^{-1} to the stretching vibration of CO adsorbed onto the low-indexed single crystal faces (110), (100) and (111), respectively. Dulaurent et al. [7] investigated the adsorption of CO on a 4.7% Cu/Al_2O_3 catalyst prepared by impregnation. They found a broad and symmetric band at 2120 cm^{-1} after adsorbing CO on the oxidized sample. After the complete reduction of the copper content in flowing hydrogen at 713 K, the adsorption of CO resulted in a broad and to lower wavenumbers asymmetric band at 2092 cm^{-1}. A 3% Cu/ZnO sample was studied by Boccuzzi and Chiorino [27]. They found only one broad and asymmetric band at 2090 cm^{-1} after adsorbing CO on the reduced sample. Topsøe and Topsøe [29] investigated the influence of the reduction temperature on the IR band of adsorbed CO using 1% and 5% Cu/ZnO samples. The maximum of the broad and asymmetric band shifted with increasing reduction temperature from 2096 cm^{-1} (453 K) to 2067 cm^{-1} (573 K). After reduction at 493 K, the band was found at 2085 cm^{-1}. The authors reported also, that no shifts were found in the case of Cu/Al_2O_3

samples.

Our FTIR results are in good agreement with the data in literature, even though the weak bands found in the case of reduced CZA2 could not be found in literature. The results obtained with CA2 confirm that the copper content of the sample is completely reduced to its zero-valent state, even after the mild reduction conditions applied. No bands can be detected above 2100 cm^{-1}. Bands in that region indicate cationic copper species [28].

The reason for the poor quality of the spectra obtained with CA2 (compared to the results with CZA2) can be explained by the copper content of 20 wt-%. The high copper content severely reduces the transparency of the sample. A comparison of the single beam spectra of the samples CZA1 and CZA2 supports this conclusion. A lower transparency results in a lower signal/noise ratio. This can be clearly seen in the spectra of the reduced samples CZA2 and CA2 in the region 1400–1600 cm^{-1} and above 3000 cm^{-1}. Thus, no information can be gained about the formation of carbonates during the adsorption of CO on the support of these samples.

The results obtained with CZA2 are similar to the results presented by Topsøe and Topsøe [29] for a Cu/ZnO sample reduced at 493 K. A comparison of these results confirm the strong influence of the ZnO on the heat of adsorption of CO found by microcalorimetry, while the alumina seems to have no effect on the heat of adsorption. The differences in the fractional coverage for a given equilibrium pressure of CO found by microcalorimetry for the catalysts CZA1 and CA1 are found analogous in the FTIR experiments. CZA2 and CA2 have nearly the same free copper surface area. Although the mass of the investigated CZA2 wafer is higher than that of the CA2 wafer, the extinction at a CO pressure of 100 Pa is significantly higher in the case of CA2. In transmission FTIR experiments, the extinction is only a function of the concentration and the extinction coefficient of the absorbing species. As the latter should be similar for CO adsorbed on CZA2 and CA2, this indicates a higher fractional coverage in the case of CA2.

It is possible to calculate a qualitative adsorption isotherm from the FTIR data by integrating the peak areas. Fig 3.10 compares the qualitative adsorption isotherms derived from the FTIR data with the adsorption isotherms calculated from the microcalorimetric results and a simulated adsorption isotherm of the Temkin type. The Temkin type adsorption isotherms were simulated using the differential heats of adsorption measured by microcalorimetry. details concerning the simulation are given in ref. [25]. The adsorption isotherms are in excellent agreement for the samples CZA1 and CZA2 indicating that the adsorption of CO follows the same adsorption

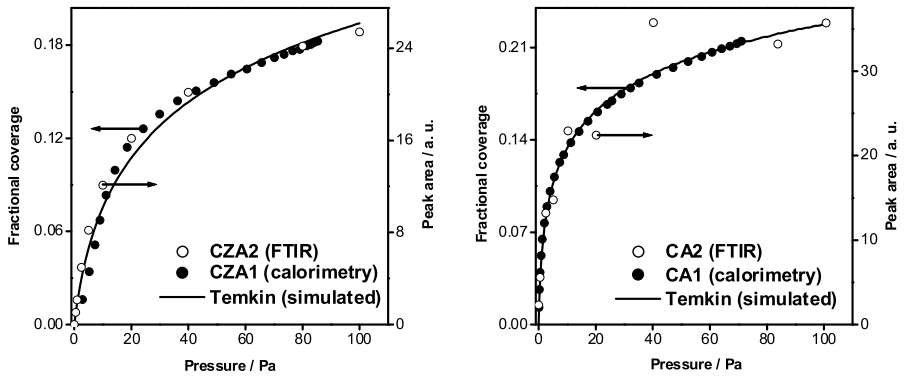

Figure 3.10: Comparison of adsorption isotherms derived from microcalorimetric results for samples of high copper content (CZA1, CA1), FTIR experiments with samples of low copper content (CZA2, CA2) and computational simulation.

kinetics on these two samples and that the microcalorimetric and the FTIR experiments were conducted under near-equilibrium conditions. In the case of CA1 and CA2 the adsorption isotherm measured by microcalorimetry and the simulated Temkin type adsorption isotherm fit very well. There is only a rough agreement with the adsorption isotherm derived from the FTIR results. This can be rationalized by the lower quality of the spectra obtained with CA2. The high noise leads to a high uncertainty of the integrated peak areas. However, the conclusions made for CZA1 and CZA2 can be also drawn for CA1 and CA2.

The shifting of the baseline observed during the adsorption of CO on CZA2 is not yet understood. Further investigations of this effect are needed.

In summary, the results by FTIR spectroscopy are in good agreement with the microcalorimetric and the TPD data, even though the copper content of the investigated samples differs. Experiments with catalysts of the same class yield analogous results. The influence of ZnO on the heat of adsorption and the higher fractional coverage of Cu/Al_2O_3 at a given equilibrium pressure were also found in the FTIR data.

3.5 Conclusions

The results demonstrate that the use of the TPD set-up for all sample pretreatments leads to well defined and reproducible catalyst states which are accessible to fundamentally different

investigation methods as transient temperature-programmed experiments, optical spectroscopy and calorimetry.

The comparison of the microcalorimetric experiments using samples of high copper content with the FTIR results obtained with samples of lower copper content supports the classification of copper catalysts as proposed by Hinrichsen et al. [23].

All experiments show that the studied copper catalysts are fully reduced by the mild pretreatment conditions chosen in this study. The strong influence of ZnO on the adsorption of CO was found by all applied investigation methods. Alumina has no effect on the heat of adsorption, but increases the fractional coverage for a given CO pressure.

The results can give a preliminary explanation for the different methanol synthesis activities of the different catalyst classes. Further investigations are needed to confirm this thesis.

Acknowledgments

Financial support by the Deutsche Forschungsgemeinschaft within the Collaborative Research Center (SFB 558) ‘Metal-Substrate Interactions in Heterogenous Catalysis’ are gratefully acknowledged.

Bibliography

[1] J.B. Hansen, in: ”Handbook of Heterogenous Catalysis”, VCH Verlagsgesellschaft, Weinheim, 4 (1997) 1856.

[2] H. Wilmer, T. Genger and H. Hinrichsen, J. Catal., 215 (2003) 188.

[3] J.B. Wagner, P.L. Hansen, A.M. Molenbroek, H. Topsøe, B.S. Clausen, and S. Helveg, J. Phys. Chem. B, 107 (2003) 7753.

[4] J.-D. Grunwaldt, A.M. Molenbroek, N.-Y. Topsøe, H. Topsøe, and B.S. Clausen, J. Catal., 194 (2000) 452.

[5] J. Pritchard, T. Catterick and R.K. Gupta, Surf. Sci., 53 (1975) 1.

[6] S. Vollmer, G. Witte and C. Wöll, Catal. Lett., 77 (2001) 97.

[7] O. Dulaurent, X. Courtois, V. Perrichon, and D. Bianchi, J. Phys. Chem. B, 104 (2000) 6001.

[8] E. Giamello, B. Fubini and V. Bolis, Appl. Catal., 36 (1988) 287.

[9] F. Boccuzzi, G. Ghiotti and A. Chiorino, Surf. Sci., 156 (1985) 933.

[10] S. Bailey, G.F. Froment, J.W. Snoeck, and K.C. Waugh, Catal. Lett., 30 (1995) 99.

[11] T. Genger, O. Hinrichsen and M. Muhler, Catal. Lett., 59 (1999) 137.

[12] H. Wilmer and O. Hinrichsen, Catal. Lett., 82 (2002) 117.

[13] B. Bems, M. Schur, A. Dassenoy, H. Junkes, D. Herein, and R. Schlögl, Chem. Eur. J., 9 (2003) 2039.

[14] O. Hinrichsen, T. Genger and M. Muhler, Chem. Eng. Technol., 11 (2000) 956.

[15] H. Bielawa, M. Kurtz, T. Genger, and O. Hinrichsen, Ind. Eng. Chem. Res., 40 (2001) 2793.

[16] B.E. Spiewak and J.A. Dumesic, Thermochim. Acta, 290 (1996) 43.

[17] ”The combined application of microcalorimetry, TPD and FTIR spectroscopy”, chapter 2.

[18] H.G. Karge and W. Nießen, Catal. Today, 8 (1991) 451.

[19] R. Naumann d’ Alnoncourt, M. Kurtz, H. Wilmer, E. Löffler, V. Hagen, J. Shen, and M. Muhler, J. Catal., 220 (2003) 249.

[20] N. Cardona-Martinez and J.A. Dumesic, Adv. Catal., 38 (1992) 149.

[21] J.C. Tracy, J. Chem. Phys., 56 (1972) 2748.

[22] G.D. Borgard, S. Molvik, P. Balaraman, T.W. Root, and J.A. Dumesic, Langmuir, 11 (1995) 2065.

[23] M. Kurtz, H. Wilmer, T. Genger, O. Hinrichsen, and M. Muhler, Catal. Lett., 86 (2003) 77.

[24] J.J.F. Scholten and J.A. Konvalinka, Trans. Faraday Soc., 65 (1969) 2465.

[25] J. Strunk, R. Naumann d'Alnoncourt, M. Bergmann, O. Hinrichsen, and M. Muhler, to be published.

[26] J.A. Dumesic, D.F. Rudd, L.M. Aparicio, J.E. Rekoske, and A.A. Treviño, ACS Professional Reference Book, Washington, DC, (1993).

[27] F. Boccuzzi and A. Chiorino, J. Phys. Chem., 100 (1996) 3617.

[28] K.I. Hadjiivanov and G.N. Vayssilov, Adv. Catal., 47 (2002) 307.

[29] N.-Y. Topsøe and H. Topsøe, Top. Catal., 8 (1999) 267.

4 Part II: The state of the catalyst after pretreatment in CO

Abstract

The influence of the strong metal-support interactions between copper and zinc oxide on the adsorption of carbon monoxide are studied in this contribution. Samples containing only copper and alumina as an inert supporting material are included for comparison. The samples are pretreated under strongly reducing conditions prior to the adsorption of carbon monoxide. The adsorption of carbon monoxide is investigated in microcalorimetric, temperature-programmed desorption and infrared spectroscopic experiments. A comparison of the results with already reported results obtained after the reduction of the samples with hydrogen shows that the adsorption of carbon monoxide is strongly influenced by the interactions between copper and zinc oxide, while alumina has only negligible effects on the adsorption behavior of the samples.

4.1 Introduction

Copper catalysts are industrially used for the synthesis of methanol. These catalysts are ternary systems containing copper (Cu), zinc oxide (ZnO) and alumina (Al_2O_3) [1]. Several recent studies [2, 3, 4, 5, 6] indicate there are strong metal-support interactions (SMSI) between copper and zinc oxide in these catalysts.

In 1978 Tauster et al. [7] reported that noble metal catalysts using TiO_2 show different behavior in the adsorption of hydrogen and carbon monoxide after low-temperature reduction and high-temperature reduction. The adsorption capacity of the samples decreased to nearly zero after high-temperature reduction, but was fully restored by an oxidizing treatment. Using electron microscopy and x-ray diffraction the authors showed that this loss of adsorption capacity was not due to metal agglomeration or encapsulation. They concluded that the loss of adsorption capacity should be related to the formation of bonds between the noble metal atoms and titanium atoms or cations of the support, thus changing the electronic properties of the metal clusters. They referred to these processes as strong metal-support interactions (SMSI).

Based on in situ EXAFS and XRD experiments Grunwaldt et al. [2] presented a model for the SMSI between copper and ZnO: Under the reducing conditions of methanol synthesis, metallic copper particles spread on the support and their surfaces are covered by zinc and oxygen species. Under more severe conditions, surface and bulk alloying leads to the formation of brass.

Hansen et al. [3] using in situ transmission electron microscopy gave experimental evidence of dynamic shape changes of copper nanocrystals supported on ZnO. The changes were induced by changes of the reduction potential of the surrounding gas phase and were fully reversible. The authors concluded that the changes were caused by adsorbate-induced changes of the Cu/ZnO interfacial energies. The authors assumed that oxygen vacancies in the ZnO play a role in the observed processes. Only negligible shape changes were found for copper nanocrystals supported on SiO_2.

Wagner et al. [5] investigated the SMSI between copper and ZnO by applying in situ electron energy loss spectroscopy. They found that the support induces a tensile strain in the Cu nanoclusters. The degree of this strain is dependent on the reduction potential of the surrounding gas phase. They found no indication for strained Cu nanoclusters in Cu/SiO_2 samples.

Hinrichsen and co-workers [4, 6] investigated the interaction of hydrogen and nitrous oxide with Cu/Al_2O_3, Cu/ZnO and $Cu/ZnO/Al_2O_3$ samples as a function of the pretreatment. The authors found that Cu/Al_2O_3 is hardly influenced by changes of the pretreatment, while dynamical changes of the copper content were found in the case of ZnO containing samples. The strongly reducing conditions of a pretreatment in CO led to a loss in free copper surface area due to zinc and oxygen species migrating onto the copper surface.

The present contribution investigates the influence of a strongly reducing CO pretreatment on the adsorption of carbon monoxide on copper catalysts. The investigated copper catalysts are the same samples studied by Hinrichsen and co-workers in ref. [4, 6]. The adsorption of CO is investigated by microcalorimetry, CO TPD experiments and FTIR spectroscopy in transmission mode. Many efforts were taken to assure that the pretreatment conditions are identical for all investigation methods thus giving all experimental techniques access to the copper surface in an identical state. The results in ref. [8] refer to the state of the catalysts after hydrogen reduction. The published data confirm that the results by microcalorimetry, CO TPD experiments and FTIR spectroscopy are all related to copper surfaces in an identical state for

each catalyst system, respectively.

4.2 Experimental

The investigated samples are binary and ternary catalysts containing copper, zinc oxide and alumina. The samples are identical to those in [8]. The methods of preparation and characterization of the samples are described in detail elsewhere [9, 10, 11]. Table 4.1 summarizes the main characteristics of the samples.

Table 4.1: Characterization and catalytic data

Catalyst	CZA1	CZA2	CZ1	CA1	CA2
BET surface area (m^2/g_{cat})	73	-	64	51	124
Cu content (wt% CuO)	47	7	68	76	20
Specific amount of Cu surface atoms[a] (μmol/g_{cat})	513	134	513	176	139
Specific Cu surface area[b] (m^2/g_{cat})	21	6	21	7	6
Specific methanol production rate[c] (μmol/s g_{cat})	0.112	0.065	0.077	0.015	0.012
Turnover frequency (10^{-5} s^{-1})	21.8	48.5	15.0	8.3	9.0

[a]: Derived by N_2O RFC. [b]: Assuming that 1 m^2 of Cu surface area equals 24.41 μmol Cu atoms. [c]: Obtained at ambient pressure using 100 mg catalyst in synthesis gas (72 % H_2, 10 % CO, 4 % CO_2 and 14 % He) and a volumetric flow rate of 50 cm^3 min^{-1} (STP).

This contribution includes results from adsorption microcalorimetry, TPD experiments and FTIR spectroscopy in transmission mode. All investigations focus on the adsorption of CO on the copper catlysts.The experiments were performed analogous to the experiments in [8]. Only the pretreatment conditions were changed. The samples were first reduced by flowing hydrogen as described in [8]. The reduction was followed by a treatment in a flowing 10% CO/He mixture at 498 K. The duration of this treatment was 50 h in the case of the microcalorimetric and TPD experiments, while the duration was varied in the case of the FTIR experiments (1, 18 and 50 h). All samples were flushed for at least 30 min at elevated temperatures in a flow of pure helium after the pretreatment. The flow rates were always fixed to 10 Ncm^3/min. All pretreatments were monitored by on-line mass spectrometry.

For the microcalorimetric experiments, 100 mg of the sieve fraction of 250–355 μm were pretreated in a specially designed pretreatment reactor, and then sealed in a pyrex capsule. Next,

the pyrex capsule was placed into the sample receptacle of the microcalorimeter (C80 II, Setaram). The calorimetric set-up was degassed and the capsule was broken. After reaching thermal equilibrium (at 303 K) the adsorption measurement was started. Small doses of carbon monoxide were subsequently admitted to the sample, and while the heat of adsorption was measured calorimetrically, the amount of adsorbed species was measured volumetrically. In order to test the reversibility of the observed processes the sample was evacuated overnight and the experiment was repeated. The employed measurement technique was adopted from the pioneering work by Spiewak and Dumesic [13]. The technique allows to investigate air-sensitive samples unimpaired by poisoning. A detailed description of the experimental procedure and the set-up is given elsewhere [12].

The TPD experiments were carried out in a stainless steel U-tube reactor connected to a flow set-up. Typically, 100 mg of the sieve fraction of 250–355 μm were investigated *in situ*, directly after the pretreatment. The samples were cooled from room temperature to 78 K in a flow of a 10 % CO/He mixture and afterwards heated to 450 K in a flow of ultra-pure He. The desorption of CO into the stream of helium was monitored by on-line mass spectrometry. The coverage dependence of the CO desorption was investigated by varying the initial coverage. This was achieved by heating the samples to 450 K in two steps, i. e. after dosing CO the sample was first heated to $T_{1st\ step}$ (275, 300, 325, 350, and 375 K) again cooled to 78 K, and finally heated to 450 K. The experimental conditions and the set-up are fully described elsewhere [12].

The infrared spectroscopy experiments were performed using a modified transmission IR cell designed by Karge et al. [14] in a Nicolet Nexus FTIR spectrometer. The cell was connected to a sample pretreatment section and a CO dosing system. The investigations were carried out using wafers of an area of about 2 cm^2 and a mass of less than 50 mg. After the pretreatment the wafer was brought into the IR beam and spectra (250 scans, resolution: 2 cm^{-1} in the region 800 – 6000 cm^{-1} were recorded. The pressure of CO was varied stepwise between 0–100 Pa (0, 0.5, 1, 2.5, 5, 10, 20, 40, 80, 100 Pa and evacuation), in order to investigate the adsorption of CO as a function of coverage. Details about the experimental conditions and the set-up are given elsewhere [12].

4.3 Results

The heat of adsorption was measured calorimetrically using the samples with a high copper content (CA1, CZ1 and CZA1). Fig. 4.1, 4.2 and 4.3 show the results (left: differential heat of adsorption; right: adsorption isotherm), respectively. The results of the experiments after hydrogen reduction presented in [8] are included for comparison. The adsorption of CO is strongly influenced by the pretreatment. Significant differences are found for catalysts with (CZA1, CZ1) and without ZnO (CA1).

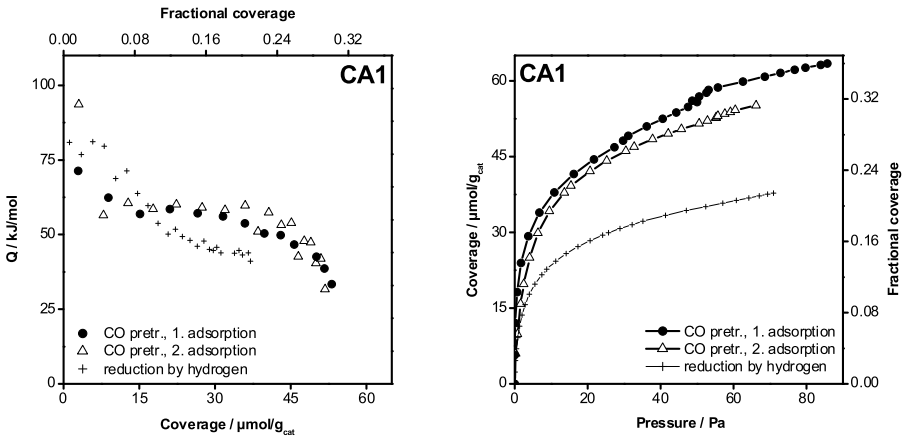

Figure 4.1: Differential heat of adsorption and adsorption isotherms of CO on CA1 at 303 K after CO pretreatment. The results obtained after hydrogen reduction are included for comparison. The sample was evacuated overnight between the first and the second adsorption experiment.

In the case of the ZnO-free sample CA1, the heat of adsorption decreases monotonically with increasing coverage from 71–33 kJ/mol (first adsorption) with a plateau around 55 kJ/mol. The range of the heat of adsorption is comparable to the results after hydrogen reduction, only that the initial and final (in the observed coverage range) heat of adsorption are slightly lower. The amount of CO adsorbed at an equilibrium pressure of 60 Pa of CO is increased by roughly 50% compared with the results after hydrogen reduction. Please note that the fractional coverages given in fig. 4.1, 4.2 and 4.3 are calculated using the specific amount of copper surface atoms as measured by nitrous oxygen reactive frontal chromatography for the sample in the state after hydrogen reduction, respectively. The reversibility of the adsorption is indicated by the results

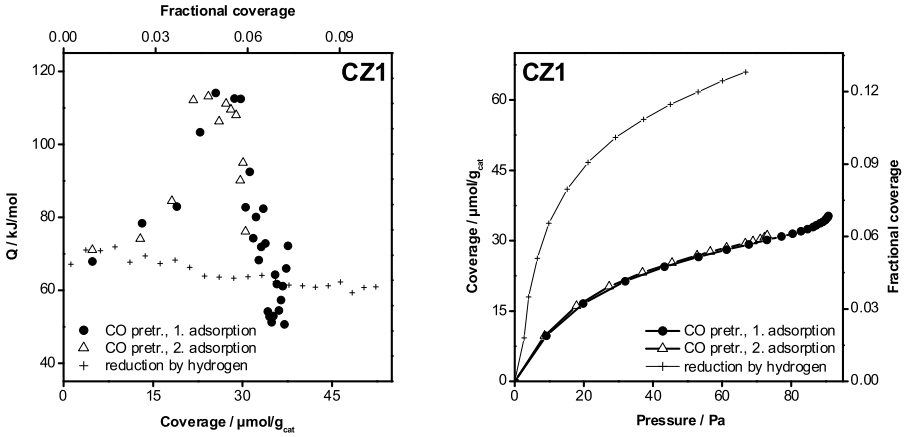

Figure 4.2: Differential heat of adsorption and adsorption isotherms of CO on CZ1 at 303 K after CO pretreatment. The results obtained after hydrogen reduction are included for comparison. The sample was evacuated overnight between the first and the second adsorption experiment.

of the second adsorption. The only differences are a slight decrease of the coverage and a higher initial value of the heat of adsorption (94 kJ/mol).

The microcalorimetric results obtained with CZ1 show completely different trends. The initial value of the heat of adsorption is similar to the value measured after hydrogen reduction, but the heat of adsorption increases with increasing coverage to a maximum at about 115 kJ/mol followed by a steep drop to about 60 kJ/mol. The final value is similar to the final heat of adsorption after hydrogen reduction, but it is measured with a large uncertainty of about 10 kJ/mol. Compared to the results after hydrogen reduction, the amount adsorbed at an equilibrium pressure of 60 Pa is drastically decreased from 64 to 28 μmol/g$_{cat}$. The second adsorption experiment implies the complete reversibility of the observed processes.

In the first adsorption experiment using CZA1 the heat of adsorption first decreases from 58 to 44 kJ/mol, then increases to 60 kJ/mol and finally decreases to 50 kJ/mol. In the second experiment the heat increases from about 40 kJ/mol to 64 kJ/mol and the decreases to 50 kJ/mol. The final values are similar to the values measured after hydrogen reduction but are measured with a large uncertainty. The equilibrium coverage at 60 Pa of CO is significantly lower after the CO pretreatment (56 μmol/g$_{cat}$) compared to the corresponding coverage after hydrogen reduction

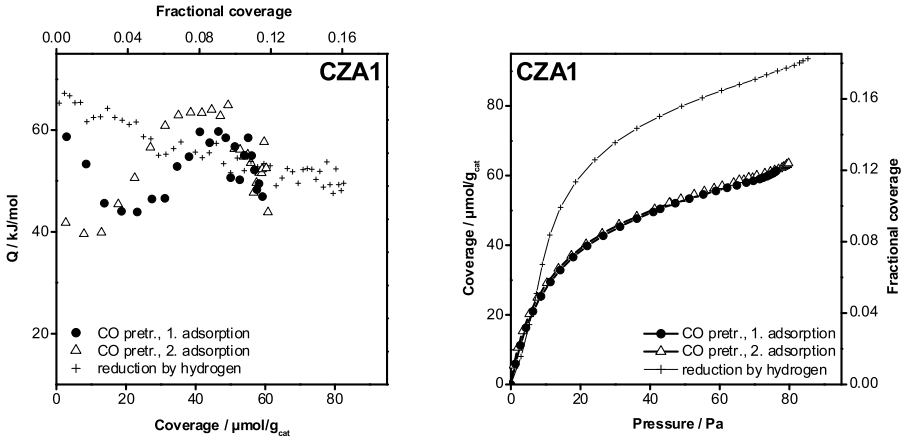

Figure 4.3: Differential heat of adsorption and adsorption isotherms of CO on CZA1 at 303 K after CO pretreatment. The results obtained after hydrogen reduction are included for comparison. The sample was evacuated overnight between the first and the second adsorption experiment.

(84 μmol/g$_{cat}$). While the adsorption isotherms shown in fig. 4.3 confirm the reversibility of the adsorption processes, the differences in the heat of adsorption between the first and the second adsorption experiment indicate non-reversible changes of the sample.

The CO TPD experiments were performed with CA1 and CZA1. Fig. 4.4 shows the results of the TPD experiments. The desorption from the fully covered copper surface of CA1 (experiment a) results in an intense peak at 110 K and a broad signal in the temperature range 200–400 K with a maximum at 283 K and a shoulder at about 345 K. The TPD profile is similar to the profile obtained after hydrogen reduction [8]. The TPD profile of the fully covered copper surface of CZA1 (experiment A) is significantly different to the corresponding profile after hydrogen reduction [8]. There is an intense peak at 105 K and a broad signal in the temperature range 200–400 K with maxima at 204 and 275 K and a shoulder at about 330 K. The amount of desorbing CO in total is lower.

In the case of CA1 and CZA1, the desorption from the partially covered surface results in a broad peak that is asymmetric to lower temperatures. The peak maximum is shifted to higher temperatures with decreasing initial coverage. Tab. 4.2 summarizes the results of the TPD experiments after CO pretreatment and hydrogen reduction. The final temperature of the first

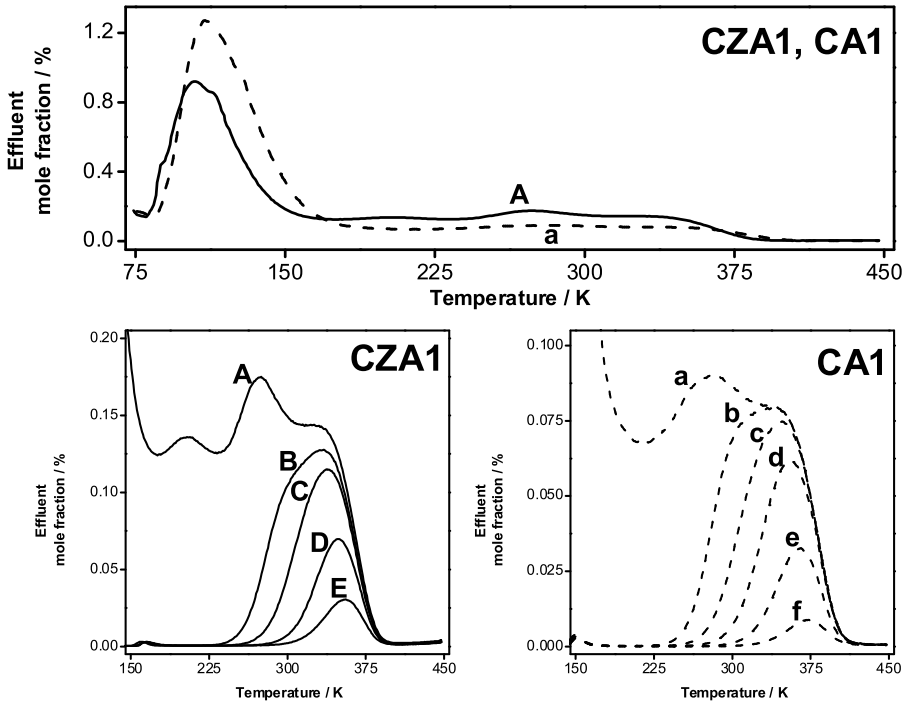

Figure 4.4: CO TPD spectra obtained with CZA1 and CA1 fully covered (A, a) and partially covered (B–E, b–f) with CO after CO pretreatment, $T_{1st\ step}$: 275 K (B, b), 300 K (C, c), 325 K (D, d), 350 K (E, e) and 375 K (f).

heating step is $T_{1st\ step}$. The temperature of the absolute peak maximum is T_{max}. The full width at half maximum is given in the column FWHM. The initial coverages are calculated by integrating the mass spectrometry traces over the complete range of the desorption peak. Only small differences in T_{max}, FWHM and initial coverage are observed in the case of CA1. A comparison of the corresponding peaks obtained with CZA1 shows that the peak maxima are shifted to lower temperatures after the CO pretreatment, the peaks are narrower and the initial coverage is significantly decreased by 45–65%.

The FTIR results of the experiments using CZA2 (42 mg/2 cm^2) and CA2 (31 mg/2 cm^2) are shown in fig. 4.5 and 4.6. In the case of CZA2, mainly one broad and to lower wavenumbers asymmetric band with a peak maximum at 2063 cm^{-1} is observed. The band becomes broader and more asymmetric with increasing coverage. Additionally, weak bands can be observed below 2000 cm^{-1} at about 1690, 1246, and 1228 cm^{-1}. No bands appear above 2100 cm^{-1}. Due to intense noise, no information can be gained in the range 1650–1300 cm^{-1} and above

Table 4.2: CO TPD data obtained with CZA1 and CA1

Sample	Peak	$T_{1st\ step}$ / K	$T_{max}{}^{a}$ / K	FWHM^{a} / K	coverage^{a} / μmol/g	$T_{max}{}^{b}$ / K	FWHM^{b} / K	coverage^{b} / μmol/g
CZA1	B	275	335	85	78	315	112	145
	C	300	338	62	53	346	87	102
	D	325	350	44	26	357	61	62
	E	350	355	44	11	367	49	33
CA1	b	275	340	100	56	336	98	58
	c	300	348	76	41	345	76	42
	d	325	354	59	27	355	59	27
	e	350	365	50	12	364	46	11
	f	375	373	44	3	369	40	2

^{a}: after CO pretreatment; ^{b}: after hydrogen reduction.

2200 cm^{-1}. It is found that the main band at 2065 cm^{-1} decreases instantly when the cell is evacuated, while the weak bands change only little in intensity. The adsorption of CO induces a baseline shift to higher extinction in the range above 1700 cm^{-1}. Shifts to lower extinction are observed at lower wavenumbers. The shifts are only partially reversible after evacuation of the cell. The spectrum of CA2 also mainly shows one broad and asymmetric band with a peak maximum at 2086 cm^{-1}. The band becomes also broader and more asymmetric with increasing coverage. Weak bands can be observed at 1246 and 1228 cm^{-1}. The baseline is shifted to higher extinction with increasing coverage in the region below 1400 cm^{-1}. Due to intense noise, no information can be gained in the range 1650–1350 cm^{-1} and above 2200 cm^{-1}.

Fig. 4.7 shows single beam spectra of CZA2 and CA2. The figures include spectra after hydrogen reduction and after CO pretreatment. The transparency of the ZnO-containing sample CZA2 decreases strongly after the CO pretreatment as a function of the pretreatment time. The single beam spectra of CA2 are not significantly influenced by the pretreatment. The single beam spectra showing gas phase contributions of carbon dioxide and water were recorded while the spectrometer was purged by a commercial air dryer, the spectra without gas phase contributions were recorded while purging with a nitrogen gas cylinder.

The influence of the pretreatment on the frequency of the main band is depicted in fig. 4.8. The CO pretreatment has a significant influence on the main band. The peak maximum shifts to lower wavenumbers and the peak area decreases. The effects are much stronger for the ZnO-containing sample and increase with the pretreatment time. The characteristics of the main

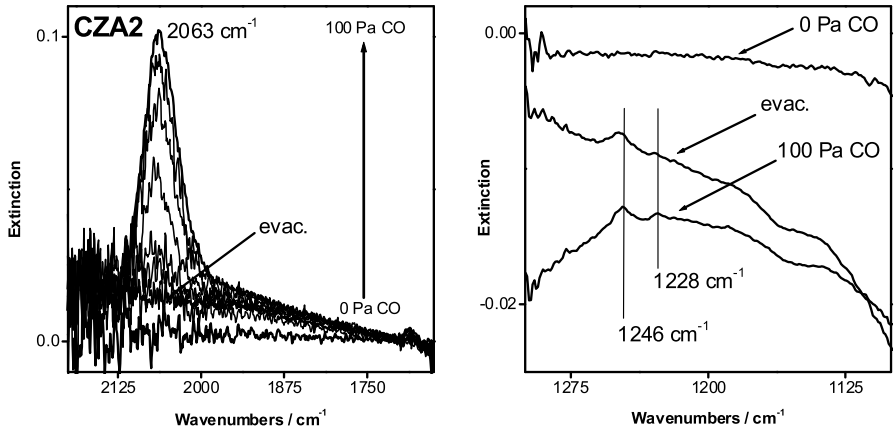

Figure 4.5: FTIR spectra obtained with CZA2 after pretreatment in CO in the pressure range of 0–100 Pa of CO and at room temperature. The left figure shows the range of the CO stretching vibration. The spectra are not corrected for the gas phase CO vibrational contribution. The right figure shows the range below the CO stretching vibration for pressures of 0 and 100 Pa of CO, and after evacuation.

band as a function of the pretreatment are summarized in table 4.3. $\tilde{\nu}$ is the wavenumber of the peak maximum, $\Delta\tilde{\nu}$ is the shift of the peak maximum relative to the maximum after hydrogen reduction. The given peak areas are normalized to the area of the peak after hydrogen reduction, respectively.

4.4 Discussion

Wilmer et al. [6, 4] investigated the interaction of hydrogen with the catalyst systems Cu/Al_2O_3 and $Cu/ZnO/Al_2O_3$ after hydrogen reduction and CO pretreatment. Both samples were influenced by the pretreatment, but the changes in the hydrogen TPD profiles of Cu/Al_2O_3 were small compared to those in the profiles of $Cu/ZnO/Al_2O_3$. After the CO pretreatment of the $Cu/ZnO/Al_2O_3$ sample an additional peak maximum was found and the free copper surface area was drastically decreased, while its size was essentially constant in the case of Cu/Al_2O_3. However, the TPD from the copper surface of Cu/Al_2O_3 after the CO pretreatment was broader and shifted to lower temperatures indicating changes in the state of the copper content. The authors concluded that under the more reducing conditions of the CO pretreatment zinc and

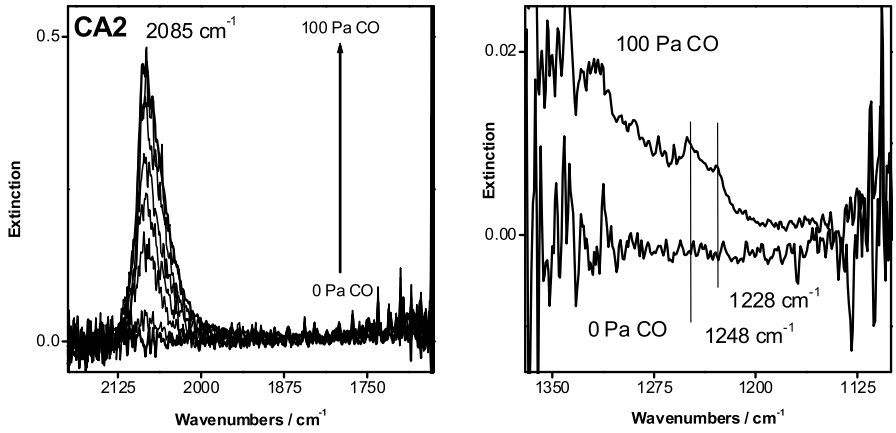

Figure 4.6: FTIR spectra obtained with CA2 after pretreatment in CO in the pressure range of 0–100 Pa of CO and at room temperature.The left figure shows the range of the CO stretching vibration. The spectra are not corrected for a baseline or the gas phase CO vibrational contribution. The right figure shows the range below the CO stretching vibration for a pressure of 0 and 100 Pa of CO.

oxygen species migrated onto the copper surface (in the case of $Cu/ZnO/Al_2O_3$), thus decreasing the free copper surface area, while the hydrogen reduction led to fully reduced and adsorbate-free copper surfaces. Kurtz et al. presented a study on the deactivation behavior of supported copper catalysts for the synthesis of methanol. Based on their findings the authors proposed a classification of the investigated copper catalyst in three classes: Cu/Al_2O_3, Cu/ZnO and $Cu/ZnO/Al_2O_3$. The three classes differ significantly in their activity for the synthesis of methanol, while the activity is linearly correlated with the free copper surface area within each class.

The microcalorimetric results support the postulated classification. The adsorption of CO on CA1, CZ1 and CZA1 is differently influenced by the CO pretreatment. CZ1 is most affected, while the changes are weakest for CA1. The ZnO-containing samples show similar tendencies, but to different extents.

The results obtained for CA1 show that the energy site distribution of the sample was altered by the CO pretreatment. The differential heats of adsorption are essentially of the same magnitude as after hydrogen reduction, but the abundance of the different adsorption sites has changed. There are less sites with heats of adsorption of more than 55 kJ/mol and more sites with lower

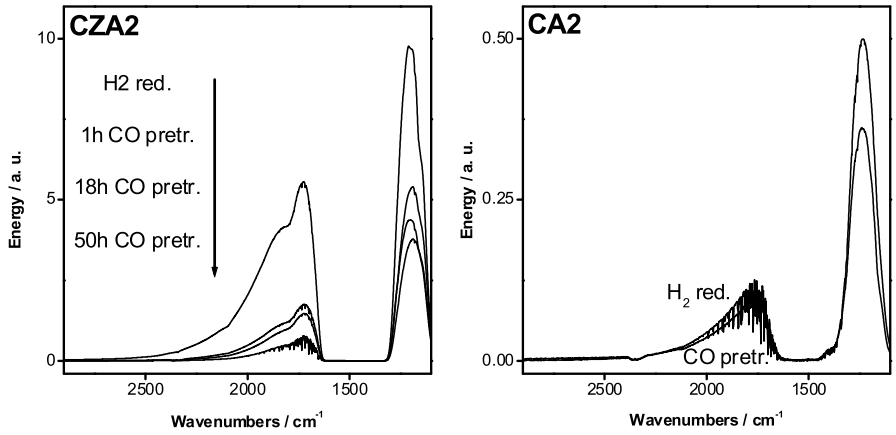

Figure 4.7: Single beam spectra obtained at room temperature with CZA2 and CA2 after different pretreatments (hydrogen reduction and CO pretreatment during 1 h, 18 h and 50 h). The single beam spectra after 50 h CO pretreatment served as background for the spectra in fig. 4.5 and 4.6, respectively.

heats of adsorption. The lower values of the heats of adsorption are found in literature for different copper single crystal surfaces [15, 16, 17, 18] while the values of the higher heats of adsorption are reported for steps, kinks and defect sites [18]. This leads to the conclusion that the morphology of the copper content of CA1 was changed by the CO pretreatment. The copper surface has less steps, kinks and defects after the CO pretreatment. The increased capacity for the adsorption of CO after the CO pretreatment can rather be rationalized by an increase of the free copper surface area than an increase of the fractional coverage. The fractional coverage of the copper surface at room temperature and low pressures of CO should not exceed 0.25 [19]. An increased copper surface area also indicates a change in the morphology of the copper particles.

The FTIR results obtained with CA2 support the microcalorimetric results. Hollins [20] investigated the influence of surface defects (including steps and kinks) of copper surfaces on the infrared spectra of adsorbed CO. The author demonstrated that dipolar coupling between different adsorbate species causes strong effects on the measured spectra. Intensity is shifted from low-frequency to high-frequency bands. In the case of copper, the low-frequency bands can be assigned to terrace places on low-indexed copper surface planes, while the high-frequency

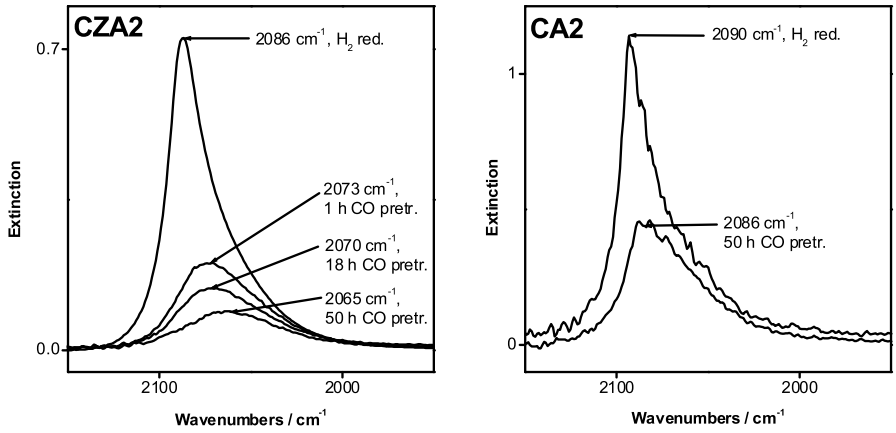

Figure 4.8: The influence of the pretreatment on the main band. The spectra are recorded after hydrogen reduction and CO pretreatment during 1 h, 18 h and 50 h at a pressure of 100 Pa of CO. The results for CZA2 are in the right figure, for CA2 in the left figure.

bands are due to CO adsorbed on defect sites. The magnitude of the intensity shift depends on the ratio of the adsorbed species. A defect/terrace site ratio of 1:10 can lead to the nearly complete absence of the low-frequency band. The spectrum is dominated by the low-frequency band if the ratio is less than 1:100. The shift of the peak maximum to lower wavenumbers observed after the CO pretreatment of CA2 can be caused by a decrease of the defect/terrace site ratio. The results presented in [8] confirm the complete reduction of the copper content of CA1 and CA2 to its zero-valent state after hydrogen reduction. Thus the differences in the results measured after hydrogen reduction and CO pretreatment cannot be explained by changes of the oxidation state of the copper content. There are no reports in literature of SMSI between copper and alumina. A change of the morphology of the copper particles of CA1 and CA2 after CO pretreatment that leads to less defect sites can explain the results by microcalorimetry and FTIR spectroscopy. It has to be noted that the FTIR results give no indication of an increased free copper surface area. The peak area of the IR band is decreased by about 40 % after the CO pretreatment. It is hard to say whether this decrease is caused by changes in the apparent absorption coefficient of the adsorbed CO or a decrease of the concentration of the adsorbed species which would indicate a loss in free copper surface area. It also has to be considered that the microcalorimetric experiments were performed using fresh samples for each experi-

Table 4.3: Influence of the pretreatment on the main IR band

Sample:	CZA2			CA2		
Pretreatment	$\tilde{\nu}$ / cm^{-1}	$\Delta\tilde{\nu}$ / cm^{-1}	peak area (norm.)[a]	$\tilde{\nu}$ / cm^{-1}	$\Delta\tilde{\nu}$ / cm^{-1}	peak area (norm.)[a]
H_2 red[b]	2086	-	1	2090	-	1
1 h CO[c]	2073	-13	0.45	-	-	-
18 h CO[d]	2070	-16	0.36	-	-	-
50 h CO[e]	2065	-21	0.24	2086	-4	0.62

[a]: the areas are normalized relatively to the area of the peak after hydrogen reduction; [b]: after hydrogen reduction; [c]: after 1 h of CO pretreatment; [d]: after 18 h of CO pretreatment; [e]: after 50 h of CO pretreatment.

ment, while the FTIR experiments after hydrogen reduction, after methanol synthesis [21] and after CO pretreatment were performed using the same wafer. Therefore sintering effects should be stronger in the FTIR experiments than in the microcalorimetric ones. The TPD experiments after the different pretreatments were also carried out with only one sample. The TPD experiments concerning CA1 give no indication of an increased free copper surface area. The results given for the different pretreatments of CA1 in table 4.2 show only small differences. The microkinetic modelling needed for a detailed interpretation of these small changes has yet to be done, but it can be said that no fundamental changes of the copper content after the CO pretreatment were detected. A similar result is found by Wilmer et al. [6] investigating the same sample after CO pretreatment in H_2 TPD experiments.

A comparison of the results obtained after CO pretreatment by microcalorimetry, FTIR spectroscopy and TPD experiments using CA1 and CA2 leads to the conclusion that the copper content is in the same oxidation state as after hydrogen reduction, but the morphology of the copper particles is slightly changed so that there are less surface defects after the CO pretreatment. This effect can be compared to the annealing of copper single crystal surfaces often carried out e.g. after sputtering. The results of the microcalorimetric and the FTIR experiments are in good agreement. The TPD experiments give no valuable information in the case of CA1, but are in general agreement with the results of the microcalorimetry and FTIR spectroscopy. In summary, analogue to literature data concerning Cu/SiO_2 [2, 3, 5] and in good agreement with the data presented by Hinrichsen and co-workers [6], no indications were found for SMSI between copper and alumina after CO pretreatment.

Hinrichsen and co-workers [4, 6] concluded that after the strongly reducing CO pretreatment the copper surface of ZnO-containing catalysts is partially covered by zinc and oxygen species. Their study included the same catalysts as those in the present contribution. The conclusions of the authors are based inter alia on the decreased capacity of CZA1 for the adsorption of hydrogen after CO pretreatment. The adsorption isotherms yielded from the microcalorimetric results are in good agreement with the results of Hinrichsen and co-workers [4, 6]. The capacity for the adsorption of CO is significantly decreased for both ZnO-containing samples. The fact that the decrease is stronger for CZ1 than for CZA1 may be due to alumina being a structural promotor as found by Kurtz et al. [22]. The CO TPD experiments using CZA1 also indicate a decreased copper surface area. The initial coverages in the TPD experiments from the partially covered surfaces are comparable to the coverages in the microcalorimetric experiments using CZA1. The decrease of the peak area of the main band in the FTIR experiments using CZA2 also indicates a decrease of the free copper surface area. The decrease in the peak area is much stronger for CZA2 than for CA2. It can be safely assumed that the decrease might be only partially due to a change in the absorption coefficient of the adsorbed CO species. Greeley et al. [23] presented a DFT study on binding energies and vibrational frequencies of CO adsorbed onto the Cu(111) single crystal plane. Their investigations include the influence of Zn adatoms and of ZnO deposited on the copper surface. At low coverages with CO the calculated values for the binding energy and the vibrational frequency are similar for the case of Zn adatoms and ZnO deposited on the copper surface. Compared to the adsorbate-free copper surface Cu(111) as reference state the authors predict a lowered binding energy and vibrational frequency of CO. The predicted decrease of the binding energy can be found in the results of the TPD experiments carried out using CZA1. A comparison of the data obtained after hydrogen reduction and CO pretreatment shows that the peak maxima are shifted to lower temperatures for experiments with the same $T_{1st\ step}$ after the CO pretreatment. This temperature shift can be interpreted as a decrease of the heat of adsorption of CO. The increase in the temperature of the peak maximum B ($T_{1st\ step}$=275 K) is due to the fact that the peak is not well resolved after hydrogen reduction but has a large contribution from the peak with its maximum around 285 K. After the CO pretreatment peak B is well resolved with nearly no contributions from the low-temperature peak which is shifted to 275 K. The decrease in the vibrational frequency predicted in ref. [23] is found in the FTIR data obtained with CZA2. The shift of the vibrational frequency is much

stronger for CZA2 than for CA2. Although the shift might be partially due to a decrease of defect sites as in the case of CA2, the main part of the shift should be caused by the effect of the zinc and oxygen species on the copper surface as indicated by the DFT study.

The microcalorimetric results concerning the heats of adsorption of CO obtained with the ZnO-containing samples CZ1 and CZA1 cannot be fully understood. As the TPD results are qualitatively confirmed by the DFT study of Greeley et al. [23] it seems likely that the heats measured by microcalorimetry are not solely the heats of adsorption of CO on copper. An increase of the heat of adsorption with increasing coverage can be rationalized by surface reactions with consecutive desorption of products. Such surface reactions may need a certain threshold coverage in order to proceed with measurable rates. In such a case the amount of adsorbed species is calculated to low, and the combined heats of adsorption, reaction and desorption are misinterpreted as heat of adsorption. This leads to an overestimation of the heat of adsorption. An example of such a process is described in [24]. A possible reaction in our experiments would be the oxidation of CO by the oxygen species present on the copper surface after CO pretreatment. However, this seems unlikely as the observed processes are reversible, while a reaction of CO and oxygen with consecutive desorption of carbon dioxide should be irreversible. A possible explanation for a reversible reaction of carbon monoxide with atomic oxygen is given in fig. 4.9. If the presence of Zn and O species on the copper surface stabilizes a state that can

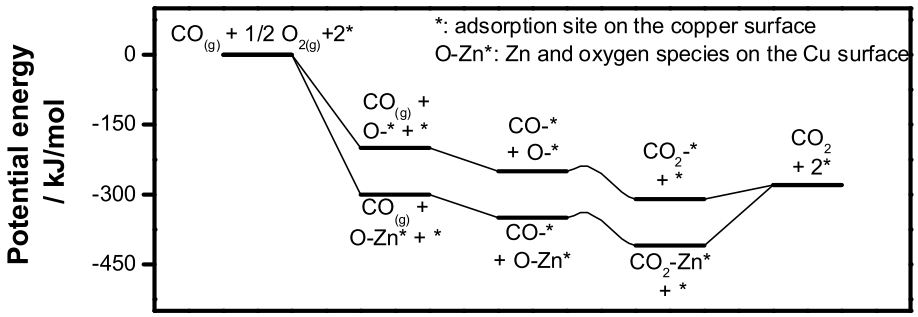

Figure 4.9: The potential energy diagram shows the reaction of CO and oxygen on a copper surface. The presence of Zn species on the copper surface could inhibit the desorption of carbon dioxide thus leading to the reverse reaction including the desorption of CO.

be formally described as carbon dioxide bound to copper and zinc, the reverse reaction may

be favorable to the desorption of carbon dioxide. This can be rationalized by the fact that a desorption of CO_2 from the described state would result in the reduction of the Zn atom. If no surface reaction of CO and atomic oxygen occurs, an unknown exothermic process must be assumed in order to interpret the calorimetric results. The process has to be reversible and should be related to ZnO, even though not necessarily to the Zn and oxygen species on the copper surface. The process does not occur after hydrogen reduction and is stronger in the absence of alumina. There are indications in the FTIR results for an influence of the CO pretreatment on the ZnO support. The single beam spectrum of CZA2 after CO pretreatment differs strongly from the spectrum after hydrogen reduction, while the single beam spectrum of CA2 is hardly influenced by the pretreatment. The loss in transparency observed for CZA2 after CO pretreatment could be explained by oxygen vacancies in the ZnO. The oxygen vacancies would result in partially filled valence bands of the semiconducting ZnO. The electrons in the partially filled valence bands would be excited by the IR beam and thus increase the absorption of the light. Fig. 4.10 shows preliminary results derived from microcalorimetric experiments using coprecipitated ZnO/Al_2O_3 samples after different pretreatments. The results after hy-

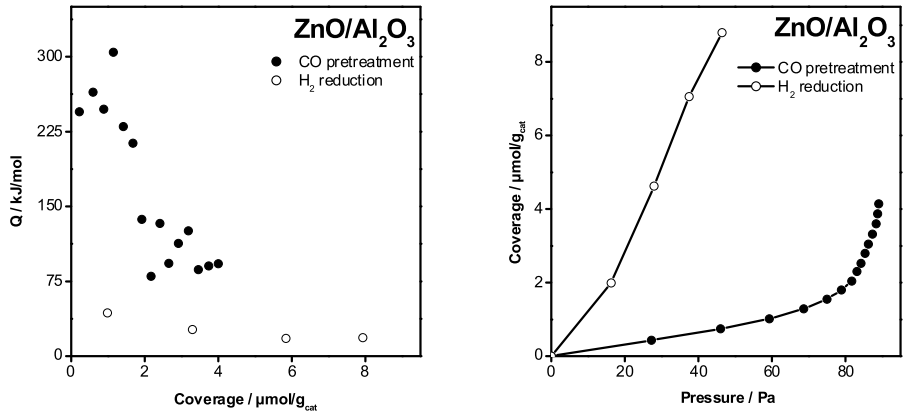

Figure 4.10: Preliminary results of experiments measuring the differential heat of adsorption and adsorption isotherms of CO on ZnO/Al_2O_3 at 303 K after CO pretreatment and hydrogen reduction.

drogen reduction are similar to literature values [25] obtained with commercial available ZnO (Kadox25) and precipitated ZnO. The increase of the heat of adsorption of CO on ZnO after CO pretreatment is not reported in literature. The results suggest that CO is strongly bound to

oxygen vacancies in the ZnO, but a certain threshold pressure of CO has to be exceeded. The threshold pressure would result in CO being first loosely bound to sites on the copper surface, and then strongly bound to the oxygen vacancies. The stronger influence of these processes on the heat of adsorption of CO on CZ1 can be rationalized by the fact that the free copper surface area after CO pretreatment is much smaller in the case of CZ1 compared to CZA1. The initial value of the heat of adsorption is slightly lower on CZ1 and significantly lower on CZA1 compared to the values after hydrogen reduction, respectively. There is even a further decrease of the heat of adsorption during the first five doses of CO in the case of CZA1. This agrees qualitatively with the results of the CO TPD experiments from CZA1 and the calculations of Greeley et al. [23]. The measured increase of the heat of adsorption is already found for the second adsorptive dose in the experiments using CZ1, while the increase occurs only after five doses in the case of CZA1. Please note that the measured equilibrium pressure of CO is similar in both cases when the increase of the heat of adsorption begins, about 20 Pa.

In summary, although the results by microcalorimetry and CO TPD experiments obtained with CZA1 are not in good agreement, all results of the experiments using ZnO-containing samples indicate an influence of the SMSI between Cu and ZnO on the adsorption of CO. The microcalorimetric results are not fully understood yet, but there are indications that the heat of adsorption of CO on copper is lowered after the CO pretreatment and that the measured increase of the heat of adsorption may be due to the adsorption on oxygen vacancies in the ZnO. The presence of oxygen vacancies after a strongly reducing pretreatment is also mentioned in literature [2, 3, 5]. Further experiments are needed for an interpretation of the microcalorimetric results.

4.5 Conclusions

The results obtained using CA1 and CA2 confirm the absence of SMSI between copper and alumina. The differences found in the comparison of the results after hydrogen reduction and after CO pretreatment are only small compared to those in the case of ZnO-containing samples. The observed differences can be explained without considering an influence of the support.

All experiments using ZnO-containing samples show that the adsorption of CO on copper is strongly influenced by the SMSI between copper and ZnO. The TPD and FTIR results are in

qualitative agreement with theoretical studies in literature. The microcalorimetric experiments are not fully understood, but there are indications for a lowered heat of adsorption of CO on copper. The measured increase of the heat of adsorption may be due to CO strongly bound to oxygen vacancies in the ZnO.

In summary, the results obtained after CO pretreatment in the present contribution together with those measured after hydrogen reduction in ref. [8] support the dynamic alloying model proposed by Grunwaldt et al. [2] for ZnO-containing copper catalysts.

Acknowledgments

Financial support by the Deutsche Forschungsgemeinschaft within the Collaborative Research Center (SFB 558) ‘Metal-Substrate Interactions in Heterogenous Catalysis’ are gratefully acknowledged.

Bibliography

[1] J.B. Hansen, in: ”Handbook of Heterogenous Catalysis”, VCH Verlagsgesellschaft, Weinheim, 4 (1997) 1856.

[2] J.-D. Grunwaldt, A.M. Molenbroek, N.-Y. Topsøe, H. Topsøe, and B.S. Clausen, J. Catal., 194 (2000) 452.

[3] P.L. Hansen, J.B. Wagner, S. Helveg, J.R. Rostrup-Nielsen, B.S. Clausen, and H. Topsøe, Science, 295 (2002) 2053.

[4] H. Wilmer and O. Hinrichsen, Catal. Lett., 82 (2002) 117.

[5] J.B. Wagner, P.L. Hansen, A.M. Molenbroek, H. Topsøe, B.S. Clausen, and S. Helveg, J. Phys. Chem. B, 107 (2003) 7753.

[6] H. Wilmer, T. Genger and H. Hinrichsen, J. Catal., 215 (2003) 188.

[7] S.J. Tauster, S.C. Fung and R.L. Garten, J. Am. Chem. Soc., 100 (1978) 170.

[8] ”Part I: The reduced catalyst”, chapter 3.

[9] B. Bems, M. Schur, A. Dassenoy, H. Junkes, D. Herein, and R. Schlögl, Chem. Eur. J., 9 (2003) 2039.

[10] O. Hinrichsen, T. Genger and M. Muhler, Chem. Eng. Technol., 11 (2000) 956.

[11] H. Bielawa, M. Kurtz, T. Genger, and O. Hinrichsen, Ind. Eng. Chem. Res., 40 (2001) 2793.

[12] ”The combined application of microcalorimetry, TPD and FTIR spectroscopy”, chapter 2.

[13] B.E. Spiewak and J.A. Dumesic, Thermochim. Acta, 290 (1996) 43.

[14] H.G. Karge and W. Nießen, Catal. Today, 8 (1991) 451.

[15] J.C. Tracy, J. Chem. Phys., 56 (1972) 2748.

[16] J. Kessler and F. Thieme, Surf. Sci., 67 (1977) 405.

[17] P. Hollins and J. Pritchard, Surf. Sci., 89 (1979) 486.

[18] S. Vollmer, G. Witte and C. Wöll, Catal. Lett., 77 (2001) 97.

[19] G.E. Parris and K. Klier, J. Catal., 97 (1986) 374.

[20] P. Hollins, Surf. Sci. Rep., 16 (1992) 53.

[21] ”Part III: The state of the catalyst after methanol synthesis”, chapter 5.

[22] M. Kurtz, H. Wilmer, T. Genger, O. Hinrichsen, and M. Muhler, Catal. Lett., 86 (2003) 77.

[23] J. Greeley, A.A. Gokhale, J. Kreuser, J.A. Dumesic, H. Topsøe, N.-Y. Topsøe, and M. Mavrikakis, J. Catal., 213 (2003) 63.

[24] J. Shen, J.M. Hill, R.M. Watwe, B.E. Spiewak, and J.A. Dumesic, J, Phys. Chem. B, 103 (1999) 3923.

[25] E. Giamello and B. Fubini, J. Chem. Soc., Farraday Trans. 1, 79 (1983) 1995.

5 Part III: The state of the catalyst after methanol synthesis

Abstract

The adsorption of carbon monoxide was used to probe the state of copper after the synthesis of methanol. The investigated samples were binary and ternary catalysts containing copper, zinc oxide and alumina. All samples were pretreated under identical conditions resulting in reproducible states of the catalysts. A comparison of the results with a study on the same samples after hydrogen reduction shows that copper is reduced to its zero-valent state after methanol synthesis in the case of all investigated samples. The microcalorimetric results indicate that the adsorbed carbon monoxide reacted with adsorbates on the copper surface left from the synthesis of methanol.

5.1 Introduction

Copper catalysts are industrially used for the synthesis of methanol. These catalysts are ternary systems containing copper (Cu), zinc oxide (ZnO) and alumina (Al_2O_3) [1].

Numerous studies investigating these catalysts in situ under the conditions of methanol synthesis are found in literature, e. g. [2, 3]. Important questions are inter alia the state of copper during methanol synthesis and the reaction mechanism of the synthesis of methanol. Klier [4] proposed that copper species are incorporated into the ZnO in interstitial and substitutional sites. Nakamura and coworkers [5, 6, 7] reported that Cu(I) species are stabilzed under reducing conditions by ZnO_x species migrated onto the copper surface. Chinchen et al. [8] identified metallic copper as the active component in methanol synthesis and ZnO as inert support that stabilizes a high copper surface area. Askgaard et al. [9] presented a detailed kinetic model of the methanol synthesis based on surface science studies. The model includes the water-gas shift reaction and a route to formaldehyde as by-product. The main carbon source for the synthesis of methanol on copper is carbon dioxide. Carbon monoxide is part of the water-gas shift reaction which is important in order to remove water formed by the synthesis of methanol from

the copper surface thus keeping copper in a reduced state.

In this contribution, the adsorption of carbon monoxide on copper catalysts is studied by microcalorimetry, temperature-programmed desorption (TPD) experiments and Fourier transform infrared (FTIR) spectroscopy. The samples are pretreated by a reduction in hydrogen followed by the synthesis of methanol. The results in ref. [10] show that the applied techniques and the used equipment allow to study the samples in reproducible states with the different investigation methods. Results obtained with catalysts of different copper content are directly compared based on the classification of copper catalysts postulated by Hinrichsen and coworkers [11] .

5.2 Experimental

The investigated samples are binary and ternary catalysts containing copper, zinc oxide and alumina. The samples are identical to those in [10, 12]. The methods of preparation and characterization of the samples are described in detail elsewhere [13, 14, 15]. Table 5.1 summarizes the main characteristics of the samples.

Table 5.1: Characterization and catalytic data

Catalyst	CZA1	CZA2	CZ1	CA1	CA2
BET surface area (m^2/g_{cat})	73	-	64	51	124
Cu content (wt% CuO)	47	7	68	76	20
Specific amount of Cu surface atoms[a] (μmol/g_{cat})	513	134	513	176	139
Specific Cu surface area[b] (m^2/g_{cat})	21	6	21	7	6
Specific methanol production rate[c] (μmol/s g_{cat})	0.112	0.065	0.077	0.015	0.012
Turnover frequency (10^{-5} s^{-1})	21.8	48.5	15.0	8.3	9.0

[a]: Derived by N_2O RFC. [b]: Assuming that 1 m^2 of Cu surface area equals 24.41 μmol Cu atoms. [c]: Obtained at ambient pressure using 100 mg catalyst in synthesis gas (72 % H_2, 10 % CO, 4 % CO_2 and 14 % He) and a volumetric flow rate of 50 cm^3 min^{-1} (STP).

This contribution includes results from adsorption microcalorimetry, TPD experiments and FTIR spectroscopy in transmission mode. All investigations focus on the adsorption of CO on the copper catlysts.The experiments were performed analogous to the experiments in [10]. Only the pretreatment conditions were changed. The samples were first reduced by flowing hydrogen as described in [10]. The reduction was followed by 12 h of methanol synthesis in a

gas mixture consisting of 72 % H_2, 10 % CO, 4 % CO_2 and 14 % He at 498 K. All samples were flushed for at least 30 min at elevated temperatures in a flow of pure helium after the pretreatment. As an example, in fig. 5.1 the helium flushing is shown after methanol synthesis using CZ1. The flow rates were always fixed to 10 Ncm^3/min. All pretreatments were monitored by

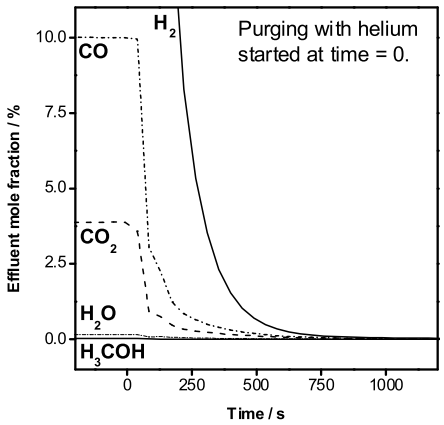

Figure 5.1: The mass spectrometry traces of hydrogen, carbon monoxide, carbon dioxide, water, and methanol recorded while flushing the sample with pure helium at 498 K. The flushing out of educts and products is almost completed after 10 min, but is carried on for at least 20 min more.

on-line mass spectrometry.

For the microcalorimetric experiments, 100 mg of the sieve fraction of 250–355 μm were pretreated in a specially designed pretreatment reactor, and then sealed in a pyrex capsule. Next, the pyrex capsule was placed into the sample receptacle of the microcalorimeter (C80 II, Setaram). The calorimetric set-up was degassed and the capsule was broken. After reaching thermal equilibrium (at 303 K) the adsorption measurement was started. Small doses of carbon monoxide were subsequently admitted to the sample, and while the heat of adsorption was measured calorimetrically, the amount of adsorbed species was measured volumetrically. In order to test the reversibility of the observed processes the sample was evacuated overnight and the experiment was repeated. The employed measurement technique was adopted from the pioneering work by Spiewak and Dumesic [16]. The technique allows to investigate air-sensitive samples unimpaired by poisoning. A detailed description of the experimental procedure and the set-up is given elsewhere [17].

The TPD experiments were carried out in a stainless steel U-tube reactor connected to a flow set-up. Typically, 100 mg of the sieve fraction of 250–355 μm were investigated *in situ*, directly after the pretreatment. The samples were cooled from room temperature to 78 K in a flow of a 10 % CO/He mixture and afterwards heated to 450 K in a flow of ultra-pure He. The desorption of CO into the stream of helium was monitored by on-line mass spectrometry. The coverage dependence of the CO desorption was investigated by varying the initial coverage. This was achieved by heating the samples to 450 K in two steps, i. e. after dosing CO the sample was first heated to $T_{1st\ step}$ (275, 300, 325, 350, and 375 K) again cooled to 78 K, and finally heated to 450 K. The experimental conditions and the set-up are fully described elsewhere [17].

The infrared spectroscopy experiments were performed using a modified transmission IR cell designed by Karge et al. [18] in a Nicolet Nexus FTIR spectrometer. The cell was connected to a sample pretreatment section and a CO dosing system. The investigations were carried out using wafers of an area of about 2 cm^2 and a mass of less than 50 mg. After the pretreatment the wafer was brought into the IR beam and spectra (250 scans, resolution: 2 cm^{-1} in the region 800 – 6000 cm^{-1} were recorded. The pressure of CO was varied stepwise between 0–100 Pa (0, 0.5, 1, 2.5, 5, 10, 20, 40, 80, 100 Pa and evacuation), in order to investigate the adsorption of CO as a function of coverage. Details about the experimental conditions and the set-up are given elsewhere [17].

5.3 Results

The heat of adsorption was measured calorimetrically using the samples with a high copper content (CA1, CZ1 and CZA1). Fig. 5.2, 5.3 and 5.4 show the results (left: differential heat of adsorption; right: adsorption isotherm), respectively. The results of the experiments after hydrogen reduction presented in [10] are included for comparison. Please note that the fractional coverages given in fig. 5.2, 5.3 and 5.4 are calculated using the specific amount of copper surface atoms as measured by nitrous oxygen reactive frontal chromatography for the sample in the state after hydrogen reduction, respectively. The sorption capacities of the three catalyst samples were differently influenced by the methanol synthesis. Compared to the state after hydrogen reduction, the equilibrium coverage of the sample at a pressure of 60 Pa of CO was significantly increased in the case of CA1 (20 %), nearly the same for CZ1, and signif-

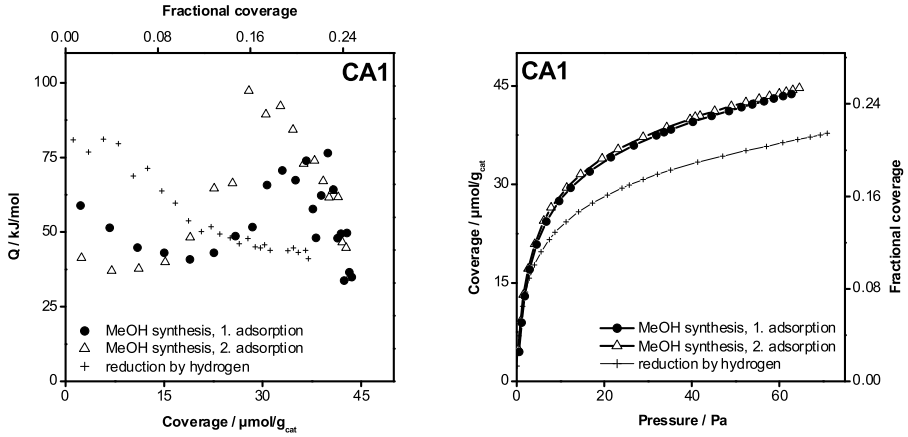

Figure 5.2: Differential heat of adsorption and adsorption isotherms of CO on CA1 at 303 K after methanol synthesis. The results obtained after hydrogen reduction are included for comparison. The sample was evacuated overnight between the first and the second adsorption experiment.

icantly decreased for CZA1 (12 %). The effect of the pretreatment on the heat of adsorption was roughly similar for the three catalysts. The initial value of the heat of adsorption indicated the complete reduction of the copper content of the samples. With increasing coverage the heat of adsorption increased, reached a maximum and steeply decreased. A comparison of the adsorption isotherms measured for the first and second adsorption indicates the reversibility of the adsorption processes, only in the case of CZ1 a slight decrease of the adsorption capacity (8 %) was observed. Differences of the measured heat of adsorption between the first and the second adsorption experiment indicate that not all processes are fully reversible and that the catalyst surface was changed after the first adsorption experiment.

In the case of CA1, the heat of adsorption (first adsorption) decreased with increasing coverage from 59–41 kJ/mol followed by an increase to a maximum of 77 kJ/mol. After reaching the maximum the heat dropped to 34 kJ/mol. The start of the increase can be correlated by the adsorption isotherm to a CO pressure of about 5 Pa. The maximum was measured at a CO pressure of about 32 Pa. The adsorption isotherm was exactly reproduced in the second adsorption experiment, while the measured heat of adsorption was different. The heat of adsorption first decreased from 41–37 kJ/mol, then increased to a maximum of 97 kJ/mol and dropped to

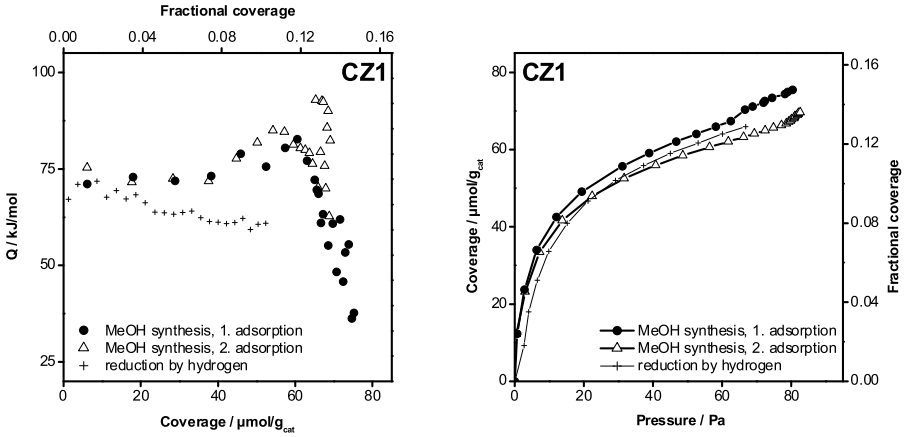

Figure 5.3: Differential heat of adsorption and adsorption isotherms of CO on CZ1 at 303 K after methanol synthesis. The results obtained after hydrogen reduction are included for comparison. The sample was evacuated overnight between the first and the second adsorption experiment.

45 kJ/mol. The start of the increase and the maximum are found at lower pressures.

The initial value of the heat of adsorption of CO on CZ1 was equal to the value measured after hydrogen reduction. The heat of adsorption stayed at a constant level for coverages up to 42 μmol/g$_{cat}$, but the heat measured in the second pulse is already increased compared to the results after hydrogen reduction. The plateau was followed by an increase to a maximum of 83 kJ/mol and a steep drop to about 35 kJ/mol. The increase started at a pressure of about 12 Pa of CO, and the maximum was measured at a pressure of about 45 Pa. The results concerning the heat of adsorption were reproduced in the second adsorption experiment with only small differences up to a coverage of about 65 μmol/g$_{cat}$. For higher coverages, the heat of adsorption varied irregularly between 93 and 63 kJ/mol. The adsorption isotherm measured in the second adsorption experiment indicates irreversibly adsorbed species.

In the first adsorption experiment using CZA1 the heat of adsorption was constant at about 52 kJ/mol in the coverage range 0–25 μmol/g$_{cat}$, then increased to 100 kJ/mol and finally decreased to 45 kJ/mol. The increase started at a pressure of about 4 Pa of CO, and the maximum was measured at a pressure of about 20 Pa. In the second adsorption experiment, the adsorption isotherm was exactly reproduced. The heat of adsorption was reproduced with small differ-

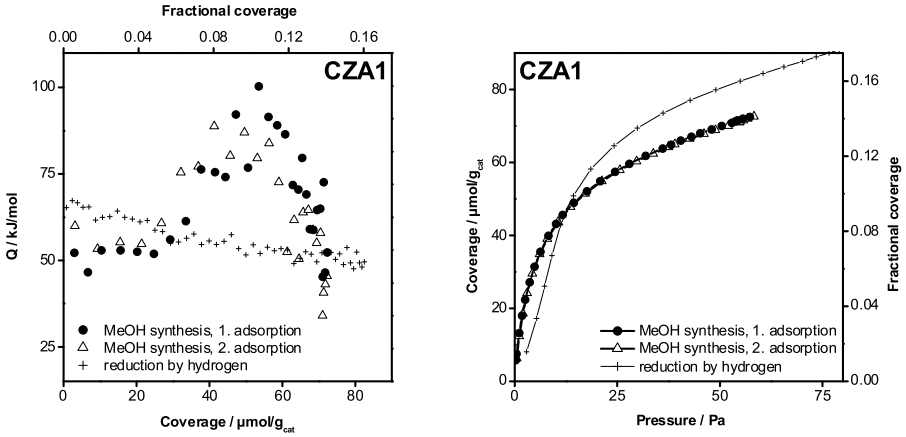

Figure 5.4: Differential heat of adsorption and adsorption isotherms of CO on CZA1 at 303 K after methanol synthesis. The results obtained after hydrogen reduction are included for comparison. The sample was evacuated overnight between the first and the second adsorption experiment.

ences. The initial heat of adsorption was slightly higher at 60 kJ/mol, decreasing to a plateau at 54 kJ/mol in the coverage range 10–24 μmol/g$_{cat}$. The heat of adsorption increased to a maximum of 89 kJ/mol and dropped then to 34 kJ/mol. The start of the increase and the maximum were measured at slightly lower pressures.

The CO TPD experiments were performed with CA1 and CZA1. Fig. 5.5 shows the results of the TPD experiments. The desorption from the fully covered copper surface of CA1 and CZA1 (experiment a and A) resulted in an intense peak at 112 K and a broad signal in the temperature range 200–400 K with a maximum at about 280 K and a shoulder at about 340 K, similar to the TPD profiles obtained after hydrogen reduction [10], respectively. For both samples the amount of desorbing CO in total was slightly lower compared to the experiments after hydrogen reduction.

In the case of CA1 and CZA1, the desorption from the partially covered surface resulted in a broad peak that is asymmetric to lower temperatures. The peak maximum was shifted to higher temperatures with decreasing initial coverage. Tab. 5.2 summarizes the results of the TPD experiments after methanol synthesis and hydrogen reduction. The final temperature of the first heating step is T$_{1st\ step}$. The temperature of the absolute peak maximum is T$_{max}$. The full

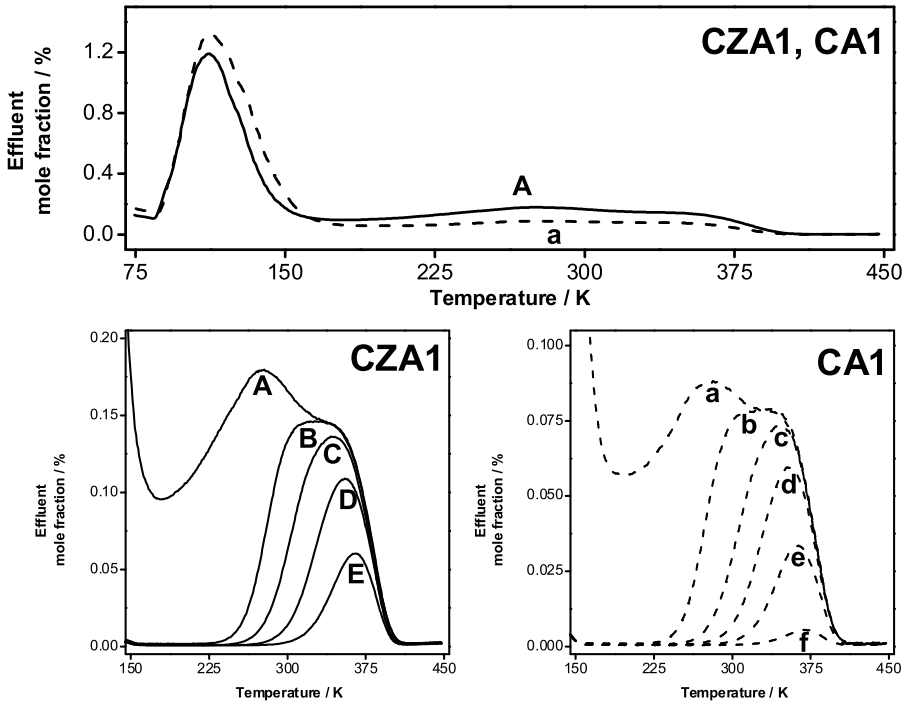

Figure 5.5: CO TPD spectra obtained with CZA1 and CA1 fully covered (A, a) and partially covered (B–E, b–f) with CO after methanol synthesis, $T_{1st\ step}$: 275 K (B, b), 300 K (C, c), 325 K (D, d), 350 K (E, e) and 375 K (f).

width at half maximum is given in the column FWHM. The initial coverages were calculated by integrating the mass spectrometry traces over the complete range of the desorption peak. The results obtained with CA1 after the two different pretreatment are essentially the same. In the case of CZA1 only small differences in T_{max} and FWHM were observed, while the initial coverages of corresponding experiments are significantly decreased after methanol synthesis.

The FTIR results of the experiments using CZA2 (42 mg/2 cm^2) and CA2 (31 mg/2 cm^2) are shown in fig. 5.6 and 5.7. In the case of CZA2, mainly one broad and to lower wavenumbers asymmetric band with a peak maximum at 2084 cm^{-1} was observed. The band became broader and more asymmetric with increasing coverage. Additionally, weak bands were observed below 2000 cm^{-1} at about 1685, 1228, 1246 and 1164 cm^{-1}. No bands appeared above 2100 cm^{-1}. Due to intense noise, no information can be gained in the range 1650–1300 cm^{-1} and above 2200 cm^{-1}. It is found that the main band at 2065 cm^{-1} decreased instantly when the cell was evacuated, while the weak bands changed only little in intensity. The baseline

Table 5.2: CO TPD data obtained with CZA1 and CA1

Sample	Peak	$T_{1st\ step}$ / K	$T_{max}{}^{a}$ / K	FWHM^{a} / K	coverage^{a} / μmol/g	$T_{max}{}^{b}$ / K	FWHM^{b} / K	coverage^{b} / μmol/g
CZA1	B	275	331	100	108	315	112	145
	C	300	345	77	78	346	87	102
	D	325	355	58	50	357	61	62
	E	350	365	46	24	367	49	33
CA1	b	275	338	104	58	336	98	58
	c	300	345	74	39	345	76	42
	d	325	354	57	25	355	59	27
	e	350	365	47	11	364	46	11
	f	368	373	43	2	369	40	2

^{a}: after methanol synthesis; ^{b}: after hydrogen reduction.

was shifted to lower extinction in the region below 1350 cm^{-1}. The spectrum of CA2 shows only one broad and asymmetric band with a peak maximum at 2091 cm^{-1}. The band became also broader and more asymmetric with increasing coverage. No additional bands were found. The baseline was shifted to higher extinction with increasing coverage in the region below 1350 cm^{-1}. Due to intense noise, no information can be gained in the range 1650–1350 cm^{-1} and above 2200 cm^{-1}.

5.4 Discussion

The TPD experiments and the FTIR experiments indicate that the copper content of the samples CZA1 and CZA2, and CA1 and CA2 are after methanol synthesis in nearly the same state as after hydrogen reduction [10], while the calorimetric results after these two pretreatments show some differences.

If the differences in the microcalorimetric results are not related to differences in the state of the copper content as indicated by the two other investigation methods, they must be related to differences in the state of the supporting material or to the presence of adsorbates left on the catalyst surface from the synthesis of methanol. The microcalorimetric results obtained with CZA1 and CA1 indicate that the effects on the heat of adsorption caused by the methanol synthesis pretreatment are not directly related to ZnO. The results obtained with CZA1 and CA1 are comparable, although CA1 is free of ZnO. A comparison of the microcalorimetric results

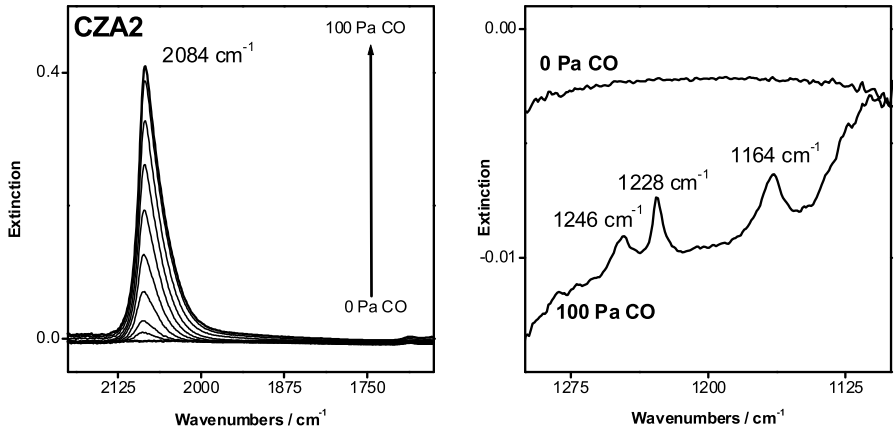

Figure 5.6: FTIR spectra obtained with CZA2 after after methanol synthesis in the pressure range of 0–100 Pa of CO and at room temperature. The left figure shows the range of the CO stretching vibration. The spectra are not corrected for a baseline or the gas phase CO vibrational contribution. The right figure shows the range below the CO stretching vibration for pressures of 0 and 100 Pa of CO.

obtained with CZA1 and CZ1 leads to the conclusion that the observed effects of the methanol synthesis might have the same cause, but the effects are less strong in the case of CZ1. The fact that CZ1 is affected by similar effects as CZA1, but already at much lower coverages is analogous to the findings after CO pretreatment [12]. After the CO pretreatment, the effects on the adsorption of CO on CZ1 were much stronger than the effects concerning CZA1. This was rationalized by the free copper surface areas of the samples. After CO pretreatment, the free copper surface area was significantly smaller in the case of CZ1 than in the case of CZA1, while the opposite was found after methanol synthesis. This might explain why CZA1 is more strongly influenced as CZ1. The assumption that the effect on the heat of adsorption after methanol synthesis is caused by only one process leads to the conclusion, that the effect is not directly related to the supporting material. However, the results obtained after hydrogen reduction [10] show that even in the absence of the strong metal-support interactions (SMSI) found after CO pretreatment [12], there are influences of the supporting material on the adsorption of CO on copper.

Askgaard et al. [9] presented a detailed kinetic model of the methanol synthesis. Possible adsorbates left on the catalyst surface from the methanol synthesis are atomic oxygen, formate,

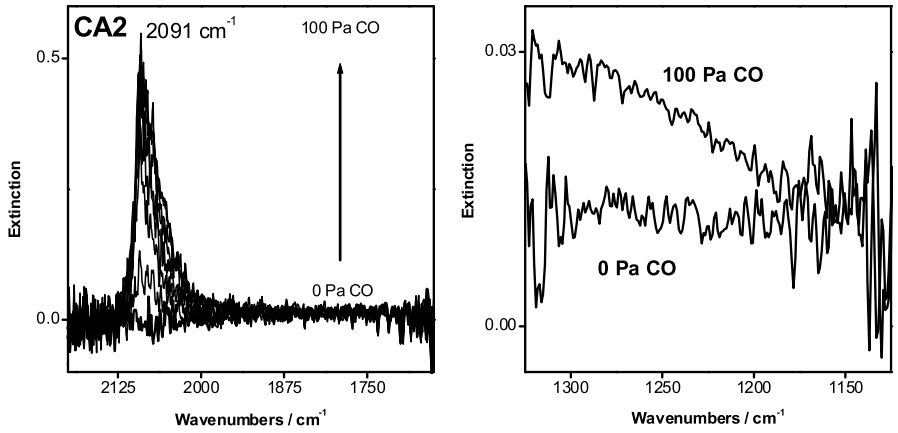

Figure 5.7: FTIR spectra obtained with CA2 after after methanol synthesis in the pressure range of 0–100 Pa of CO and at room temperature. The left figure shows the range of the CO stretching vibration. The spectra are not corrected for a baseline or the gas phase CO vibrational contribution. The right figure shows the range below the CO stretching vibration for a pressure of 0 and 100 Pa of CO.

formaldehyde and methoxy species. Formate, formaldehyde and methoxy species should be removed by the purging of the sample at elevated temperatures in pure helium that followed each pretreatment. Atomic oxygen is therefore the most likely adsorbate to be left on the copper surface. Unfortunately, the removal of the other adsorbate species can not be confirmed by the FTIR spectroscopy results in this contribution, as the noise is to intense in the region of the vibrational frequencies of these adsorbates (below 1100 cm^{-1}, above 2500 cm^{-1} and 1650–1350 cm^{-1}, [3, 19, 20].

A reaction of CO with atomic oxygen forming carbon dioxide, followed by desorption or the formation of carbonates on the supporting material can explain the increase of the heat of adsorption found in the experiments after methanol synthesis. The formation of carbon dioxide and carbonates are exothermic processes that would increase the measured heat and thus lead to an apparent increase of the heat of adsorption of CO. In the case of desorption of carbon dioxide without formation of carbonates, i. e. if carbon dioxide stays in the gas phase, the partial pressure calculated for CO would be overestimated, while the amount adsorbed CO would be calculated too low. This would result in a flattening of the shape of the adsorption isotherm. Such a flattening is not found in the calorimetric results after methanol synthesis. A comparison

of the adsorption isotherms obtained after methanol synthesis and hydrogen reduction leads to the conclusion, that the state of the copper is similar after both pretreatments. The observed differences can be correlated with changes of the free copper surface area. The measured heats of adsorption are in direct contradiction to this conclusion. This contradiction strongly indicates the occurrence of additional processes such as the formation of carbon dioxide and carbonates. The assumption that a certain pressure of CO or a certain surface coverage with CO has to be exceeded to start the reaction results in the conclusion that the initial heats of adsorption are measured correctly. The initial heats of adsorption are in all cases comparable to the initial heats measured after hydrogen reduction. This also confirms the conclusion drawn from the TPD data, the FTIR data and the adsorption isotherms that the copper content of the catalysts is completely reduced after methanol synthesis and in a state that is comparable to the state after hydrogen reduction.

An example of an adsorption process followed by a surface reaction is given in ref. [21]. The authors reported that a certain threshold pressure or surface coverage was needed to start the reaction. Therefore, the heat of adsorption was measured correctly at low coverage. At higher coverages the measured heat of adsorption increased significantly. Unfortunately, the authors did not include the measured adsorption isotherm.

The reaction of CO with adsorbed oxygen and the formation of carbon dioxide or carbonates are irreversible processes. Further investigations are needed to explain the apparent reversibility of the adsorption processes. It has to be considered that the samples are evacuated overnight between the adsorption experiments. Slow processes like the diffusion of atomic oxygen dissolved in the copper (subsurface or bulk) onto the copper surface thus restoring the initial coverage with oxygen could be the reason for the apparent reversibility.

In summary, the results show that the copper content of all investigated samples after methanol synthesis is in a state which is comparable to the state after hydrogen reduction. The microcalorimetric results are yet not fully understood, but a surface reaction of adsorbed carbon monoxide and atomic oxygen is a reasonable assumption. The classification of copper catalysts into three classes by Kurtz et al. [11] is supported by the presented results. The effect of the methanol synthesis pretreatment on all samples is generally the same, but significant differences between the samples of different classes are found by all investigation methods.

5.5 Conclusions

All results indicate that copper is completely reduced to its zero-valent state under the conditions of methanol synthesis, regardless of the supporting material. The SMSI observed after CO pretreatment of the ZnO-containing samples are not found after methanol synthesis.
There are strong indications for the presence of atomic oxygen on the copper surface after methanol synthesis. Atomic oxygen reacts with adsorbed carbon monoxide thus increasing the measured heat of adsorption. Further investigations are needed to explain the reversibility observed in the microcalorimetric experiments.
The results support the classification of copper catalysts postulated by Hinrichsen and coworkers [11].

Acknowledgments

Financial support by the Deutsche Forschungsgemeinschaft within the Collaborative Research Center (SFB 558) ‘Metal-Substrate Interactions in Heterogenous Catalysis’ are gratefully acknowledged.

Bibliography

[1] J.B. Hansen, in: ”Handbook of Heterogenous Catalysis”, VCH Verlagsgesellschaft, Weinheim, 4 (1997) 1856.

[2] M. Muhler, E. Törnqvist, L.P. Nielsen, B.S. Clausen and H. Topsøe, Catal. Lett., 25 (1994) 1.

[3] S. Bailey, G.F. Froment, J.W. Snoeck, and K.C. Waugh, Catal. Lett., 30 (1995) 99.

[4] K. Klier, Adv. Catal., 31 (1982) 243.

[5] I. Nakamura, T. Fujitani, T. Uchijima, and J. Nakamura, J. Vac. Sci. Technol. A, 14 (1996) 1464.

[6] I. Nakamura, T. Fujitani and T. Uchijima, and J. Nakamura, Surf. Sci., 400 (1998) 387.

[7] Y. Kanai, T. Watanabe, T. Fujitani, M. Saito, J. Nakamura, and T. Uchijima, Energy Convers. Mgmt, 36 (1995) 649.

[8] G.C. Chinchen, K.C. Waugh and D.A. Whan, Appl. Catal., 25 (1986) 101.

[9] T.S. Askgaard, J.K. Nørskov, C.V. Ovesen and P. Stoltze, J. Catal., 156 (1995) 229.

[10] ”Part I: The reduced catalyst”, chapter 3.

[11] M. Kurtz, H. Wilmer, T. Genger, O. Hinrichsen, and M. Muhler, Catal. Lett., 86 (2003) 77.

[12] ”Part II: The state of the catalyst after pretreatment in CO”, chapter 4.

[13] B. Bems, M. Schur, A. Dassenoy, H. Junkes, D. Herein and R. Schlögl, Chem. Eur. J., 9 (2003) 2039.

[14] O. Hinrichsen, T. Genger and M. Muhler, Chem. Eng. Technol., 11 (2000) 956.

[15] H. Bielawa, M. Kurtz, T. Genger, and O. Hinrichsen, Ind. Eng. Chem. Res., 40 (2001) 2793.

[16] B.E. Spiewak and J.A. Dumesic, Thermochim. Acta, 290 (1996) 43.

[17] ”The combined application of microcalorimetry, TPD and FTIR spectroscopy”, chapter 2.

[18] H.G. Karge and W. Nießen, Catal. Today, 8 (1991) 451.

[19] S.G. Neophytides, A.J. Marchi and G.F. Froment, Appl. Catal., A, 86 (1992) 45.

[20] J.F. Edwards and G.L. Schrader, J. Phys. Chem., 89 (1985) 782.

[21] J. Shen, J.M. Hill, R.M. Watwe, B.E. Spiewak, and J.A. Dumesic, J, Phys. Chem. B, 103 (1999) 3923.

6 Conclusions

Microcalorimetry, TPD experiments and FTIR spectroscopy were successfully combined in the investigation of the adsorption of CO on copper catalysts after various pretreatments. The results obtained after hydrogen reduction confirm that all samples were pretreated under identical conditions. All presented data show clearly that applying identical pretreatment conditions leads to reproducible and fully comparable states of the catalyst surface. To the best of our knowledge, the present contribution shows for the first time results measured by fundamentally different investigation methods concerning samples both prepared and pretreated under identical conditions.

All results support a grouping of copper catalysts in three classes as proposed by Hinrichsen and co-workers [1]: ternary catalysts consisting of Cu, ZnO and Al_2O_3 ($Cu/ZnO/Al_2O_3$), binary catalysts consisting of Cu and ZnO (Cu/ZnO), and binary ZnO-free catalysts such as Cu supported on Al_2O_3 (Cu/Al_2O_3). After a specific pretreatment samples of one class showed similar behavior in the adsorption of CO, while all three classes were differently influenced by the pretreatment conditions. The interaction of copper catalysts with hydrogen was not significantly influenced by the supporting material [2, 3], while a strong influence of the catalyst support on the adsorption of CO was found after all applied pretreatment conditions.

After hydrogen reduction the copper content of all samples was completely reduced to its zero-valent state. The copper surfaces were clean and free of adsorbates, but the FTIR results suggest that there was a significant amount of defect sites. The initial heat of adsorption of CO was lowered significantly by the presence of ZnO. Catalysts containing alumina showed higher fractional coverages for a given pressure of CO. Although ZnO influences the adsorption of CO, the effects observed after hydrogen reduction cannot be classified as SMSI as described by Tauster et al. [4].

SMSI between copper and ZnO can be clearly seen in the results after CO pretreatment. The results support the dynamic alloying model presented by Grunwaldt et al. [5]. The free copper surface area of ZnO-containing samples was drastically decreased due to Zn and O species migrated onto the copper surface. The microcalorimetric results showed that the initial heat of adsorption of CO was lower than after hydrogen reduction, but the heat increased with increas-

ing coverage. The increase of the heat of adsorption can be rationalized by Zn and O species on the copper surface or by oxygen vacancies in the supporting ZnO providing sites with higher heat of adsorption. The population of these sites seems to be a slightly activated process. The TPD data give no indication of an increase of the heat of adsorption with increasing coverage. Compared to the state after hydrogen reduction, the state of copper in Cu/Al_2O_3 samples can be described as completely reduced with less surface defects, as indicated by all investigation methods.

The data measured after methanol synthesis show that copper was completely reduced to its zero-valent state although the copper surface was partly covered with atomic oxygen. The atomic oxygen reacted with adsorbed CO and resulted in the formation of carbon dioxide and carbonates. The observed reversibility of the adsorption of CO can be rationalized by the existence of a second oxygen species. This second species can restore the consumed atomic oxygen on the copper surface. The results show that the SMSI observed after CO pretreatment of the ZnO-containing samples play only a small or even no role under the methanol synthesis conditions of the present study.

In summary, the results support the classification of copper catalysts proposed in ref. [1] and the dynamic alloying model presented in ref. [5]. SMSI between copper and ZnO were observed after CO pretreatment but not after hydrogen reduction or methanol synthesis. Copper was partly covered by atomic oxygen after methanol synthesis but was in a completely reduced state.

More investigations are needed for a thorough understanding of the increase of the measured heat of adsorption after CO pretreatment. The exact role of ZnO under these conditions has not yet been determined. The increase of the fractional coverage in the presence of alumina observed after hydrogen reduction also needs further inquiry. At last, the observed reversibility of the adsorption of CO after methanol synthesis is not yet understood.

Bibliography

[1] M. Kurtz, H. Wilmer, T. Genger, O. Hinrichsen, and M. Muhler, Catal. Lett., 86 (2003) 77.

[2] H. Wilmer and O. Hinrichsen, Catal. Lett., 82 (2002) 117.

[3] H. Wilmer, T. Genger and H. Hinrichsen, J. Catal., 215 (2003) 188.

[4] S.J. Tauster, S.C. Fung and R.L. Garten, J. Am. Chem. Soc., 100 (1978) 170.

[5] J.-D. Grunwaldt, A.M. Molenbroek, N.-Y. Topsøe, H. Topsøe, and B.S. Clausen, J. Catal., 194 (2000) 452.

Appendix:
A detailed description of the adsorption microcalorimetry set-up and its operation

6.1 Introduction

The most direct way to study the strength of the interaction between adsorbed species and the adsorbent is to measure the heat of adsorption by microcalorimetry. Adsorption is a spontaneous process and is therefore generally an exothermic process. The heat evolved during the process is the heat of adsorption. The heat of adsorption can be determined as integral heat of adsorption or as differential heat of adsorption. The integral heat of adsorption q^{int} is defined by eq. (6.1):

$$q^{int} = \frac{Q}{n_{ads}} \tag{6.1}$$

Q is the total amount of heat evolved during the adsorption of the complete amount n_{ads} of the adsorptive on the adsorbent. The differential heat of adsorption q^{diff} is related to q^{int} according to eq. (6.2).

$$q^{diff} = \frac{\partial q^{int}}{\partial n_{ads}} \tag{6.2}$$

The differential heat of adsorption can be measured by giving small amounts Δn_{ads} of adsorptive subsequently to the adsorbent. Depending on the experimental conditions, the heat Q equals a change in the internal energy U or a change in the enthalpy H. If the adsorption experiment is carried out in a twin-type calorimeter (e. g. a Tian-Calvet calorimeter), the measured heat Q equals the change in the enthalpy H as the work of expansion is compensated:

$$q^{diff} = \Delta H_{ads}^{diff} \tag{6.3}$$

A comprehensive description of the thermodynamics of adsorption can be found in ref. [1].
Tian-Calvet microcalorimeters are differential scanning calorimeters (DSC). A DSC consists of two thermally decoupled measuring cells, the sample cell and the reference cell. The measured signal is a differential signal measured between the two cells. Thus, all external influences on the measurement are compensated as they should have the same effect on the sample and

reference cell (assumed the cells are completely identical). Tian-Calvet microcalorimeters can be further classified as heat flux DSCs. In a heat flux DSC, a defined exchange of the heat to be measured with the environment takes place via a well-defined heat conduction path with given thermal resistance. The primary measurement signal is a temperature difference, which determines the intensity of the heat exchange. The temperature difference ΔT can be converted into the heatflow $\dot{Q}$ using a calibration factor k (eq. (6.4)) [2].

$$\dot{Q} = k \times \Delta T \tag{6.4}$$

6.2 Experimental

6.2.1 Connectors and flanges

The choice of connectors used to build a vacuum system is a very important issue, as the connectors have a strong influence on the tightness of the system. Three types of connectors are present in the adsorption microcalorimetry set-up: Swagelok fittings, Cajon VCR fittings, and CF flanges. A KF flange is only used to connect a rough vacuum pump to the set-up.

6.2.1.1 Swagelok connectors and tube fittings

Swagelok connectors and tube fittings are used to connect two metal tubes or a metal tube to a special part like a valve. A Swagelok fitting consists of a body, a nut and two ferrules. Fig. 6.1 shows its working mechanism: The elements of the fitting are depicted in cross-section prior to make-up: the fitting nut (top), the back ferrule (left), the front ferrule (center), and the fitting body (right). The tube wall section is shown below the ferrules and body. During make-up, the front ferrule (center) is driven into the body of the fitting (right) and the tube (bottom) to create primary seals (tube and body), while the back ferrule (left) hinges inward to create a strong grip on the tube. A Swagelok tube fitting can be reusable until the edge of the front ferrule nearly reaches the edge of the back ferrule. If that happens, cut a small segment of the tube with the ferrules and use a pair of new ferrules.

Swagelok tube fittings are specified according to the outer diameter (o. d.) of the used tube. Tube fittings for tubes of metric and fractional (inch) o. d. may not be interchanged. All metric tube fittings have a stepped shoulder on the body hex (fig. 6.2). Shaped fittings, such as elbows,

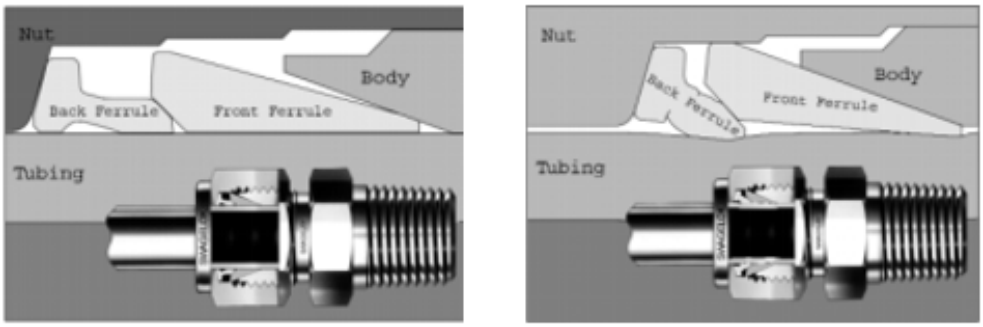

Figure 6.1: The Swagelok connection, before (left) and after (right) make-up [3].

crosses, and tees, are stamped MM for metric tubing instead of having a stepped shoulder.

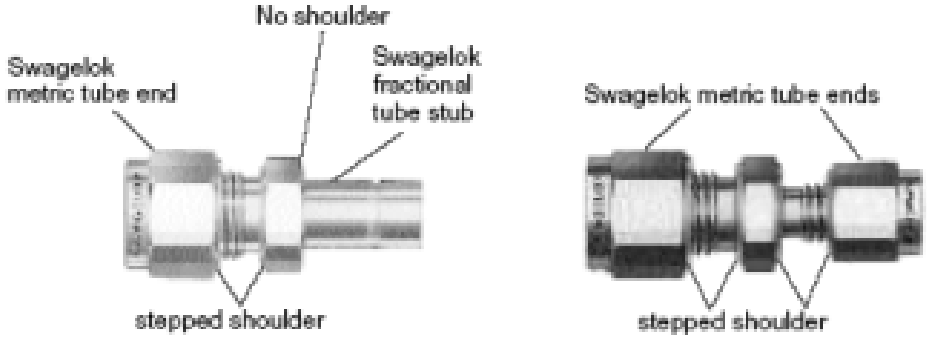

Figure 6.2: Metric and fractional (inch) fittings [3].

To install a new Swagelok tube fitting (for o. d. of less than 1 in. / 25 mm), insert the tubing into the Swagelok assembled tube fitting. Make sure that the tubing rests firmly on the shoulder of the tube fitting body and that the nut is finger-tight. Then mark the nut at the 6 o'clock position. While holding the fitting body steady, tighten the nut 1 1/4 turns to the 9 o'clock position (fig. 6.3). In the case of reusing a Swagelok tube fitting, just tighten it for 1/2 turn.

6.2.1.2 The Cajon VCR connection

A Cajon VCR connection consists either of two glands, a gasket, a female and a male nuts or a gland, a body, a gasket and a nut (fig. 6.4). Many special parts, e.g. valves or pressure gauges, are commercially available with Cajon VCR connectors. The sealing face of the glands is polished very finely and demands careful handling. Even light scratches will cause a poor seal. Several types of gaskets are available: made of stainless steel, of silver-plated stainless steel

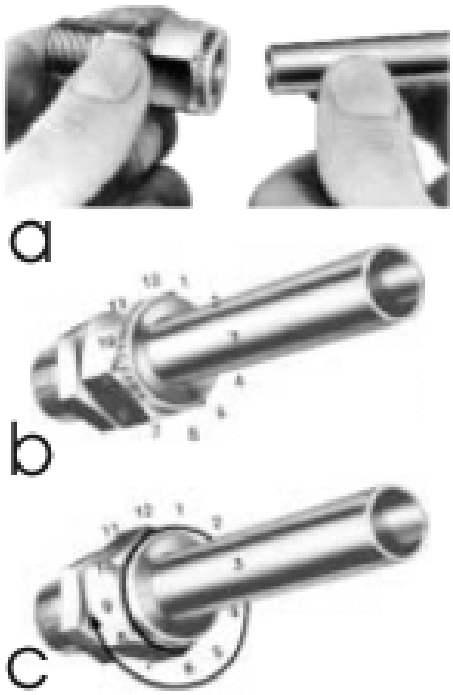

Figure 6.3: Installation of a Swagelok tube fitting [3].

and of copper. Harder gaskets give lower leakage rates, while the use softer gaskets avoids damaging of the sealing faces during assembly. Therefore, copper gaskets should be used for frequently disassembled connections.

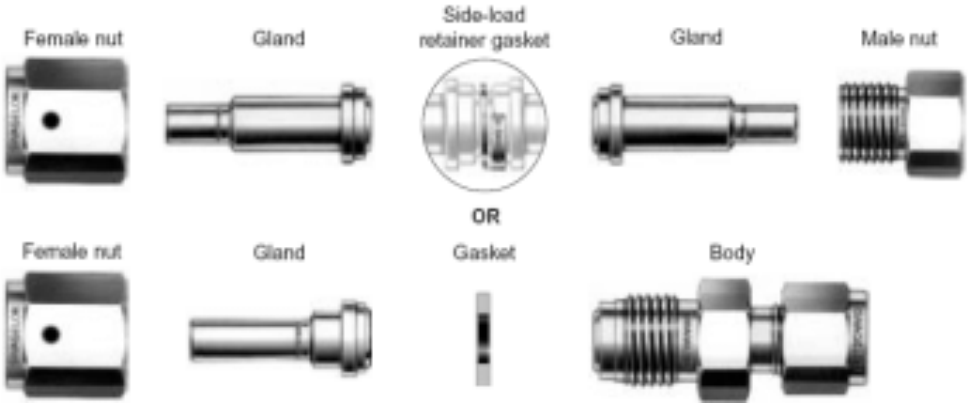

Figure 6.4: The Cajon VCR connection [4].

The installation instruction for a Cajon VCR connection is shown in fig. 6.5. First, place a suitable gasket between the glands and tighten the two nuts finger-tight. The gasket may not be touched without gloves, otherwise it will be contaminated by skin fat and cause a poor seal.

Then use two wrenches to tighten the connection (45 ˚ using stainless steel gaskets, 90 ˚ using copper gaskets).

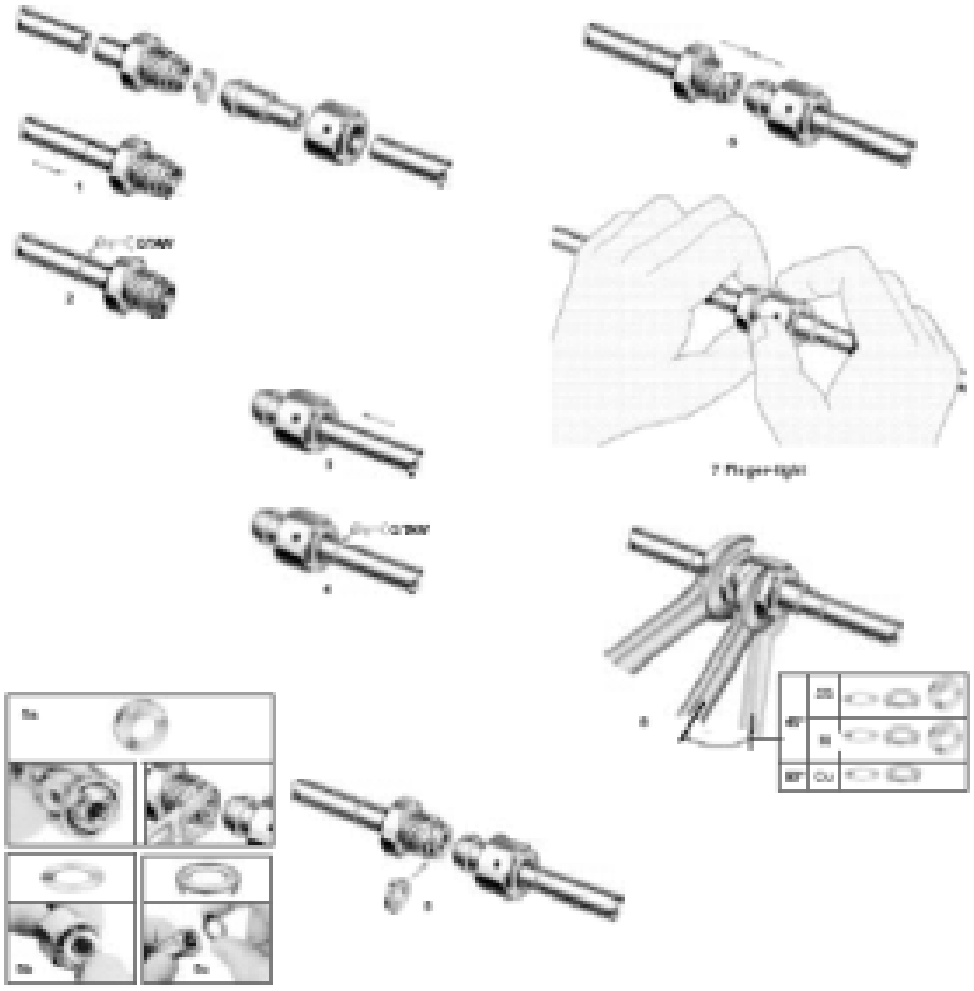

Figure 6.5: The installation of a Cajon VCR connection [4].

6.2.1.3 The CF Flange

CF flanges are used at frequently disassembled positions, especially if tubes of a large diameter are connected. To connect two CF flanges, place a copper gasket against the knife edge seal of one of the flanges, preferably the flange most likely to hold and support the gasket from falling. With the gasket in place arrange the second flange in a suitable bolt hole orientation. After hand tightening all bolts, use two wrenches for further tightening. The tightening process must be done gradually in 1/4 to 1/2 turns of each bolt in an alternating crisscross pattern until

the desired torque ratings have been achieved (fig. 6.6). This procedure ensures a reliable seal due to even gasket compression and deformation. CF flanges are suitable even for vacuum conditions below 1x10^{-11} Pa. They can be opened and closed for over 5000 times without a loss in sealing quality.

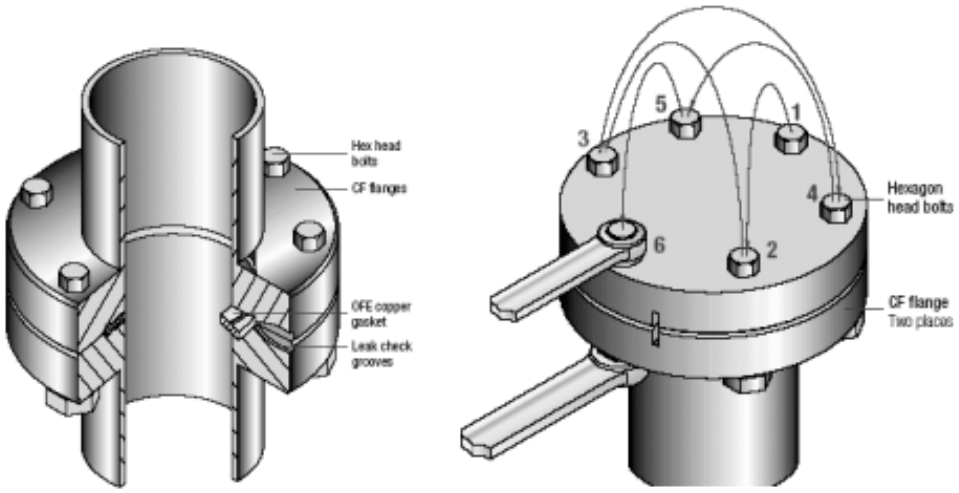

Figure 6.6: The installation of a CF connection [5].

6.2.1.4 The KF Flange

A KF connection consists of two flanges, a viton O-ring with a centering ring and a clamp (fig. 6.7). It can quickly be connected and disconnected . The viton O-ring can be re-used and has a long life time. KF flanges can be used under vacuum conditions down to 1x10^{-6} Pa.

6.2.2 The adsorption microcalorimetry set-up

The adsorption microcalorimetry set-up consists of the microcalorimeter itself, a volumetric dosing section in a thermostated box, additional heating elements, the microcalorimetric measuring cells, a gas supply, two vacuum pumps, and two pressure gauges. It is mainly used to measure the heat of adsorption of CO.

The set-up is based on the works of Spiewak and Dumesic [1]. The main modification is the change from glass to stainless steel as construction material. The complete set-up is metal-tightened and made of components suitable for ultrahigh vacuum (UHV) conditions. The set-up is also thermostated and suitable for experiments above room temperature. A schematic

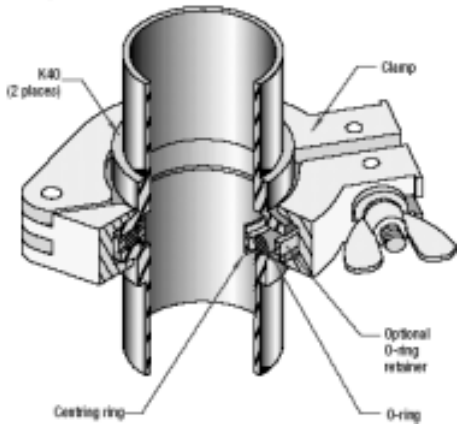

Figure 6.7: The KF connection [6].

diagram of the set-up is shown in fig. 6.8. Fig. 6.9 is a photography of the front side of the set-up, the photography in fig. 6.10 shows the personal computers used for data logging and controlling the set-up, and the rack that houses the turbomolecular pump and several pressure displays.

6.2.2.1 The microcalorimeter

The central piece of the set-up is the calorimeter itself. It is a commercially available Tian-Calvet heat-flux microcalorimeter (Setaram C80 II). It can be operated from room temperature up to 573 K. The Tian-Calvet sensor gives a high calorimetric resolution of 0.1 μW and a low detection limit of 2–5 μW. The high sensitivity of the calorimeter is needed to detect the usually low heats evolved during adsorption processes. Fig. 6.11 shows a schematic diagram of a Tian-Calvet sensor. The sample cell and the reference cell are surrounded by thermopiles connecting the cells with the calorimetric block. The thermopiles consist of many thermocouples connected in series. The voltage generated by a thermopile is a function of the number of joined thermocouples. The resulting voltage can be used to measure the mean temperature difference between each cell and the calorimetric block. As the calorimetric block is considered to have a constant temperature profile, the temperature difference between the cells can be measured by measuring the thermopiles in difference. The high sensitivity of a Tian-Calvet sensor is due to the amplifying effect of the thermopiles and due to the fact that the thermopiles are the main heat conducting path. Thus, the amount of heat lost undetected is minimized.

The complete calorimeter consists of the calorimetric block (including the sensor) in an insulat-

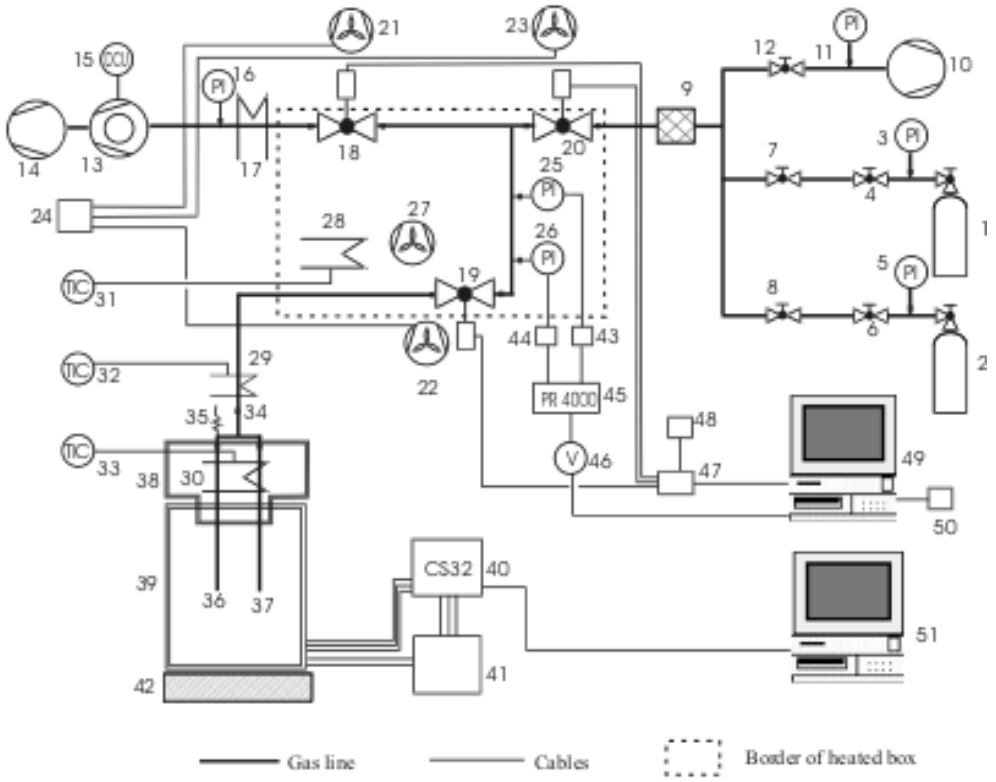

Figure 6.8: The adsorption microcalorimetry set-up; 1: CO gas bottle; 2: nitrogen gas bottle; 3 + 5: pressure gauges; 4 + 6: pressure reducing valves; 7, 8, 12: shut-off valves; 9: filter; 10: rotary vane pump; 11: Pirani gauge; 13: turbomolecular pump; 14: membrane pump; 15: control unit; 16: full range pressure gauge; 17: heating element; 18 - 20: pneumatic valves; 21 - 23: fans; 24: power supply unit; 25 + 26: Baratron pressure gauges; 27: heater fan; 28 - 30: heating elements; 31 - 33: temperature controllers; 34: CF flange; 35: linear motion feedthrough; 36 + 37: measuring cells; 38: insulation; 39: calorimetric block; 40: CS 32 controller; 41: power supply unit; 42: Linear motion device; 43 + 44: signal conditioners; 45: power supply and pressure display unit; 46: Voltmeter; 47: control unit; 48: power supply unit; 49 + 51: personal computer; 50: safety switch.

ing shell, a controlling unit (CS 32) and a power module. The CS 32 controller is used to operate the calorimeter via a personal computer. It controls the oven and the fan of the calorimeter and collects the measured data. The calorimetric block is mounted on a linear motion device as it has to be lowered to introduce or remove the calorimetric measuring cells (see fig. 6.9.).

6.2.2.2 The volumetric dosing section

The volumetric dosing section consists of three pneumatic valves (Swagelok SS-4BG-VCR-3C, see fig. 6.12) and two Baratron pressure gauges (MKS 121AA01000B and MKS 121AA00001B) connected by stainless steel tubing (1/4”). The pneumatic valves are connected

Figure 6.9: The adsorption microcalorimetry set-up (front view).

to the gas supply, the turbomolecular pump and the measuring cells. The internal volume of the dosing section is mainly determined by the volume of the two Baratron pressure gauges (ca. 15 cm^3 per gauge). The pneumatic valves are operated via solenoid valves. The solenoid valves are connected directly to the actuator of the pneumatic valves in order to minimize the opening time of the pneumatic valves. Helium is used as actuator gas for the same reason, due to its lower viscosity compared to compressed air. The helium is taken from the central gas supply of the laboratory. A pressure of about 0.6 MPa is needed to operate the pneumatic valves. Minimum opening times are typically 20 ms.

All parts of the dosing section contributing to the internal volume are placed in a thermostated box. Only the actuators of the pneumatic valves with the attached solenoid valves are placed outside of the box. The maximum working temperature of the solenoid valves is 321 K, while the parts in the box can be heated up to 418 K. Three fans are used to cool the solenoid valves if the temperature of the box is raised above 320 K (e.g. during degassing of the set-up, vide infra). If possible, the fans should not be operated during a calorimetric measurement as the flowing air disturbs the heat flow measurement.

Figure 6.10: The adsorption microcalorimetry set-up (personal computers and pressure displays).

6.2.2.3 Controlling the temperature of the set-up

A constant temperature profile of the set-up during a measurement is absolutely necessary as the amount of adsorbed gas is determined volumetrically. Therefore, the set-up includes several controlled heating units. The calorimetric block in the calorimeter is a controlled heating unit in itself. The parts of the measuring cells which are not in contact with the calorimetric block are thermostated by an additional heating unit that fits exactly into the upper part of the calorimeter (replacing part of the insulation). The volumetric dosing section is thermostated in an insulated box equipped with a fan and a heating element. The connection between the dosing section and the measuring cells is thermostated by a heating tape that can be easily detached for disconnecting the measuring cells. With exception of the calorimetric block each heating unit is controlled by a programmable temperature controller (Eurotherm 2416). The calorimeter includes a controller (Setaram CS32) that controls the temperature of the calorimetric block.

During an adsorption experiment, the temperature of the calorimetric block typically is set to 303 K, while the three additional heating elements are set to a slightly higher temperature

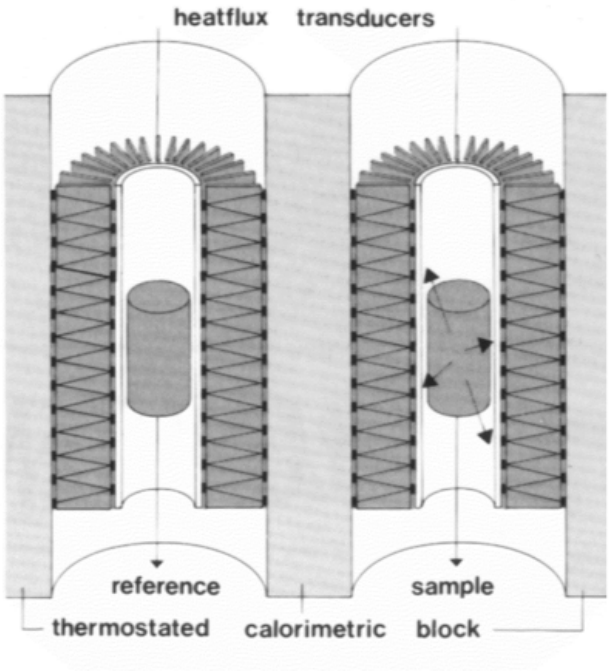

Figure 6.11: A schematic diagram of a Tian-Calvet sensor.

(313 K). A temperature difference of 10 K between the calorimetric block and the rest of the set-up has been found suitable to avoid measurement artifacts when the gas dose expands into the calorimetric cells. Prior to each adsorption experiment the complete set-up is degassed. During degassing all temperatures typically are set to 418 K. The temperature controllers of the calorimeter, the heating element fitted into the calorimeter and the heated box may be set directly from room temperature to 418 K, as these heating elements rise the temperature slowly without any overshooting. The temperature controller of the heating tape attached to the connection between the dosing section and the calorimetric cell may only be set stepwise and carefully to higher temperatures. The heating tape can produce fast temperature increases leading to a large overshooting. The temperature of the thermostated box may not be risen above 418 K, otherwise the Baratron pressure gauges will be seriously damaged.

6.2.2.4 The measuring cells

The microcalorimetric cells are shown in Fig. 6.13. They fit exactly into the calorimeter and the inset heating element (vide supra). The cells are designed as symmetrically and simply as possible. They are made of five parts: the central part is a tee piece with two double-

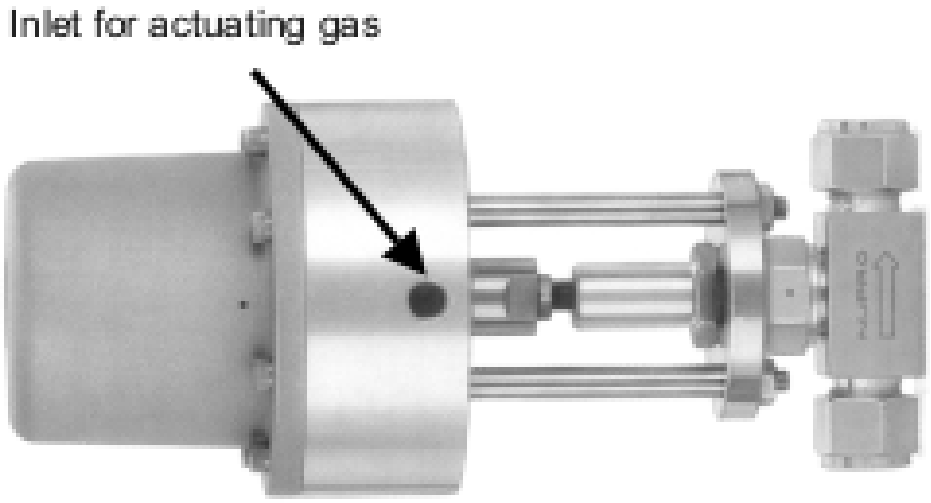

Figure 6.12: A pneumatic valve (Swagelok SS-4BG series).

sided DN40 CF vacuum flanges and one standard DN40 CF vacuum flange. Two identical receptacles for the sample and the reference sample are connected to the two double-sided flanges. A bellows-sealed linear motion feedthrough and a dummy resembling the form of the half-expanded feedthrough are connected to the other side of the flanges. The linear motion feedthrough can be used to crush a pyrex capsule in the sample receptacle via a steel rod. The standard flange is used to connect the cells to the volumetric dosing section. All parts of the cells are made of stainless steel and are UHV tight.

After a microcalorimetric experiment the cells are disconnected from the dosing section. To clean the sample receptacle, only the flange connecting the receptacle and the tee piece has to be opened.

6.2.2.5 The gas supply system

The gas supply system consists of two gas lines and a vacuum line. CO is used as probe molecule in the adsorption experiments. Nitrogen is used as inert gas, e. g. for the calibration of the volume of the dosing section or the measurement of the volume of the measuring cells. Nitrogen is preferable to helium, as nitrogen is more similar to CO in terms of thermal conductivity and viscosity. The vacuum line can be used to evacuate the gas lines or the dosing section.

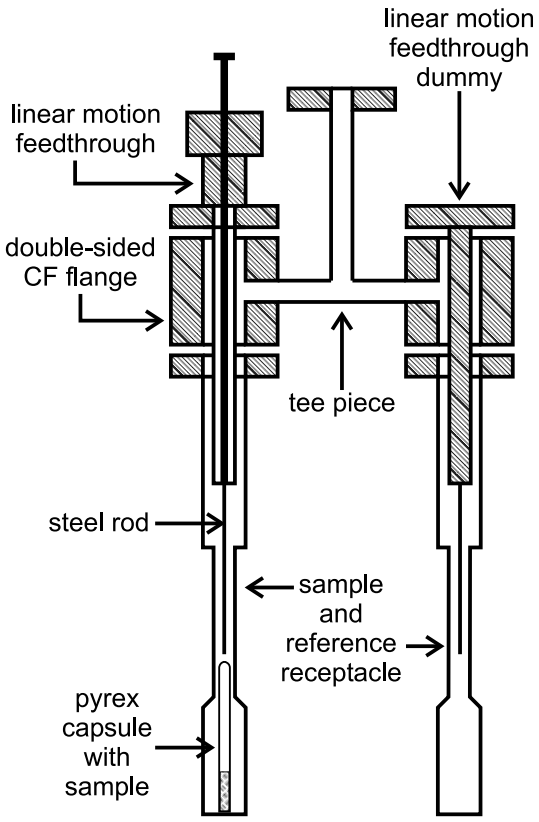

Figure 6.13: A schematic diagram of the microcalorimetric measuring cells.

Both gas lines consist of a gas bottle, a pressure reducing valve and a shut-off valve. The purity of the used gases is 99.997 % and 99.99990 % for CO and nitrogen, respectively. The 10 l CO bottle is stored in a vented gas cupboard equipped with an additional pressure reducing valve and a solenoid shut-off valve for safety reasons (fig. 6.14). The 50 l nitrogen bottle is fixed to the wall directly behind the set-up (fig. 6.15). The pressure of the two used gases should be set to low values (i. e. about 0 bar excess or 1 bar absolute) to allow the dosing of small gas quantities. The vacuum line is connected to a rotary vane pump. Fig. 6.16 shows a part of the gas supply system, i. e. the shut-off valves of the gas lines and the vacuum line, the Pirani pressure gauge of the vacuum line and the rotary vane pump. The gas supply is connected to the dosing section via a filter in order to prevent damaging of the pneumatic valves by dust particles.

Figure 6.14: The CO gas bottle stored in a vented gas cupboard.

6.2.2.6 The vacuum system

Two pumps are included in the set-up, a rotary vane pump and a turbomolecular pump. The rotary vane pump (Pfeiffer DUO 2.5) can be used to evacuate the gas lines, the dosing section, or the complete set-up. A final pressure of less than 2-5 Pa in the dosing section can be achieved using the rotary vane pump (depending on the experimental conditions). The rotary vane pump is also used to lower the pressure of helium in the process of sealing a pretreated sample (vide infra). The operation of the pump is monitored by a Pirani gauge. The turbomolecular pump (Pfeiffer TMP 071P) is used to evacuate the dosing section and the measuring cell to pressures below 10^{-5} Pa (UHV). The turbomolecular pump uses an oil-free membrane pump as backing pump. The operation of the turbomolecular pump is monitored by a full range pressure gauge (Pfeiffer PKR 251, 10^{5}–10^{-7} Pa).

In order to achieve UHV conditions, the connecting line between the dosing section and the turbomolecular pump is always thermostated at 348 K. Raising the temperature above 350 K will lead to severe damage of the full range gauge and the turbomolecular pump. To prevent severe damaging of the turbomolecular pump, the pneumatic valve between the dosing section and the turbomolecular pump may never be opened while the pressure in the dosing section exceeds 10 hPa. The turbomolecular pump should be switched off only for maintenance rea-

Figure 6.15: The nitrogen gas bottle at the backside of the set-up.

sons to prolong the lifetime of the pump. The exhaust ports of the rotary vane pump and the turbomolecular pump always need to be directly connected to the air ventilation system of the laboratory. Otherwise considerable quantities of carbon monoxide may flow into the atmosphere of the laboratory.

6.2.2.7 The Baratron pressure gauges

A Baratron pressure gauge is an absolute capacitance manometer of high accuracy (about 0.1 % of reading). It includes a signal conditioning unit that is part of the calibrated sensor. The sensor consists of rigidly attached capacitive electrodes on the reference side of a flexible metal diaphragm. Applied pressure changes the deflection of the diaphragm and thus produces a change in the distance between the electrodes and the metal diaphragm and the resulting capacitances. The capacity changes are converted into an AC voltage signal via a high impedance bridge circuit. The voltage signal is amplified and demodulated to give a stable 0-10 V DC output signal that is directly proportional to the applied pressure.

The set-up includes two Baratron pressure gauges, MKS 121AA01000B and MKS 121AA00001B, with a range of 0-100.00 kPa and 0-100.00 Pa respectively. The gauges are connected to a power supply and pressure display unit (MKS PR4000). The MKS PR4000 unit is connected to a personal computer via a voltmeter equipped with a RS 232 output (Voltcraft

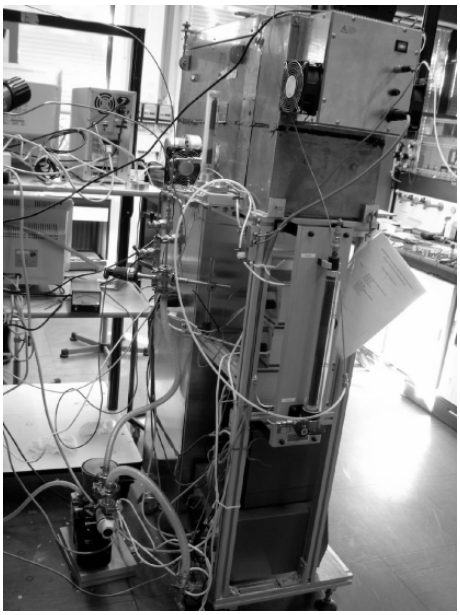

Figure 6.16: Part of the gas supply.

M-4660A). A program based on the software package LabView is used for data logging. Typically, the data measured by the gauge with the lower range is stored by the LabView program. The signal generated by a Baratron pressure gauge is sensitive to temperature changes. Therefore, reliable pressure measurement can only be achieved after reaching thermal equilibrium of all thermostated parts. Prior to each adsorption experiment the zero point of the pressure gauges needs resetting (when evacuated to pressures lower than 10^{-5} Pa and thermally equilibrated). The maximum working temperature of the gauges is 423 K and their burst pressure is 0.24 MPa, both values may never be exceeded.

6.2.3 Operation of the adsorption microcalorimetry set-up

6.2.3.1 Controlling the calorimeter via the Setsoft 2000 software

A detailed description of the Setsoft 2000 software is given in the user manual. A short description only of the parts necessary for a typical experiment is given below.

The Setsoft 2000 program can be run under Microsoft Windows NT. It is designed to control many different devices including the C80 II microcalorimeter. The Setsoft 2000 consists of five modules. Of these modules only the acquisition module is needed during a calorimetric experiment. After starting the programme and logging-in with a user name and password, the

acquisition module can be started by moving the mouse pointer to the left side of the active program window. A tool bar with five buttons will appear (see fig. 6.17). Pressing the first button will activate the acquisition module.

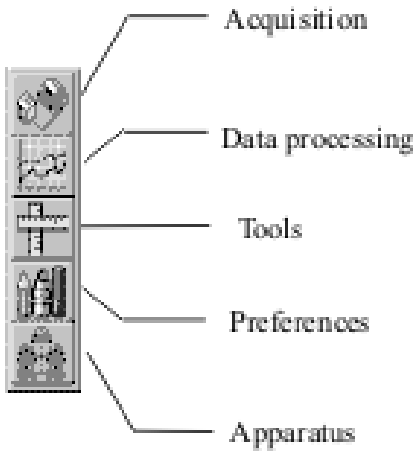

Figure 6.17: The toolbar of the Setsoft 2000 program.

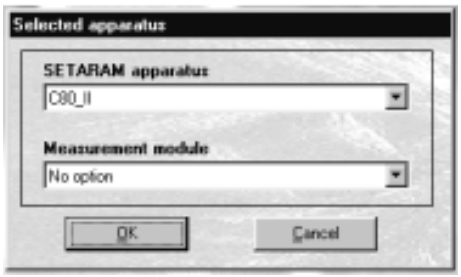

Figure 6.18: Choosing the measurement device.

To start an experiment click on the ”New Collection” menu item in the ”Collection” drop-down menu. In the appearing pop-up window (see fig. 6.18), select ”C80_II” in the ”SETARAM apparatus” drop-down menu and click the ”OK” button. In the appearing window (see fig. 6.19), the experiment has to be described. Only defining an experiment name that serves also as file name is mandatory, all other information is only used for file management. Each calorimetric experiments consists of at least one zone. Up to 15000 data points can be collected in each zone. Given a frequency of one data point per second, a zone lasts about 4 h. The duration of the complete experiment defines the number of zones of the experiment. Each zone consists of

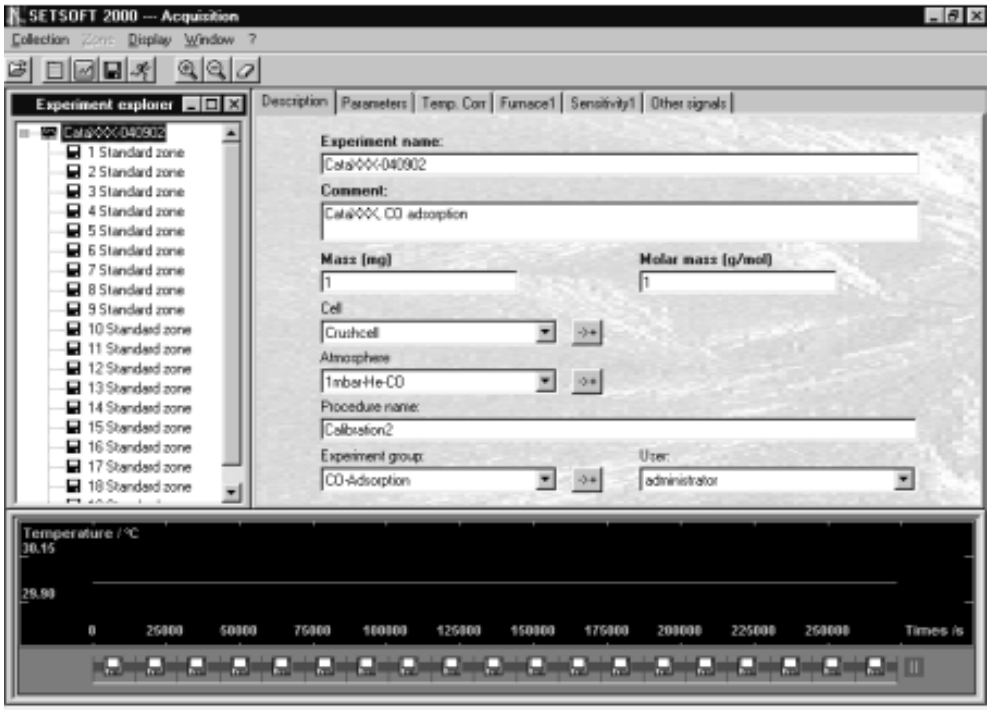

Figure 6.19: Description of the experiment.

at least one sequence. For each sequence, an initial and final temperature, a heating rate (max. 2 K/min) and the duration of the sequence have to be specified (see fig. 6.20). The calorimeter is equipped with a fan to increase the speed of cooling (rates up to 1 K/min can be achieved). The operation of the fan can be defined for each sequence (the switch controlling the fan has to be set to ”automatic”, see the C80 II user manual). Data storage can be activated for each zone. The acquisition time and thus the number of data points per zone (Standard: 4966 Points) has to be defined for each zone individually by filling in the desired values into the pop-up window (see fig. 6.21) appearing after clicking ”acquisition period” in the ”Zone” drop-down menu. To add a zone to an experiment just right-click the last zone in the ”Experiment explorer” area and select ”Add zone”, ”Standard zone”. A typical zone of an adsorption experiment consists of only one sequence in isothermal mode (initial=final temperature, 303 K) with 14400 data points, an acquisition period of 1 s, and a duration of 4 h in total. The first zone may differ, if degassing of the set-up is required.

After all the zones are set, click ”Start experiment” in the ”Collection” drop-down menu. To monitor the experiment in progress click ”Real-time drawing” in the ”Display” drop-down menu. The appearing window (see fig. 6.22) displays the temperature and heat flow change

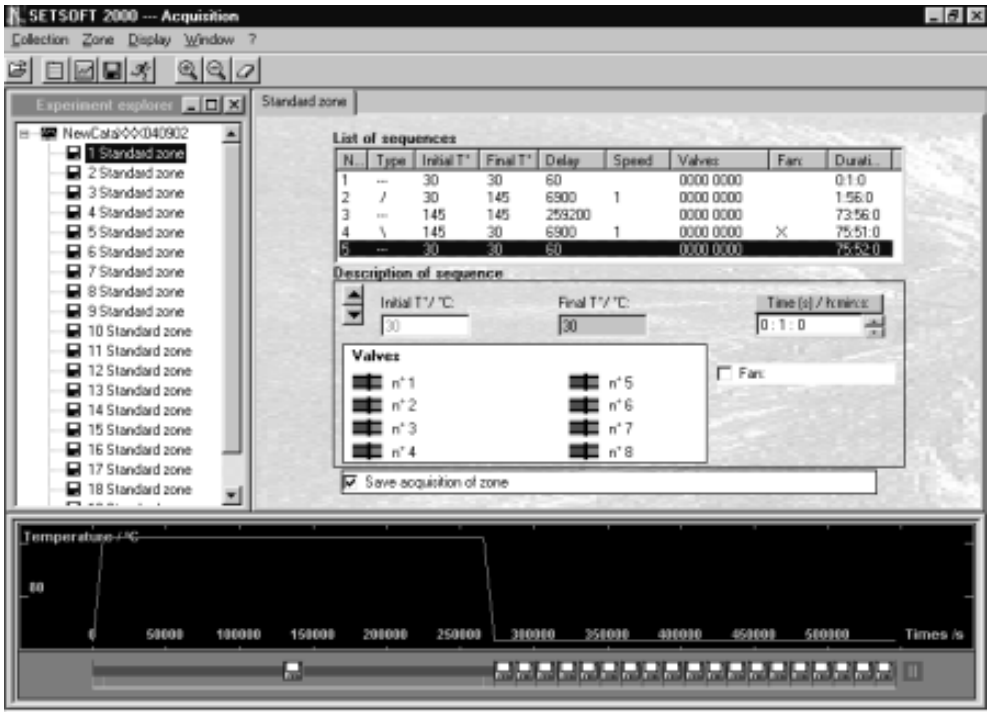

Figure 6.20: Experiments consist of zones and sequences.

versus time, typically for the last 10 min. The admission of gas into the measuring cells, i. e. the adsorption experiment itself should only be started after the heat flow reaches a stable baseline. This might take up to 1 h after starting the programmed experiment (due to the onset of the heating action). An additional window displays the parameters used for controlling the temperature of the calorimetric block (including the PID parameters, for an explanation refer to the C80 II user manual) and the measured signals. The window ”Manual programming” can be used to end an experiment manually by clicking the red square button in the upper right corner.

6.2.3.2 Controlling the volumetric dosing section via LabView programs

The valves of the volumetric dosing section can be operated via a program (Vent-Puls) based on the software package LabView. The program uses the parallel port (LPT1) to operate the valves. The pneumatic valves of the dosing section are actuated via solenoid valves that are connected to the parallel port via a controller box. The controller box is equipped with LED lights indicating the state of the solenoid valves, and switches that allow manual controlling of the solenoid valves. Fig. 6.23 shows the user interface of the Vent-Puls program. The program

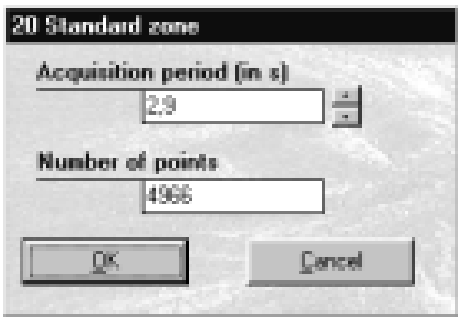

Figure 6.21: Defining the acquisition period and the number of data points for a zone.

can be used to control up to eight valves (V1-V8). The valves can be opened and closed by clicking on the grey square buttons. A red box indicates an opened valve. The valves can also be opened for a defined period. Clicking on the grey buttons labelled ”PULS” opens the valves for the time specified in the field next to the buttons, respectively. Pulses shorter than 0.20 s are to short to affect the pneumatic valves, although the solenoid valves are actuated. The program can be used to control the valves in an automatic mode using sequence files created with the LabView program ”Vent-Puls-Edit” (vide infra). To load a file click the button labelled ”Auto” and choose the appropriate file. The fields next to the ”Auto” button indicate the run time of each programmed step, its total duration, the number of the step and the total number of steps in the sequence file. Operating the volumetric dosing section in the automatic mode requires thorough knowledge of the complete set-up and careful planning. The turbomolecular pump can be easily damaged by running an unsuitable sequence file. If the valve connecting the turbomolecular pump to the volumetric dosing section is opened for a period longer than 0.20 s while the pressure in the dosing section exceeds 10 hPa, the pump will be irreversibly damaged. If the pressure exceeds 100 hPa even a short pulse might damage the turbomolecular pump. In such a case, lower the pressure using the rotary vane pump (not possible in the automatic mode). Fig. 6.24 shows the user interface of the Vent-Puls-Edit program. To create a file each step has to be programmed individually. A step is programmed by pressing the buttons analogous to using the Vent-Puls program. The duration of the step has to be defined in the field ”Zeit/sec”. The field ”Satznr.” shows the number of the present step. A step can be finished by pressing the ”replace” button. A step can be copied by pressing the ”C” button. A copied step can be inserted by pressing the ”I” button followed by the ”replace” button. If the ”replace” button was not pressed, all changes are lost when the step number is changed. The step number can

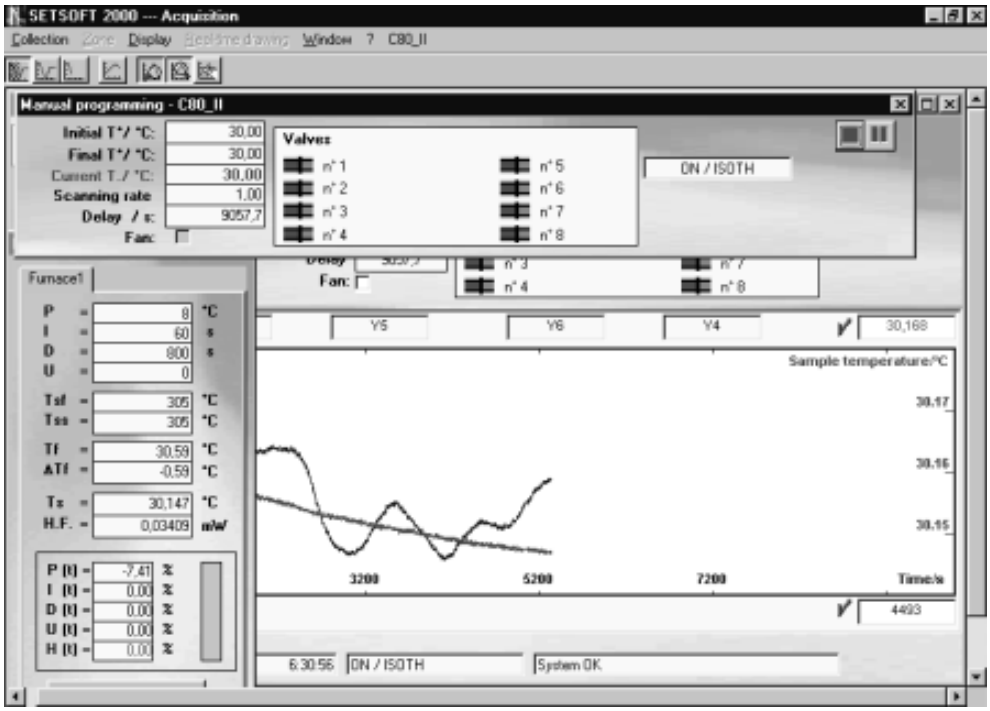

Figure 6.22: Monitoring of the experiment in the ”Real-time drawing” window.

be changed by pressing the buttons ”<” and ”>”. To save all steps up to the step displayed, press the ”write” button and define a file name. To alter an existing file press the ”read” button, choose the file, alter the steps as desired and save it (press the ”write” button).

A sequence file is stored as a simple text file. Each line represents a step and consists of 10 numbers. The first number indicates the state of all valves following a binary code. The next eight numbers are the numbers in the fields of the Vent-Puls-Edit user interface indicating the opening time for each valve (even if the valves are not operated in the pulse mode). The last number is the duration of the step. The binary code of the first number consists of 16 bits. The first eight bits indicate opened and closed valves (0=closed, 1=open), the last eight bits indicate which valves are operated in the pulse mode (0=closed, 1=pulse), e.g. a value of zero means all valves are closed, three means valve 1 and 2 are open, 1024 means only valve 3 is open (pulse mode).

A typical adsorption experiment consists of up to 50 dosing cycles. Each dosing cycle consists of up to 15 steps. The first step is the evacuation of the dosing section for about 120 s (the valve to the turbomolecular pump is open, the valves to the measuring cell and the CO gas line are closed). In the next step a small dose of CO is admitted into the dosing section by pulsing the

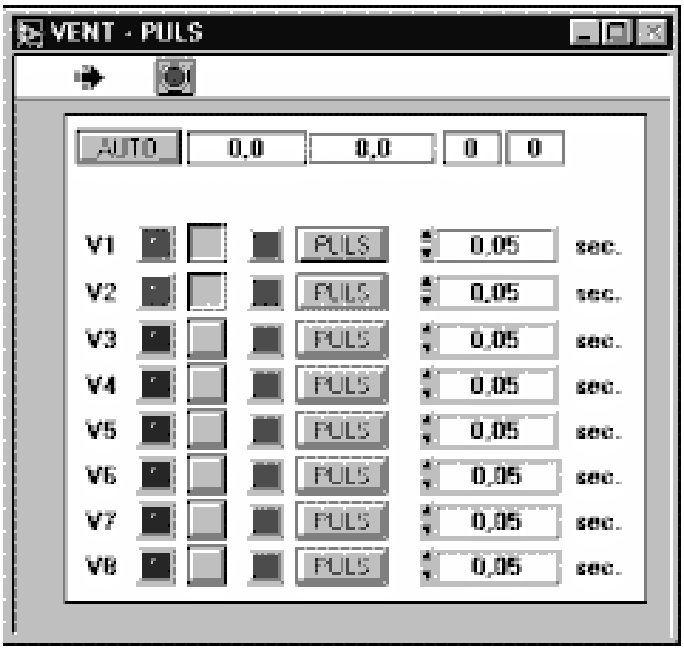

Figure 6.23: The user interface of the Vent-Puls program.

valve (0.20 s) connected to the gas line while all other valves are closed. If the resulting CO pressure is unsuitably high (but lower than 10 kPa) to lower the pressure in the dosing section the valve connected to the turbomolecular pump is pulsed several times (0.20-0.30 s) while all other valves are closed. When the pressure is in the desired range (typically 85-100 Pa), as the last step of the cycle the valve to the measuring cell is opened for about 1 h (with all other valves closed). A complete cycle should last exactly one hour.

The change of the pressure in the dosing section versus time can be monitored and stored by the LabView program ”M4660A-mV-C3”. Fig. 6.25 shows the user interface of the M4660A-mV-C3 program. The name of the data file to be stored can be defined after clicking the button ”New file”. Data is only stored when the button ”store” is activated. The field next to the button displays the run time of the stored file. The signal stored as a function of time is not directly the pressure, but the 0-10 V DC signal generated by the Baratron pressure gauge connected to the Voltmeter (vide supra). The data is stored in a two column ASCII file. The stored signal can be easily converted to a pressure value after importing the ASCII file into an Origin or Excel file. Depending on the range of the monitored Baratron pressure gauge, 10 V equals 100.00 Pa or 100.00 kPa.

A power failure of the computer that is used to run the LabView programs might have severe

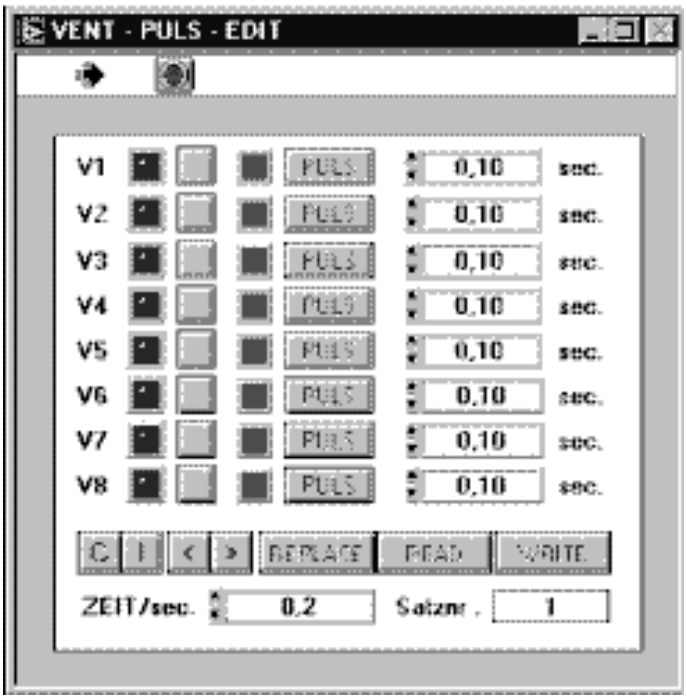

Figure 6.24: The user interface of the Vent-Puls-Edit program.

consequences. During the boot process of the computer, random signals are sent to the parallel port. If the box controlling the solenoid valves is attached to the computer during booting the valves of the dosing section will be actuated randomly. To prevent this a magnetic safety switch is inserted in the power supply of the computer. After a power failure, the valve controller is disconnected from the computer, the clearance button of the safety switch is pressed, and the computer is switched on. Only after starting the Vent-Puls program the valve controller is connected to the computer.

6.2.3.3 Volume calibration

As the amount of adsorbed species is volumetrically measured accurate values of the volumes involved is needed. Two volumes are of interest: the volume of the dosing section, and the volume of the measuring cells. The volume of the dosing section is constant. The volume needs to be calibrated only after parts of the dosing section are exchanged (e.g. for repairing or maintenance). The volume of the measuring cells is influenced by the amount of sample and the position of the linear motion feedthrough. This volume has to be measured after each adsorption experiment.

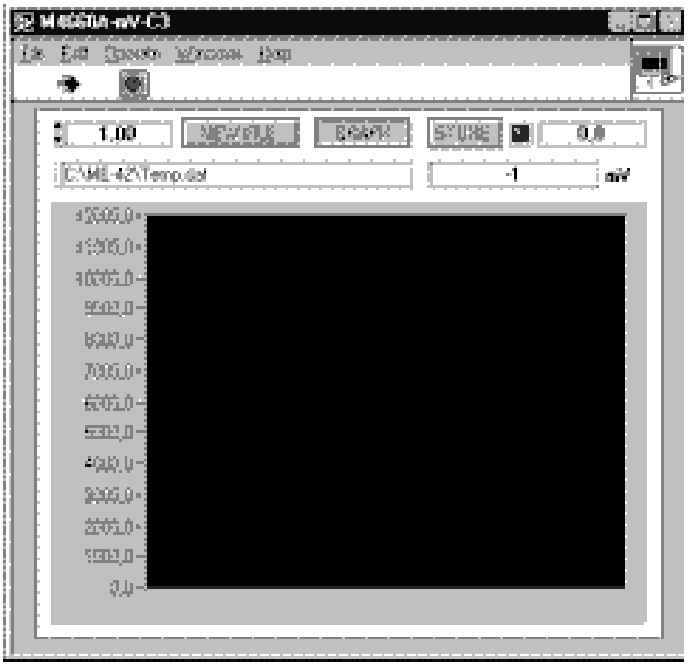

Figure 6.25: The user interface of the program ”M4660A-mV-C3”.

A special calibration chamber built of UHV tight components and a stainless steel cylinder of exactly known volume (V_C) are used to calibrate the volume of the dosing section. The cylinder can be placed into the calibration chamber. The calibration chamber is connected to the gas supply system and can be shut off by a valve (fig. 6.26). In order to determine the volume of the dosing section (V_{dose}), the dosing section, the empty calibration chamber and part of the tubing of the gas supply system are filled with nitrogen and the pressure (p_1) is recorded. The calibration chamber and the tubing together form the volume V_{out} (of unknown value). In the next step only V_{dose} is evacuated by the turbomolecular pump. In the last step the gas contained in V_{out} is expanded into the dosing section, and the pressure (p_2) is recorded. The ratio p_1/p_2 is calculated. The three steps are repeated several times to give a mean value of the pressure ratio with sufficient accuracy. The complete procedure is repeated with the cylinder placed in the calibration chamber, yielding a mean value of the ratio of the pressures p_1^* and p_2^*. Based on the universal gas equation, V_{dose} can be calculated according to eq. (6.5).

$$V_{dose} = \frac{V_C}{p_1/p_2 - p_1^*/p_2^*} \tag{6.5}$$

The main contribution to V_{dose} is the volume of the Baratron pressure gauges. V_{dose} is typically

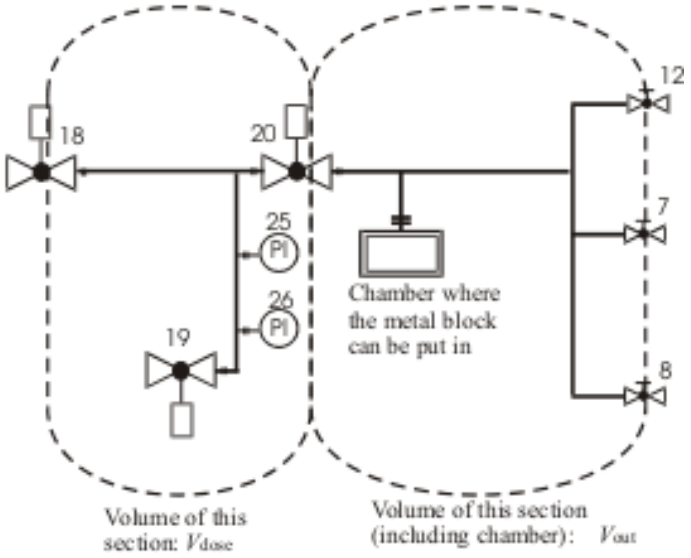

Figure 6.26: Calibration of the volume of the dosing section.

around 40 cm^3 when two Baratron pressure gauges are installed.

With V_{dose} known, the volume of the measuring cells V_{cells} is easily accessible. After evacuation of the complete set-up (first step), V_{dose} is filled with nitrogen (second step) and the pressure is recorded (p_1). In the third step the nitrogen contained in V_{dose} is expanded into V_{cells} and the pressure is recorded (p_2). The ratio p_1/p_2 is calculated. The three steps are repeated several times to give a mean value of the pressure ratio with sufficient accuracy. Based on the universal gas equation, V_{dose} can be calculated according to eq. (6.6).

$$V_{cells} = V_{dose} * (p_1/p_2 - 1) \tag{6.6}$$

Depending on the experimental conditions, it might be necessary to degas the complete set-up over night after the adsorption experiment and prior to the measurement of V_{cells}. Slowly desorbing adsorbate species would interfere with the measurement of V_{cells}.

6.2.3.4 Sample pretreatment

Typically, experiments are carried out using 100 mg of powder samples with a particle size of 250-355 μm. Pellets and powders consisting of too large particles are ground in an agate mortar. The resulting powder is sieved to obtain the desired particle size. Too fine powders are pressed to form tablets. The tablets are ground and the powder is sieved. The tools used for

grinding, pressing, and sieving have to be completely free of impurities which could change the adsorption behavior of the sample (e.g. catalyst poisons or compounds with a very high adsorption capacity).

Fig. 6.27 shows a schematic diagram of the specially designed pretreatment reactor used for the sample pretreatment. It consists of a glass-lined stainless steel U-tube, a pyrex-metal joint with a NMR tube welded to it, a manometer, and a tee piece with two CF flanges and one connection to a four-way valve. The reactor can be heated by a vertically moveable heating element. The complete reactor is metal-tightened. Samples are placed into the U-tube and kept in place by a quartz wool plug. To pretreat a sample, it is first weighed in a special glass container (see fig. 6.28). A quartz wool plug is put in the longer part of the U-tube and its position is adjusted to about 2 cm above the bending. The sample is put on top of the quartz wool plug using a small glass funnel (see fig. 6.28). The U-tube is connected to the lower CF flange of the tee piece and the VCR connector that is connected to the four-way valve. The pyrex-metal joint (equipped with a new NMR tube) is connected to the upper CF flange of the tee piece. The thermocouple used for the regulation of the heating element is fixed on the outside of the reactor at the position of the sample using metal wire. The heating element is lifted until the reactor touches the bottom of the heating element. The gas inlet and exhaust of the four-way valve, the thermocouple and the power supply of the heating element are connected to a suitable set-up and the four-way valve is opened. The desired pretreatment steps (e. g. reduction, oxidation or synthesis reactions) are carried out. After the pretreatment the reactor is purged with helium and cooled down to room temperature. The heating element is lowered and the four-way valve is closed. The complete reactor is disconnected from the set-up. The reactor is turned vertically by 180°. The pretreated sample falls into the pyrex tube while the quartz wool plug stays in the U-tube. The gas inlet and exhaust of the closed four-way valve are connected to the rotary vane pump of the microcalorimetry set-up. The pressure of helium in the reactor is lowered to 200–500 hPa by shortly opening the four-way valve. Using a small torch fuelled by liquid gas, the pyrex tube is welded to yield a sealed capsule of 95 mm length containing the pretreated sample in helium. The sealed capsule is finally placed into the sample receptacle of the measuring cells. All pretreatment procedures that can be applied to samples in a standard U-tube reactor can be carried out in the pretreatment reactor (except for high pressure treatments due to the glass part). Before the next sample pretreatment can be carried

out a new pyrex tube has to be welded to the glass-metal joint.

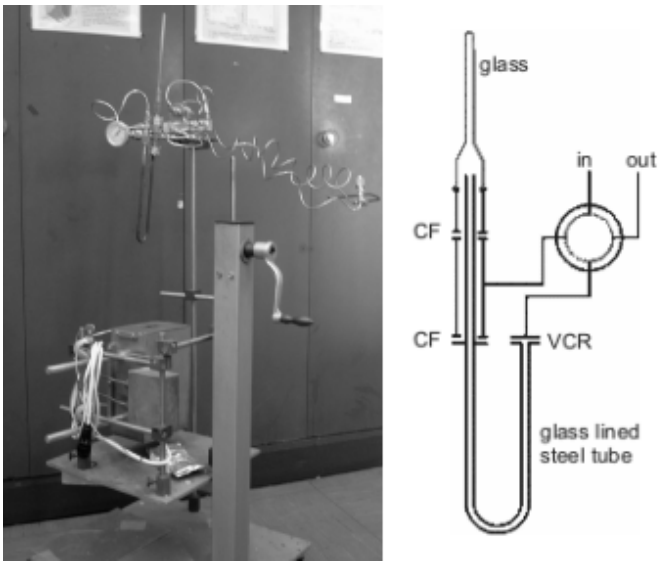

Figure 6.27: The pretreatment reactor.

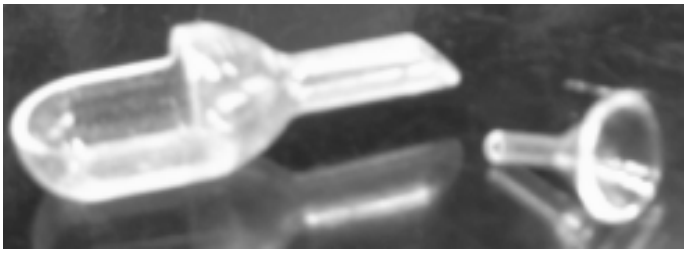

Figure 6.28: The special glass container and glass funnel.

6.2.3.5 Measurement of heats of adsorption

Prior to the measurement itself, the measuring cells containing the sealed pyrex capsule are put into the calorimeter and connected to the dosing section. The calorimeter has to be lowered down completely to introduce the measuring cells. To connect the measuring cells to the dosing section, the calorimeter has to be lifted until the CF flanges to be connected nearly touch. A copper gasket is placed between the flanges and the flanges are connected. The heating tape used to thermostat the connection between the calorimetric cells and the dosing section is put in place. A thick layer of insulating material is wrapped around the heating tape and the connection. In the next step the complete set-up is degassed for at least 72 h under static vacuum

conditions at elevated temperatures (418 K). Before the valve connected to the turbomolecular pump is opened, the set-up is first evacuated using the rotary vane pump. After degassing the calorimeter is cooled to 303 K, while the rest of the set-up is cooled to 313 K. The fans cooling the solenoid valves are switched off and the leakage rate is measured. The leakage rate is derived from the measured increasing rate of the pressure under static vacuum conditions and the volume of the dosing section and the microcalorimetric cells (app. 100 cm^3). After measuring the leakage rate the set-up is evacuated for several minutes. While only the valve connecting the volumetric dosing section and the measuring cells is opened the pyrex capsule is crushed via the linear motion feedthrough. The complete set-up is evacuated and then filled with nitrogen at a pressure of about 80–95 Pa. When the recorded heatflow signal shows a stable baseline the adsorption experiment itself is started. Typically, about fifty doses of CO are admitted to the sample while the heatflow and the pressure are recorded. When the experiment is finished (no further detectable heatflow or an equilibrium pressure of more than 80 Pa of CO) the complete set-up is degassed overnight under static vacuum conditions at room temperature. After degassing the volume of the measuring cells is measured using about twenty doses of nitrogen (vide supra). After the measurement of the cells volume the sample may be removed or a second adsorption experiment is started to investigate the reversibility of the adsorption processes. All valves should be closed when the sample is removed, and the set-up should be filled with nitrogen (not with CO).

6.3 Data processing

The collected pressure and heatflow data is best processed using the software Origin (Micro-Cal) and Excel (Microsoft). While the pressure data is directly stored in an ASCII format the heatflow data needs to be exported from the Setsoft 2000 software.

To export data from the Setsoft 2000 software click the ”Data processing” button in the tool bar (see fig. 6.17). The appearing window contains the newest collected experiment (see fig. 6.29). Any experiment may be opened by clicking the ”open” menu item in the ”Experiment” drop-down menu. Each zone has to be opened in an own window. The signals to be displayed and exported have to be added to the window by ”drag&drop” actions. Right-click on the desired signal and drop it into one of the fields labelled ”Y1”–”Y6”. The run-time of the zone is always

assigned to the x-axis. To export the zone in the active window click the ”export” menu item in the ”Zone” drop-down menu. In the appearing window (see fig. 6.30) define a file name, select an ASCII file format (typically ”fixed length”), click ”ASCII in file”, and select the signals to be exported (time and heatflow). The type of the decimal separator and the number of figures can be individually defined for each signal after clicking the ”format” button. The file is exported after clicking the ”OK” button.

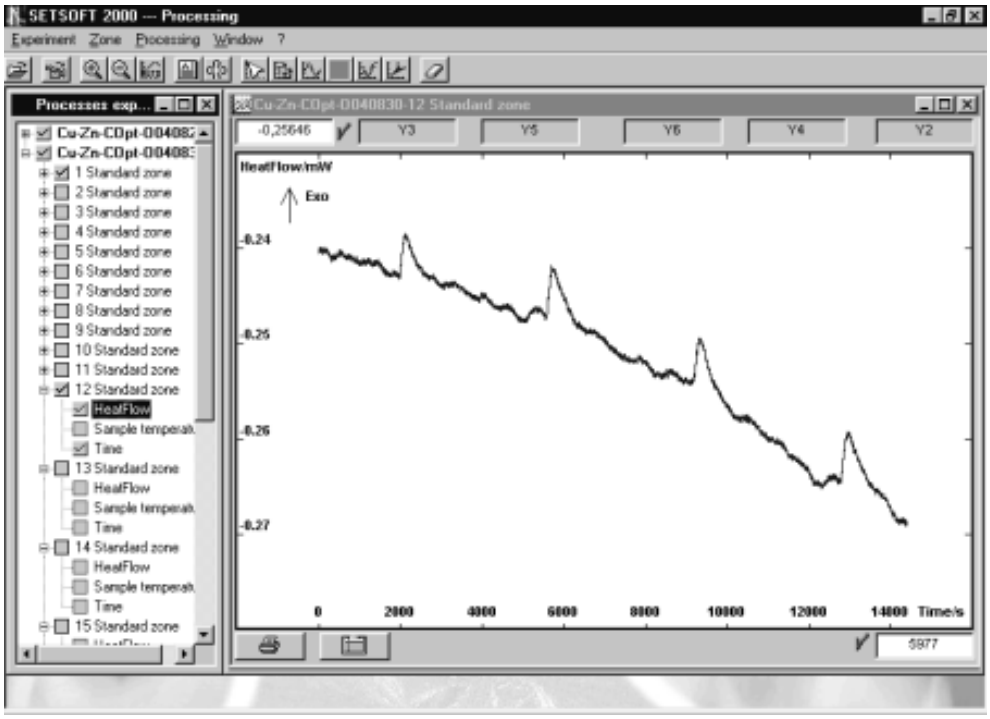

Figure 6.29: Processing an experiment.

6.3.1 Calculation of the adsorption isotherm

The adsorption isotherm is calculated from the collected pressure data only using an excel spreadsheet. The spreadsheet includes a template that shows directly the adsorption isotherm. The equations in the spreadsheet are based on the following considerations.

The measured pressure is the total pressure in the set-up, either in the volumetric dosing section alone or in the dosing section and in the measuring cells. It consists of two partial pressures (see fig. 6.31): the partial pressure of CO and the partial pressure of inert gas (nitrogen). The partial pressures of nitrogen and CO and the amount of CO adsorbed for each dose can be calculated directly from the collected pressure data.

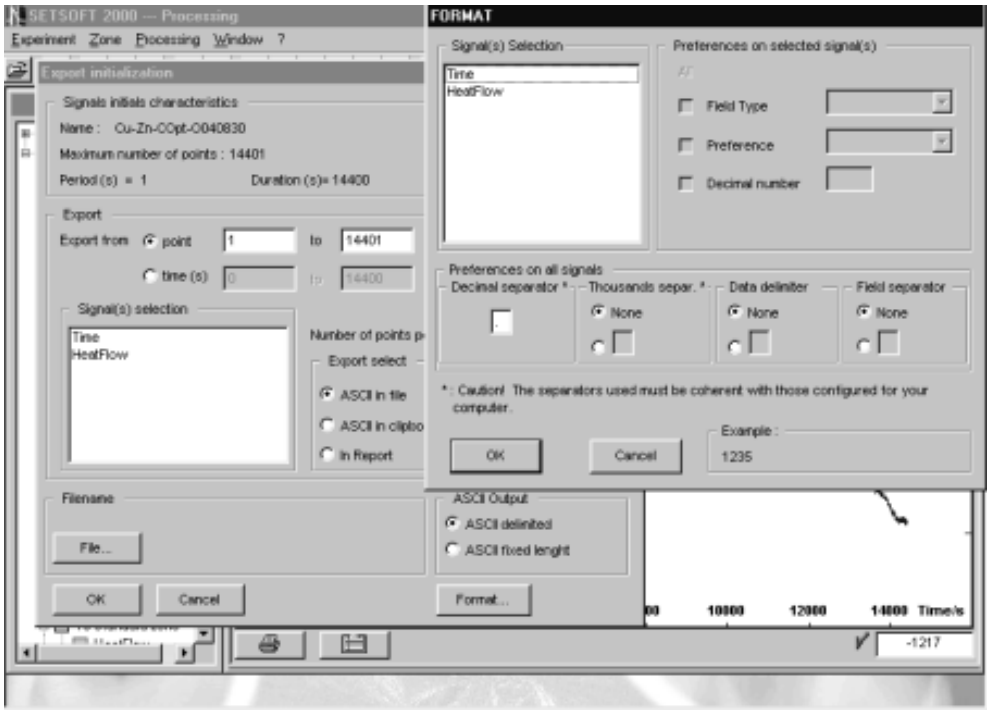

Figure 6.30: Exporting a zone.

p_{0a} is the pressure of nitrogen after the crushing of the capsule at t_{0start} in the dosing section and the measuring cells. p_{0b} is the pressure of nitrogen at t_{0end}, the increase with time is due to leakage. p_{1a} indicates a pressure of CO in the dosing section higher than the measuring range of the used Baratron pressure gauge (>100 Pa). After several pulses of the turbo pump valve the pressure of CO in the dosing section is lowered to a suitable pressure p_{1b} of 85–100 Pa. p_{1c} is the total pressure of nitrogen and CO after opening the valve connecting the dosing section to the measuring cells. p_{1d} is the total pressure of nitrogen and CO in the dosing section and the measuring cells at t_{1end}, the difference between p_{1c} and p_{1d} is due to the adsorption of CO and leakage. Based on the universal gas equation the partial pressures of nitrogen and CO can be calculated if the volume of the dosing section and the measuring cells, and the leakage rate are known. The volume of the dosing section is calibrated prior to the experiment, the volume of the measuring cells is measured after the experiment, and the leakage rate (Lrate) can be calculated from the increase of the pressure between t_{0start} and t_{0end}.

The amount of nitrogen in the set-up originates from the nitrogen filled into the measuring cells after the crushing of the capsule and from leakage. The amount of nitrogen is lowered with each dose (due to the evacuation of the dosing section between two doses) and increases

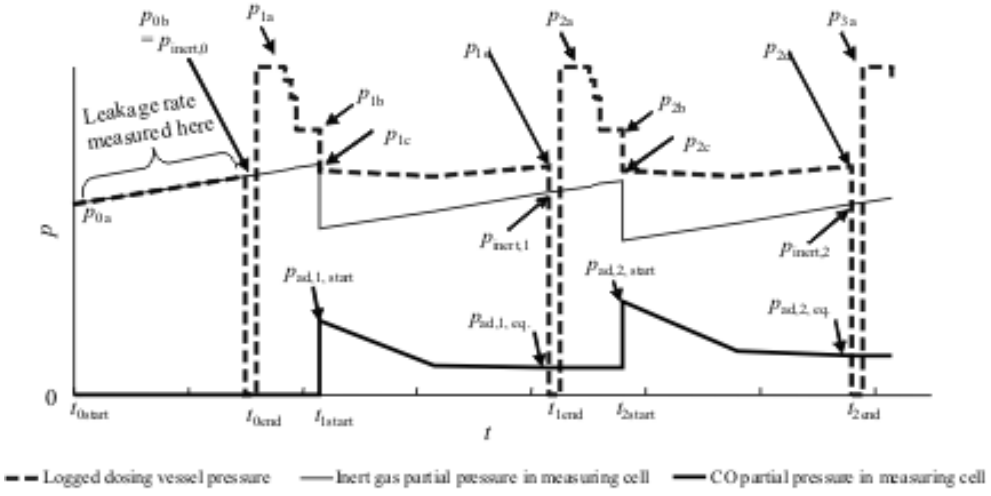
Leakage rate measured here
Logged dosing vessel pressure
Inert gas partial pressure in measuring cell
CO partial pressure in measuring cell

Figure 6.31: The logged pressure data.

linearly with time according to the leakage rate. The partial pressure of nitrogen at the end of dose n ($p_{inert,n}$) can be calculated according to eq. (6.7).

$$p_{inert,n} = p_{inert,n-1} \times V_{cells}/(V_{cells} + V_{dose}) + Lrate \times (t_{nend} - t_{n-1end}) \tag{6.7}$$

The equilibrium partial pressure of CO $p_{ad,n,eq}$ is the difference between the measured total pressure and the calculated partial pressure of nitrogen at the end of the dose n. The amount of CO adsorbed during dose n ($n_{ad,n}$) can be calculated from the pressure difference between $p_{ad,n,eq}$ and the theoretical partial pressure of CO $p_{ad,n,start}$ (eq. (6.9)). $p_{ad,n,start}$ is calculated under the assumption that no adsorption of CO occurs (eq. (6.8)).

$$p_{ad,n,start} = (p_{dose,n} \times V_{dose} + p_{ad,n-1,eq} \times V_{cell})/(V_{cell} + V_{dose}) \tag{6.8}$$

$$n_{ad,n} = (p_{ad,n,start} - p_{ad,n,eq}) \times (V_{cell} + V_{dose})/(R \times T) \tag{6.9}$$

Plotting the sum of the amounts adsorbed of the doses 1–n versus the equilibrium pressure of CO at the end of dose n yields the adsorption isotherm.

For each dose, the values of p_{nb} and p_{nd} and the length of the dose in minutes have to be inserted into the Excel spreadsheet. In addition to the pressure data, the Excel spreadsheet needs the following experimental values inserted to calculate the adsorption isotherm: the sample mass, the active sample area, the temperatures of the dosing section and the calorimeter, the dosing

section volume and the leakage rate. The volume of the measuring cells is also calculated from pressure data that have to be inserted into the appropriate cells.

6.3.2 Calculation of the differential heat of adsorption

The differential heat of adsorption $\Delta H^{diff}{}_{ads}$ can be calculated for each dose by dividing the heat generated during the dose by the amount of CO adsorbed during the dose. The heat generated during each dose can be determined by integrating the heatflow measured during the dose.

The integration of the heat flow data is best done using the software Origin (MicroCal). The ASCII file containing the exported heatflow data can be easily imported into Origin files. After creating plots of the heatflow versus the time, the heatflow can be integrated using Origins tools. The first step is to subtract a baseline from the heatflow signal. In the next step markers are used to define the part of the signal that should be integrated. The last step is the integration itself. The yielded value is the generated heat in units of mJ. The value of the generated heat can be directly inserted into the Excel spreadsheet for each dose. An included spreadsheet displays the differential heat of adsorption versus the coverage of the sample.

Bibliography

[1] N. Cardona-Martinez and J.A. Dumesic, Adv. Catal., 38 (1992) 149.

[2] Höhne G. W. H., W. F. Hemminger, and H.-J. Flammersheim , ”Differential Scanning Calorimetry”, Springer, Berlin (2003).

[3] http://www.swagelok.com/downloads/webcatalogs/MS-01-140.pdf, Sept. 22, 2004.

[4] http://www.swagelok.com/downloads/webcatalogs/MS-01-24.pdf, Sept. 22, 2004.

[5] http://www.caburn.co.uk/resources/downloads/pdfs/sec1.1.1.pdf, Sept. 22, 2004.

[6] http://www.caburn.co.uk/resources/downloads/pdfs/sec1.2.1.1.pdf, Sept. 22, 2004.

[7] B.E. Spiewak and J.A. Dumesic, Thermochim. Acta, 290 (1996) 43.

List of Tables

2.1 CO TPD data obtained with $Cu/ZnO/Al_2O_3$ (50:35:15) 21

3.1 Characterization and catalytic data 29
3.2 Calorimetric results 31
3.3 CO TPD data obtained with CZA1 and CA1 34
3.4 Simulated data 41

4.1 Characterization and catalytic data 49
4.2 CO TPD data obtained with CZA1 and CA1 55
4.3 Influence of the pretreatment on the main IR band 60

5.1 Characterization and catalytic data 70
5.2 CO TPD data obtained with CZA1 and CA1 77

List of Figures

2.1 Flow scheme of the adsorption microcalorimetry set-up. 12

2.2 Schematic drawing of the microcalorimetric cells. 13

2.3 U-tube reactor used for the pretreatment of microcalorimetric samples. 14

2.4 Flow scheme of the set-up used for CO TPD experiments and sample pretreatment. 15

2.5 Flow scheme of the transmission IR cell. 17

2.6 Differential heat of adsorption and adsorption isotherms of CO on Cu/ZnO (50:50) determined at 300 K. 19

2.7 CO TPD spectra obtained with Cu/ZnO/Al_2O_3 (50:35:15) with varying initial coverage of CO, $T_{1st\ step}$: 275 K (a), 300 K (b), 325 K (c), and 350 K (d). 21

2.8 FTIR spectra obtained with Cu/ZnO/Al_2O_3 (10:60:30) (left) and adsorption isotherms of CO obtained with Cu/ZnO/Al_2O_3 (10:60:30) and Cu/ZnO/Al_2O_3 (50:35:15) (right) determined in the pressure range of 0–100 Pa and at room temperature. 23

3.1 Differential heat of adsorption and adsorption isotherms of CO on CZA1, CZ1 and CA1 determined at 303 K. 31

3.2 The entropy of adsorption of CO on CZA1 and CA1 at 303 K and its contributions. 32

3.3 CO TPD spectra obtained with CZA1 and CA1 fully covered (A, a) and partially covered (B–E, b–f) with CO, $T_{1st\ step}$: 275 K (B, b), 300 K (C, c), 325 K (D, d), 350 K (E, e) and 375 K (f). 33

3.4 FTIR spectra obtained with CZA2 after reduction in the pressure range of 0–100 Pa of CO and at room temperature. The left side shows the range of the CO stretching vibration. The spectra are not corrected for a baseline or the gas phase CO vibrational contribution. The right side shows the range below (upper right) and above (lower right) the CO stretching vibration for a pressure of 0 and 100 Pa of CO. The upper right spectrum at 100 Pa CO is shifted by an extinction of 0.025 to allow a better comparison. 35

3.5 FTIR spectra obtained with CA2 after reduction in the pressure range of 0–100 Pa of CO and at room temperature.The left side shows the range of the CO stretching vibration. The spectra are not corrected for a baseline or the gas phase CO vibrational contribution. The right side shows the range below (upper right) and above (lower right) the CO stretching vibration for a pressure of 0 and 100 Pa of CO. The upper right and the lower right spectrum at 0 Pa CO are shifted by an extinction of -0.04 and -0.75, respectively, to allow a better comparison. 36

3.6 Single beam spectra obtained at room temperature with CZA1, CZA2 and CA2 in the calcined state (cal) and after reduction (red). The spectra of the calcined samples CZA2 and CA2 are shifted to higher energy to allow a better comparison. The single beam spectra served as background for the spectra in fig. 3.4, 3.5 and 3.7, respectively. 37

3.7 FTIR spectra obtained with CZA1, CZA2 and CA2 in the calcined state at a pressure of 100 Pa of CO and at room temperature. Only the spectrum of CZA2 is corrected for a baseline and the gas phase CO spectral contribution. . . 38

3.8 Comparison of adsorption isotherms derived from microcalorimetric results using the samples CZA1, CZ1 and CA1. The fractional coverage is calculated by dividing the amount of adsorbed CO by the specific amount of copper surface atoms, respectively. 39

3.9 Simulation of the TPD peaks obtained with CZA1 and CA1. 40

3.10 Comparison of adsorption isotherms derived from microcalorimetric results for samples of high copper content (CZA1, CA1), FTIR experiments with samples of low copper content (CZA2, CA2) and computational simulation. 43

4.1 Differential heat of adsorption and adsorption isotherms of CO on CA1 at 303 K after CO pretreatment. The results obtained after hydrogen reduction are included for comparison. The sample was evacuated overnight between the first and the second adsorption experiment. 51

4.2 Differential heat of adsorption and adsorption isotherms of CO on CZ1 at 303 K after CO pretreatment. The results obtained after hydrogen reduction are included for comparison. The sample was evacuated overnight between the first and the second adsorption experiment. 52

4.3 Differential heat of adsorption and adsorption isotherms of CO on CZA1 at 303 K after CO pretreatment. The results obtained after hydrogen reduction are included for comparison. The sample was evacuated overnight between the first and the second adsorption experiment. 53

4.4 CO TPD spectra obtained with CZA1 and CA1 fully covered (A, a) and partially covered (B–E, b–f) with CO after CO pretreatment, $T_{1st\ step}$: 275 K (B, b), 300 K (C, c), 325 K (D, d), 350 K (E, e) and 375 K (f). 54

4.5 FTIR spectra obtained with CZA2 after pretreatment in CO in the pressure range of 0–100 Pa of CO and at room temperature. The left figure shows the range of the CO stretching vibration. The spectra are not corrected for the gas phase CO vibrational contribution. The right figure shows the range below the CO stretching vibration for pressures of 0 and 100 Pa of CO, and after evacuation. 56

4.6 FTIR spectra obtained with CA2 after pretreatment in CO in the pressure range of 0–100 Pa of CO and at room temperature.The left figure shows the range of the CO stretching vibration. The spectra are not corrected for a baseline or the gas phase CO vibrational contribution. The right figure shows the range below the CO stretching vibration for a pressure of 0 and 100 Pa of CO. 57

4.7 Single beam spectra obtained at room temperature with CZA2 and CA2 after different pretreatments (hydrogen reduction and CO pretreatment during 1 h, 18 h and 50 h). The single beam spectra after 50 h CO pretreatment served as background for the spectra in fig. 4.5 and 4.6, respectively. 58

4.8 The influence of the pretreatment on the main band. The spectra are recorded after hydrogen reduction and CO pretreatment during 1 h, 18 h and 50 h at a pressure of 100 Pa of CO. The results for CZA2 are in the right figure, for CA2 in the left figure. 59

4.9 The potential energy diagram shows the reaction of CO and oxygen on a copper surface. The presence of Zn species on the copper surface could inhibit the desorption of carbon dioxide thus leading to the reverse reaction including the desorption of CO. 62

4.10 Preliminary results of experiments measuring the differential heat of adsorption and adsorption isotherms of CO on ZnO/Al_2O_3 at 303 K after CO pretreatment and hydrogen reduction. 63

5.1 The mass spectrometry traces of hydrogen, carbon monoxide, carbon dioxide, water, and methanol recorded while flushing the sample with pure helium at 498 K. The flushing out of educts and products is almost completed after 10 min, but is carried on for at least 20 min more. 71

5.2 Differential heat of adsorption and adsorption isotherms of CO on CA1 at 303 K after methanol synthesis. The results obtained after hydrogen reduction are included for comparison. The sample was evacuated overnight between the first and the second adsorption experiment. 73

5.3 Differential heat of adsorption and adsorption isotherms of CO on CZ1 at 303 K after methanol synthesis. The results obtained after hydrogen reduction are included for comparison. The sample was evacuated overnight between the first and the second adsorption experiment. 74

5.4 Differential heat of adsorption and adsorption isotherms of CO on CZA1 at 303 K after methanol synthesis. The results obtained after hydrogen reduction are included for comparison. The sample was evacuated overnight between the first and the second adsorption experiment. 75

5.5 CO TPD spectra obtained with CZA1 and CA1 fully covered (A, a) and partially covered (B–E, b–f) with CO after methanol synthesis, $T_{1st\ step}$: 275 K (B, b), 300 K (C, c), 325 K (D, d), 350 K (E, e) and 375 K (f). 76

5.6 FTIR spectra obtained with CZA2 after after methanol synthesis in the pressure range of 0–100 Pa of CO and at room temperature. The left figure shows the range of the CO stretching vibration. The spectra are not corrected for a baseline or the gas phase CO vibrational contribution. The right figure shows the range below the CO stretching vibration for pressures of 0 and 100 Pa of CO. 78

5.7 FTIR spectra obtained with CA2 after after methanol synthesis in the pressure range of 0–100 Pa of CO and at room temperature. The left figure shows the range of the CO stretching vibration. The spectra are not corrected for a baseline or the gas phase CO vibrational contribution. The right figure shows the range below the CO stretching vibration for a pressure of 0 and 100 Pa of CO. . 79

6.1 The Swagelok connection, before (left) and after (right) make-up [3]. 91

6.2 Metric and fractional (inch) fittings [3]. 91

6.3 Installation of a Swagelok tube fitting [3]. 92

6.4 The Cajon VCR connection [4]. 92

6.5 The installation of a Cajon VCR connection [4]. 93

6.6 The installation of a CF connection [5]. 94

6.7 The KF connection [6]. 95

6.8 The adsorption microcalorimetry set-up; 1: CO gas bottle; 2: nitrogen gas bottle; 3 + 5: pressure gauges; 4 + 6: pressure reducing valves; 7, 8, 12: shut-off valves; 9: filter; 10: rotary vane pump; 11: Pirani gauge; 13: turbomolecular pump; 14: membrane pump; 15: control unit; 16: full range pressure gauge; 17: heating element; 18 - 20: pneumatic valves; 21 - 23: fans; 24: power supply unit; 25 + 26: Baratron pressure gauges; 27: heater fan; 28 - 30: heating elements; 31 - 33: temperature controllers; 34: CF flange; 35: linear motion feedthrough; 36 + 37: measuring cells; 38: insulation; 39: calorimetric block; 40: CS 32 controller; 41: power supply unit; 42: Linear motion device; 43 + 44: signal conditioners; 45: power supply and pressure display unit; 46: Voltmeter; 47: control unit; 48: power supply unit; 49 + 51: personal computer; 50: safety switch. 96

6.9 The adsorption microcalorimetry set-up (front view). 97

6.10 The adsorption microcalorimetry set-up (personal computers and pressure displays). . . . 98
6.11 A schematic diagram of a Tian-Calvet sensor. . . . 99
6.12 A pneumatic valve (Swagelok SS-4BG series). . . . 100
6.13 A schematic diagram of the microcalorimetric measuring cells. . . . 101
6.14 The CO gas bottle stored in a vented gas cupboard. . . . 102
6.15 The nitrogen gas bottle at the backside of the set-up. . . . 103
6.16 Part of the gas supply. . . . 104
6.17 The toolbar of the Setsoft 2000 program. . . . 105
6.18 Choosing the measurement device. . . . 105
6.19 Description of the experiment. . . . 106
6.20 Experiments consist of zones and sequences. . . . 107
6.21 Defining the acquisition period and the number of data points for a zone. . . . 108
6.22 Monitoring of the experiment in the ”Real-time drawing” window. . . . 109
6.23 The user interface of the Vent-Puls program. . . . 110
6.24 The user interface of the Vent-Puls-Edit program. . . . 111
6.25 The user interface of the program ”M4660A-mV-C3”. . . . 112
6.26 Calibration of the volume of the dosing section. . . . 113
6.27 The pretreatment reactor. . . . 115
6.28 The special glass container and glass funnel. . . . 115
6.29 Processing an experiment. . . . 117
6.30 Exporting a zone. . . . 118
6.31 The logged pressure data. . . . 119

Curriculum Vitae

Persönliche Daten

Name	Raoul Naumann d'Alnoncourt
Geburtsdatum	10. Juli 1972
Geburtsort	Göttingen

Schulbesuch

1978	Grundschule Neu-Aubing, München
1978–1980	Montessorischool, Amsterdam, Holland
1980–1982	Grundschule, Utting
1982–1983	Städtisches Gymnasium, Weilheim
1983–1985	Collegium Josephinum, Bonn
1985–1988	Reuchlin-Gymnasium, Pforzheim
1988–1991	Carl-Humann-Gymnasium, Essen
24. Mai 1991	Abitur

Wehrdienst

Aug. 1991–Sep. 1992	Zivildienst, Alfried-Krupp-Krankenhaus, Essen

Hochschulausbildung

20. Sep. 1992	Immatrikulation an der Universität Dortmund
23. Okt. 1995	Vordiplom in Chemie
26. Okt. 1995	Immatrikulation an der Universität zu Köln
Jan.–Juli 2001	Diplomarbeit zum Thema: Untersuchungen zur Wechselwirkung von Wirkstoffen und Polymeren mit Lösungsmitteln und Additiven in Formulierungen
21. Aug. 2001	Diplom in Chemie
Dez. 2001– Dez.2004	Dissertation am Lehrstuhl für Technische Chemie der Ruhr-Universität Bochum Lehrstuhlinhaber: Prof. Dr. M. Muhler